INSTRUMENTATION FOR MEASUREMENT OF COSMIC NOISE AT 750, 1225, AND 2000 kHz FROM A ROCKET

Technical Report
NASA Grant NsG 572

By:

W. J. Lindsay
H. W. Estry
D. D. Majeske
R. L. Miller
D. Walsh

SUBMITTED BY:

Fred T. Haddock
Project Director

THE UNIVERSITY OF MICHIGAN
RADIO ASTRONOMY OBSERVATORY

DEPARTMENT OF ASTRONOMY
DEPARTMENT OF ELECTRICAL ENGINEERING

February 1967

PREFACE

This is the final technical report concerning the instrumentation for measurement of cosmic noise at 0.75, 1.225, and 2.0 MHz flown aboard rocket NASA 11.03 UR in June, 1965. The work was supported under NSG-572. The scientific aspects of this program will be published separately.

TABLE OF CONTENTS

TABLE OF CONTENTS (Continued)

TABLE OF CONTENTS (Concluded)

LIST OF TABLES

LIST OF FIGURES

Figure

Figure

Figure

Figure

ABSTRACT

This report describes design considerations and performance characteristics of a complete rocket-borne instrumentation system for absolute intensity measurements of radio frequency noise energy. The instrumentation was designed to make simultaneous cosmic noise measurements at frequencies of 750, 1225, and 2000 kHz, while immersed in, or above, the ionosphere. The instrumentation includes an antenna impedance measuring system which operates during flight.

Procedures used for preflight and in-flight noise calibrations are discussed. A description is given of the ground equipment used to prepare the flight telemetry data for computer processing.

The payload was launched June 30, 1965 from Wallops Island, Virginia, to an altitude of 1,057 statute miles and all instrumentation functioned perfectly. The scientific aspects and results of this program will be published in a separate report.

I. INTRODUCTION

This report describes design considerations and performance characteristics of a complete rocket-borne instrumentation system for absolute intensity measurements of the radio frequency noise energy which is of galactic and extra-galactic origin. All portions of the system shown in Figure 1 utilize fail-safe circuits, alternate channel redundancy, and conservative design techniques wherever possible. The payload is an improved version of a previous experiment conducted in 1962. The present payload is actually the prototype of this earlier experiment with various modifications and additions. Simultaneous cosmic noise measurements can be made while immersed in, or above, the ionosphere at frequencies of 0.75, 1.225, and 2.0 MHz. The radio astronomy antenna impedance is affected by the ionosphere, and is therefore measured periodically throughout the flight.

The instruments described herein were successfully fired to an altitude of 1701 kilometers on June 30, 1965. The rocket was designated NASA 11.03 UR. The scientific results of the flight will be reported separately.

The radio astronomy antenna diagrammed in Figure 1 consists of a 71.5-foot tip-to-tip balanced electric dipole deployed from the instrumentation package after last stage rocket burnout and nose cone ejection. Three radiometers operating simultaneously from one antenna are alternately switched between the receiving dipole and an electrical equivalent dummy antenna for in-flight noise calibration. For 5 seconds out of every 15 seconds throughout the flight, the antenna is switched to a circuit which measures the antenna impedance at 0.75 and 1.225 MHz. At these frequencies, the antenna is electrically very short. Therefore its terminal impedance appears almost completely capacitive in free space.

Since free electrons present in the ionosphere affect the dielectric properties of the medium, the antenna impedance will vary as the electron density varies. Local measurement of the antenna impedance is necessary in order to derive the absolute level of the cosmic noise. These measurements can also be used to estimate local electron densities, and possibly to evaluate ionospheric focusing effects.

Figure 2 is a photograph of the flight payload. For clarity, a metal cylindrical outer shield normally placed around the instrumentation section is not included.

The above system was designed to be carried aboard an Argo D-8 rocket as shown in Figure 3. The 11.03 payload has a predicted[1] peak altitude of 1840 kilometers for a gross payload weight of 140 pounds. Of the total

weight, 89 pounds is scientific payload. The remaining weight is allocated to the rocket nose cone, despin system, and the other necessary hardware. The total usable measurement interval is approximately 1500 seconds with apogee predicted for 865 seconds after rocket takeoff. The actual flight trajectory for this payload is shown in Figure 4.

II. DETAILED DESCRIPTION OF PAYLOAD

A. RADIOMETER ANTENNA

1. General Operation

An antenna with accurately known electrical properties is an essential part of any system for absolute intensity measurement at medium or low radio frequencies. In addition, an antenna for use aboard a spin stabilized rocket payload must meet stringent requirements as to physical size, weight, deployment, and environmental capabilities.

A balanced electric dipole antenna was chosen for this flight and consists of two DeHavilland Aircraft of Canada, Ltd., Type A-18 antenna units, with slight modifications. Each unit contains a 35-foot element. The elements are colinearly deployed from the payload perpendicular to the Z-axis. The payload structure is 1.5 feet in diameter, making the dipole 71.5 feet tip-to-tip.

2. Antenna Elements

The antenna element is a beryllium copper alloy strip, 2 inches wide, 0.002 inch thick, and weighs 0.0141 lb/ft. The strip is tempered by heat-treating in a manner which causes it to spring into a 0.5-inch diameter thin-walled tube on deployment. The partially deployed antenna elements may be seen in Figure 2. For storage, each element is uncurled and wound on a cylinder. Each unit has a self-contained 12-volt DC electric motor and gear train which deploys the 35 feet of antenna element in approximately 100 seconds. As the antenna element is deployed from the spinning payload it is subjected to a bending moment. The maximum[2] bending moment experienced during deployment for a given payload and initial spin rate, is directly proportional to the rate at which the antenna is deployed. The maximum deployment rate is therefore limited by the maximum allowable bending moment for the antenna element. The rate selected for this experiment assures a large safety factor.

3. Modifications to A-18 Unit

One modification of the A-18 unit was the installation of a Globe LL-24 motor with a 20:1 gear head, replacing the standard motor provided in the A-18 unit. This modification provides the desired deployment rate and insures

sufficient power for retracting the antenna during ground tests. No provision is made for retraction during flight.

The other modification to the A-18 unit was the addition of a spring actuated linear potentiometer for monitoring the antenna position during deployment. The potentiometer shaft rides on a polished, specially built cam locked to the deploy unit shut-off shaft. The shut-off shaft has a Lexan cam that follows the element supply spool. Thus, as the diameter of the supply spool decreases, the potentiometer wiper picks off the related fraction of the potentiometer supply voltage (see Figure 5). When all of the element has been deployed the Lexan follower falls into a slot, shutting off power to the deployment motor and causing the potentiometer wiper to pick off maximum voltage. The potentiometer signals from each antenna are telemetered to the ground so that antenna deployment may be confirmed.

4. Mechanical

The two antenna units are mounted on "A" Deck of the payload as shown in Figure 6. A modified A-18 antenna unit with 35 feet of antenna element weighs 2.79 pounds exclusive of wiring and mounting brackets. The maximum dimensions for each unit exclusive of mounting brackets but including the length sensor is 8.0 inches long, 4.1 inches high, and 4.2 inches wide.

5. Antenna Equivalent Circuit

The dipole antenna may be represented by either of the two equivalent circuits shown in Figure 7. The first equivalent circuit emphasizes the fact that we are dealing with a balanced circuit. The junction point of the two voltage generators is at ground potential. C_A and R_A are measured every 15 seconds during flight by the antenna impedance measuring circuit. The approximate free space value of R_A may be computed from:

$$R_A = \frac{80\pi^2}{\lambda^2} h^2$$

where h is the dipole half length, λ the free space wavelength, and R_A is in ohms. The effects on R_A of antenna tubing diameter and conductor losses are not considered in this equation. These effects are negligible.

The free space reactive component of antenna impedance represented by C_A is given approximately by:

$$C_A = \frac{\pi\epsilon_o h}{\ell n(h/a)-1}$$

where:

h = dipole half length
a = antenna wire radius.

For h = 35 feet and a = 0.25 inch, these equations predict the following values for free space conditions:

R_A = 0.56 ohm at 0.75 MHz
R_A = 1.46 ohm at 1.225 MHz
R_A = 4.00 ohm at 2.0 MHz
C_A = 46 pf.

C_B in the antenna equivalent circuit is stray capacitance. The stray capacitance is due to the proximity of grounded conductors and surfaces adjacent to the DeHavilland antenna unit, the antenna switch, and the signal leads. As installed in the rocket payload, $2C_B$ was measured as 31.9 pf for the left antenna (stub only). The right antenna had slightly less stray capacity than this so a small adjustable capacitor was added as shown in Figure 8 to maintain the balanced circuit. This capacitor was adjusted so that the total capacitance from the right antenna element stub to ground was also 31.9 pf.

Note in the second equivalent circuit in Figure 7 that C_B forms a capacitive voltage divider with C_A which decreases the signal voltage at the input to the preamplifier. For this reason, every effort in design and component layout was made to minimize the value of C_B.

The values of R_A and C_A vary greatly from their free space values as the antenna moves through the ionosphere. Since the antenna impedance does change during the flight, it is not possible to have an impedance match between the antenna and the preamplifier. The approach used for this payload was to have the input impedance to the preamplifier fairly high at all three frequencies. This results in a high noise figure for the receiver, but since the levels to be measured are on the order of 10^7°K ohm, a low noise figure is not required.

6. Antenna Length and Payload Stability

A final consideration for the dipole antenna is overall length. A very long antenna is desirable from a signal standpoint. However, the payload is initially spin stabilized about the axis of least moment of inertia (Z-axis). To insure that the payload remains stable, the Z-axis must remain the axis of least moment of inertia. If the antenna element were to exceed 40 feet the Y-axis would become the axis of least moment of inertia and this stability condition would be violated. The 35-foot elements are therefore a compromise between signal level and payload stability.

B. RADIOMETER

1. General Operation

The payload block diagram, Figure 1, shows the functional relationship between the various parts of the radiometer. These units are the antenna, the antenna switch, the preamplifier first-stage, the preamplifier second-stage, and the three receivers.

2. Antenna Switch

The relation of the antenna switch to other parts of the payload is outlined in the diagram, Figure 1. Figure 8, the antenna switching circuit diagram, shows the complete electrical details. The antenna is switched by Wafers C and D which alternately connect the balanced preamplifier input terminals to the receiving antenna or the dummy antenna. When the preamplifier is connected to the dummy antenna, the antenna switch also connects the receiving antenna to a circuit for measurement of antenna impedance. One complete rotation of the antenna switch corresponds to one 90-second payload cycle.

Antenna switch Wafer B is used to synchronize the antenna Ledex switch and the audio commutator switch. Wafer A controls the timing of the switching intervals and application of power to the antenna impedance system and noise diode.

Balanced series resonant 240.2 MHz trap circuits at the antenna terminals and parallel resonant traps at the preamplifier input terminals effectively prevent transmission of telemetering interference to the radiometer preamplifier and the antenna impedance measuring circuit.

3. Preamplifier

The preamplifier circuit diagram is shown in Figure 9. It consists of a stable, high input impedance, broadband, low-noise, cascode amplifier feeding three cathode followers. Each cathode follower has a nominal 50-ohm output impedance and serves to isolate the input of each receiver. This feature makes it unnecessary to control the receiver input impedance except at its own operating frequency. The receiver input impedance is a nominal 50 ohms at band center and decreases sharply outside the operating bandwidth. This decreases the gain of the cathode follower off the band center and thus effectively reduces input signal levels except at the appropriate operating frequency. Spurious receiver responses are thereby minimized.

Of particular interest are the construction techniques used to obtain the balanced broadband preamplifier input transformer T_1. The transformer core is a Siemens No. 550M25-AL60, 23x17 mm, air gapped pot core. The center-tapped primary winding consists of 64 bifilar, spaced, pi-wound turns at one end of the coil form. The 89-turn secondary winding is pi-wound at the opposite end of the coil form to minimize stray capacitance between the secondary and primary windings. A 7x44 Litz wire is used in all windings. This construction minimizes transformer electrical unbalance.

A General Electric ceramic-and-metal planar triode, type 7462, is used in the first stage of the cascode amplifier. It is operated at a plate current of 5.6 milliamperes. This operating point yields a typical g_m of 9500 micromhos, a plate resistance of 10K ohms, and a mu of 95. Under these conditions the equivalent series noise resistance is approximately 250 ohms. The B+ power required for the complete preamplifier is 33 milliamperes at 200 volts DC.

It will be noted in Figure 9 that all tube filaments in the second-stage preamplifier are wired in series. Since a tube failure in any of the three cathode followers only affects its respective channel, Zener diodes are placed across each of the filaments so that preamplifier operation will be unaffected by one or more cathode follower filament failures. The total filament current required is 400 milliamperes at -25 volts. Vacuum tubes rather than transistors were used in the radiometer preamplifier and receivers because the radiometer is the modified prototype of NASA 11.02 UR rocket payload,[3] which was designed before suitable transistors were available for low noise RF work.

The preamplifier is physically separated into two sections. The first section containing the first stage is packaged with the antenna switch, dummy antenna, and antenna impedance measurement circuit as shown in Figure 10(b). The second section consisting of the second stage of the cascode amplifier and the three output cathode followers shown in Figure 11 weighs 14 ounces and occupies 37 cubic inches.

Figure 12 is a plot of the preamplifier frequency response from the input terminals of the dummy antenna to the resistively terminated output. Figure 13 is a curve of the preamplifier self-noise, $T_A R_A$ product in °K·ohms, as C_A in the dummy antenna is varied above and below the antenna free space capacitance at 0.75 MHz.

The noise performance of the preamplifier with the antenna as a source impedance can also be characterized by a set of noise parameters as discussed by the IRE Subcommittee 7.9 on Noise.[4] These parameters have been measured on the flight preamplifier and are tabulated below.

PREAMPLIFIER NOISE PARAMETERS

Frequency (MHz)	F_M	G_o(mhos)	B_o(mhos)	R_n(ohms)
2.00	2.460	1.336×10^{-4}	-2.00×10^{-4}	3182.9
1.225	1.808	2.297×10^{-4}	1.791×10^{-4}	1156.2
0.75	1.691	3.939×10^{-4}	4.369×10^{-4}	602.4

Using these values, the noise performance can be predicted by using the following equation:

$$T_r = T_o\{F_m - 1 + R_n/G_a[(G_A-G_o)^2 + (B_A-B_o)^2]\}$$

where

$$T_o = 290°K$$

$$G_A = \frac{R_A}{R_A^2+X_A^2} = \text{antenna conductance}$$

and

$$B_A = \frac{-X_A}{R_A^2+X_A^2} = \text{antenna susceptance .}$$

4. Receivers

The three radiometer receivers (each driven from a separate cathode follower in the preamplifier) are conventional superheterodynes as shown in Figure 14. A cascode RF amplifier is followed by a pentode mixer with a separate local oscillator stage. Two pentode intermediate frequency amplifiers with delayed AGC, operating at 450 kHz are followed by a full wave bridge second detector. The detector drives a transistor audio amplifier and an RC filter with a time constant of 0.1 second. The RC filter is followed by a cathode follower stage which establishes the optimum DC level and output impedance for the telemetry system. The audio output is also telemetered so that man-made or atmospheric noise leakage through the ionosphere, or abnormal receiver performance, can be monitored. The character of the signal present at the antenna terminals can be determined in a gross way from this audio output.

Figure 15 shows a typical receiver CW bandwidth curve, obtained by varying frequency with signal input level constant and the output voltage maintained below the AGC threshold at all times. The noise bandwidth is typically 8.73 kHz.

In the receiver schematic, Figure 14, note that all three receivers are basically identical. R_4 in the cascode amplifier output tank is used to set the receiver gain for signal levels below AGC threshold. The IF traps in the first stage provide additional rejection at 450 kHz for the 0.75 MHz and 1.225 MHz receivers. No IF rejection filter is required in the 2.00 MHz receiver. Figure 16 shows the receiver construction.

The receiver overall dynamic response characteristic is determined by delayed AGC. The AGC action does not begin until well above the expected cosmic noise level.

The overall gain characteristic of the dynamic response is determined by the value of cathode and grid bias on V_4 and V_5 (see Figure 14). Cathode bias is fixed by Zener diode D_8 and emitter-follower Q_1 and is independent of cathode current. The fixed gain portion of the dynamic response is determined by Zener diode D_7, which supplies grid bias through series pass diode D_6. The AGC portion of the dynamic response is determined by the AGC amplifier, which amplifies the detector output, feeding the amplified signal through pass diode D_5 to the grids of V_4 and V_5. AGC amplifier gain is determined by the value of R_{31} and R_{32}.

Diodes D_6 and D_5 select either the voltage on Zener diode D_8 or the AGC amplifier output, whichever is more negative for application to the grids of V_4 and V_5. The receiver gain and the point at which AGC takes over are determined by the values of Zeners D_7, D_8, and resistors R_{31} and R_{32}.

When the signal input is low, grid bias is taken from Zener D_8 and receiver gain is constant. As the signal input is increased, the AGC amplifier output eventually exceeds the voltage on Zener D_8 and receiver gain becomes a function of the signal input and AGC action occurs.

The Zener diodes D_7 and D_8 are temperature compensated types. Diodes D_9, D_{10}, and D_{11} provide circuit temperature compensation. Thus the AGC characteristic is carefully temperature compensated through the fixed gain range, with only moderate drift in the delayed AGC range.

Power requirements for each receiver are 130 volts DC at 18.6 milliamperes and 25.6 volts DC at 300 milliamperes.

All components were carefully selected for stability and ruggedness and particular attention was paid to the construction techniques used. After adjustment, each transformer and inductor tuning slug is locked in place

with beeswax so that the ferrite cores are not detuned by vibration. Each receiver weighs 1.88 pounds and occupies 74 cubic inches.

C. ANTENNA IMPEDANCE MEASURING SYSTEM

1. Introduction

Proper interpretation of the cosmic noise levels measured during flight requires that the impedance of the receiving antenna be known. The antenna impedance measuring system designed for this payload measures the antenna impedance at 0.75 MHz and 1.225 MHz once every 15 seconds during flight. The instrument can measure values of antenna impedance equivalent to a capacitance between -40 pf and +70 pf at 1.225 MHz and between -36 pf and +92 pf at 0.75 MHz. Antenna resistance values up to 1000 ohms may be measured at either frequency.

2. Simplified Circuit

The telemetered data from the antenna impedance measuring circuit consists of two waveforms which must be measured simultaneously. The first waveform represents the response of a resonant circuit and is telemetered via the 40 kHz VCO. The second waveform is a measure of the bias sweep voltage applied to a varactor diode and is telemetered via the 30 kHz VCO. Both of these waveforms are shown in the sample of telemetry data in Figure 78.

The circuit for measuring antenna impedance is a modification of the familiar "Q-Meter" circuit. Basically, the circuit consists of a series resonant RLC circuit as shown in Figure 17(a), in which the X_R and R_R are known functions of the antenna impedance. The value of C is varied by use of a varactor diode to obtain a complete resonance response curve. The sweeping bias voltage to the varactor diode is monitored so the value of C is known at all times. The unit contains two constant amplitude excitation oscillators, one for 0.75 MHz and one for 1.225 MHz. The radio frequency voltage across the circuit C is the output signal. A computer program has been written to determine R_A and X_A from the shape of this response curve.

Figure 17(b) shows a simplified schematic diagram of the antenna impedance measuring circuit. A transformer is used to couple the antenna impedance to the resonant circuit. The impedance seen looking into the secondary winding of the transformer is designated Z_R for reflected impedance and is equal to R_R plus jX_R as indicated in Figure 17(a). Preflight calibration of this circuit consists in part of determining the function which allows X_R and R_R to be calculated from X_A and R_A and vice versa.

3. Detailed Circuit

a. Antenna Coupling Transformer.—Figure 18 shows the complete schematic diagram of the resonant circuit. The antenna coupling transformer is designated as T_1, and the varactor diode as D_1. The oscillator input signal is injected into the circuit as a nominal 0.33 mv rms across the 0.5 ohm resistor R_5. Capacitors C_1, C_2, and C_3 parallel D_1 and are part of the series C. Capacitors C_2 and C_3 are used only during the measurement at 0.75 MHz. The RF signal across the varactor diode is taken off via emitter-follower Q_1, so as not to load the resonant circuit.

The antenna coupling transformer T_1 was developed for use in this circuit. A pot core was used in the transformer because of its self-shielding, high coupling coefficient and small size. An air gap in the core improves temperature stability. Losses in the transformer were minimized so that small values of antenna resistance could be measured. The turns ratio is one-to-one and consists of basket wound Litz wire. One half of the primary was wound on each side of the secondary so that the stray capacitance would be balanced. The balance of each primary half was checked by applying a signal to the secondary winding and then comparing the induced signals in each half of the primary as to amplitude and phase. Fine balancing was accomplished by adjusting the relative position of the primary half coils.

The inductance of the secondary winding provides the L in the series resonant circuit. The secondary winding was designed to have an inductance of 106 microhenries so that at 1.225 MHz the circuit could resonate when the antenna reactance was equivalent to a C_A of -40 pf. This resonance occurs when the varactor diode is at its maximum value of capacitance. For minimum varactor diode capacitance, resonance occurs for a C_A of 70 pf. To obtain the proper C_A range at 0.75 MHz, a 270 pf capacitor is switched in parallel with the varactor diode.

b. Varactor Diode.—Operation of the circuit is such that the sum of C_A and the varactor diode capacitance is nearly constant at circuit resonance. The range over which C_A may be measured is therefore approximately equal to the range over which the varactor diode capacitance may be varied. A 1N952 varactor diode was selected because it can be varied by at least 125 pf, has a high Q and is quite stable with temperature. The capacitance of the diode may be calculated very accurately from:

$$C_D = \frac{K}{(V_o+V)^n}$$

where

C_D = diode junction capacitance

K, V_o, and n = constants for a given diode

V = instantaneous value of the bias sweep voltage.

When C_D is measured in pf and V is measured in volts, the flight diode values are K = +143.0, V_o = 0.5958, and n = 0.4766. The value of C_D is 157 pf when V = +0.30 volts and 26.1 pf when V = +35.0 volts.

c. Sweep Voltage Generator.—The bias sweep voltage is generated by an RC discharge circuit shown in Figure 19. The sweep waveform is generated by C_{10} discharging through the series combination of R_{10} and R_{13}. The sweep voltage decays exponentially from 35 volts to 0.3 volt in approximately 0.5 second. The sweep capacitor is recharged through the silicon controlled rectifier, Q_3. The free running multivibrator, consisting of Q_1 and Q_2, generates a positive pulse every 0.5 second which is coupled through C_8 and triggers the SCR, allowing C_{10} to charge back up to +35 volts. The repetition rate is such that approximately five resonant response curves are obtained at each measurement frequency.

d. Excitation Oscillators.—The two crystal controlled oscillators which provide the input signal to the series resonant circuit are of the Colpitts type. Construction details are shown in Figure 20. The schematic diagram of the oscillator circuit board is shown in Figure 21. These oscillators are temperature stable in amplitude and frequency. A monitor circuit is provided which measures the oscillator amplitude at the collector and provides a DC level which is telemetered along with the other data. The proper measurement frequency is selected by a relay which applies -23 volts to only one of the oscillators at a time. The relay is controlled by the payload sequence timer.

e. Signal Amplifier and Envelope Detector.—As mentioned previously, the RF signal appearing across the varactor diode is coupled to the amplifier via an emitter-follower. The amplitude of this signal changes as the varactor diode capacity is swept through its full range. The envelope formed by this amplitude variation goes through a resonant peak and is a measure of the response of the series resonant circuit.

Following the emitter-follower, the RF signal is amplified and then the envelope is detected. The circuit is shown in Figure 22. Two stages of amplification are provided by Q_1 and Q_2. A reactive load is used for Q_2 to improve linearity and produce equal gain at 0.75 MHz and 1.225 MHz. The envelope detector consists of D_1 and D_2 connected as a voltage doubler. Signal levels are high enough so that this detector produces a linear response.

The diodes have high forward conductance and exceedingly low reverse leakage. The detector time constant is set by R_6 and C_5 to be approximately 1/10 that of the series resonant circuit. This allows the detector to faithfully follow the envelope.

Driver stage Q_3 couples the detected envelope signal to the telemetry (40 kHz VCO) input. Diode D_3 temperature compensates Q_3 and at the same time sets the bias level so that any signal detected will produce an output at the driver.

4. Flight Operation Sequence

Figure 23 shows the time relationship between the antenna impedance measurement intervals and all other payload switching functions. In the basic pattern power is supplied to the antenna impedance measurement circuit for 5 out of every 15 seconds. The antenna impedance is measured at 1.225 MHz during the first half of the 5-second interval and at 0.75 MHz during the second half.

Note in Figure 23 that the antenna impedance is measured in four different intervals during one complete 90-second payload switching sequence. In addition, the interval between the 10-second mark and the 15-second mark is used to measure the impedance of a known capacitor to provide an in-flight check of the circuit calibration. During the interval between the 55-second mark and the 60-second mark the antenna impedance circuit is not energized. Therefore oscillator leakage cannot interfere with the radiometer "noise" and "no-noise" calibration.

5. Mechanical Layout

The antenna impedance measuring circuit was assembled in two boxes designated the antenna switch box and the oscillator and sweep generator box. The antenna switch was integrated into a single package along with the antenna impedance tank envelope output circuit and the radiometer first-stage preamplifier. Figure 10(b) is a photograph showing the mechanical assembly of the antenna switch and the impedance tank envelope output circuits. Shielding is accomplished by providing separate compartments for the circuits. A side cover plate and a shielding plate have been removed for clarity. The circuit boards are secured on three sides by slots milled into the vertical sides of the package. Figure 10(a) is another view of the antenna switch box showing the plug-in calibration capacitor for the impedance measuring system. The total weight of the switch box unit is 2.45 pounds and it measures 7.50 inches long, 4.25 inches wide, and 4.25 inches high. The housing is fabricated from magnesium.

The excitation oscillators and sweep generator are housed in a common box on "B" Deck. The complete unit weighs 0.79 pound and measures 4.50 inches long, 3.83 inches wide, and 3.83 inches high. The housing is magnesium.

D. SWITCHING SEQUENCE TIMER

1. General Operation

In order to perform the various measurements and calibrations during flight the switching sequence requires a rather complicated timer. The time relationships can best be illustrated by referring to Figure 23 which shows a complete sequence of switching events. Note that 90 seconds are required for one complete switching sequence. In that interval the radiometer data and antenna impedance sequence repeats 6 times, the radiometer audio output commutator sequence repeats twice and the telemetering VCO channel calibration occurs once for each bank of VCO's. The Ledex steps at 10-second and 5-second intervals for the radiometer data and antenna impedance measurement intervals, respectively. The payload block diagram, Figure 1, shows the relationship of the various sections of the timer and their influence on payload operation. The control functions of the timer are as follows:

1. Antenna switching, which also controls all other timing functions.

2. Antenna impedance measurement turn-on and sequencing.

3. Radiometer "no noise" and "noise" calibration sequencing.

4. VCO calibration sequencing.

5. Antenna impedance measuring system calibration.

6. Radiometer audio commutator sequencing.

Referring to Figure 24, the basic timing interval is generated by the astable multivibrator labeled "Antenna Timer." The output of this timer is a -34-volt pulse with a duration of approximately 50 milliseconds. The pulse is used to drive two power amplifiers, which in turn energize the antenna Ledex and the audio commutator Ledex. The antenna Ledex shown in Figure 8 is a 12-position 4-wafer switch. Wafers C and D are 2-pole, 6-position switches which are used to switch the radiometer preamplifier and antenna impedance measuring system between the antenna, radiometer calibrating dummy antenna, and impedance calibrating capacitor. Wafer B is used to synchronize the audio commutator to the antenna Ledex. Wafer A is a 2-pole, 6-position switch, one pole of which switches a timing capacitor in and out of the antenna switch multivibrator to provide variable timing. The other pole

switches -23-volt regulated power to the antenna impedance system. The audio commutator Ledex shown in Figure 25 is a 4-wafer switch with half of Wafer D wired as a 3-position switch to sample the audio output of each of the three receivers sequentially. The audio output of each receiver is sampled for 15 seconds. Only during the first 10 seconds of this interval is the audio output due to galactic background noise. During the final 5 seconds the antenna impedance is being measured and the audio output is meaningless. The other half of Wafer D supplies -34 volts from the VCO calibration timer to two groups of VCO calibration relays. Wafer C supplies +9 volts through several resistor networks for the establishment of a computer control voltage. Wafer B supplies -23 volts to the noise generator control, VCO calibration control, and antenna impedance measuring circuit. The fourth wafer is part of a homing circuit to slave the audio commutator to the antenna Ledex.

Several fail-safe features were incorporated in the switching sequence. In both the delay circuits and the calibration timer, a circuit failing, in either the energized or de-energized position, will be switched out within 5 seconds by the antenna timer so that radiometer data will still be provided. Further, if either or both the antenna Ledex or the audio commutator Ledex should malfunction, the antenna timer will continue to pulse them in an attempt to restore normal action. Under these circumstances, the audio commutator Ledex will be resynchronized to the antenna Ledex within 90 seconds.

2. Description of Circuits

A simplified antenna timer circuit is shown in Figure 26. Applicable waveforms for this and other timing circuits to be discussed are shown in Figure 23. The basic antenna timer is a conventional astable multivibrator with unsymmetrical on-off times. Referring to Figure 24, when terminal C43 is not connected to terminal C44, the discharge time of C_5 through R_3 produces a 1/2 cycle time of 1.5 seconds, and C_8 in parallel with C_{13} discharging through R_2 produces a 1/2 cycle time of 3.5 seconds. The total is then 5.0 seconds. When terminals C43 and C44 are connected, C_9 and C_{12} are in parallel with C_5 and the discharge time becomes 6.5 seconds, which, in combination with the 3.5-second time, gives a period of 10 seconds. Terminals C43 and C44 are alternately connected and disconnected, producing alternate 10- and 5-second periods, respectively. The output relay RY_6 is placed in series with a capacitor from the collector of Q_8 to ground. When Q_8 is cut off, C_4 charges through R_4 and the relay coil. Since the relay is a magnetically biased, polarized type, the charging current does not operate the relay. When Q_8 conducts, C_4 discharges through the relay coil. The current direction is now correct and the relay operates. The time constant of the relay coil and C_4 is adjusted so that the relay remains closed for approximately 50 milliseconds. Diode D_7 prevents the relay coil back-EMF from damaging capacitor C_4.

The second basic circuit is the delay-on timer which is used in the VCO calibration sequences, the VCO calibration sequence delay, the noise generator delay and the antenna impedance measuring system delay timers. Referring to the simplified circuit in Figure 27, transistor Q_1 is cut off and C_1 initially is not charged. When $-E_{cc}$ is applied, E_b begins falling toward $-E_{cc}$ as the capacitor charges. When E_b reaches about -0.2 volt, the transistor conducts and relay RY_1 is energized. R_3 limits collector current.

In the circuits for the antenna impedance measuring system delay and VCO calibration delay shown in Figure 24, additional resistors (R_{13} and R_{24}) have been provided to discharge the timing capacitor. They are switched across the timing capacitor when the associated relays are energized.

The delay-off gate shown in Figure 28 and used in the VCO calibration timer is the last basic type of delay circuit used. In this case, audio commutator Ledex Wafer B provides the initiating power, $-E_{cc}$, to the circuit. Relay RY_1 is energized immediately and is de-energized 2 seconds later. Delay-off was used for the VCO calibration timer because it can be wired failsafe in the event of audio commutator Ledex malfunction in the VCO calibrate position. If such a malfunction occurs, the delay-off timer will "time out" and the system will revert to a data taking mode. Circuit operation is then basically the same as that of the delay-on gate previously described except that, instead of using Q_2 to energize a relay, the rise in collector voltage when Q_2 conducts is used to cut off Q_1 and thereby de-energize RY_1.

The audio commutator and antenna Ledex stepping switches each require a 28-volt, 3-ampere pulse for proper actuation. The Ledex coils must not remain energized for extended periods because of their limited duty cycle rating. The Ledex solenoids are energized through power transistors Q_{11} and Q_{12} shown in Figure 24. Their bases are normally reverse biased by the +14-volt supply through relay RY_6 and drive resistors R_6 and R_7. When RY_6 closes for 50 milliseconds the bases are forward biased from the -34-volt supply, the transistors saturate, the Ledexes actuate and step one position.

To prevent Ledex switching transients from interfering with proper timer performance, it is necessary to operate the collector of Q_8 from the separate Zener regulator diode, D_8. Precision control of the delay circuit timing requires a stable voltage for the bias circuits. Zener diode D_9 provides a regulated source of +10 volts from the unregulated +14-volt battery.

3. Components

All timing capacitors in the circuits of Figure 24 are hermetically sealed, sintered anode, wet slug tantalum type XT capacitors manufactured by P. R. Mallory. The switching transistors used are all from the Motorola Meg-A-Life series, which are specially constructed to have a low failure rate.

All timer circuits are mounted together in the subassembly shown in Figure 29. The unit weighs 38 ounces, exclusive of the Ledex actuators, and occupies 81 cubic inches.

E. IN-FLIGHT CALIBRATION

1. Noise Calibrator

a. General.—The requirement for a reliable and rugged in-flight calibrator for the radiometer poses a rather difficult design problem because of the 7.6×10^7 °K·Ω signal level required. Continuous wave, pulse, or amplitude modulated carriers require the generation of constant amplitude signals. If the radiometer center frequency or bandwidth shifts somewhat during flight a CW or pulse type calibration will result in a misleading interpretation of the changed response of the radiometer to the actual cosmic noise being measured. The only completely satisfactory solution is the in-flight use of a wideband random noise generator. The noise generator is used to supply a known input signal level periodically so the radiometer dynamic response may be monitored in flight.

With the above considerations in mind a study was made to obtain the best possible means of in-flight noise generation. A solid state noise diode[5] was selected on the basis of its high output and its ruggedness.

b. Noise Diode Selection.—Since relatively little was known about the diode as far as stability, spectrum, and reliability, a test circuit was assembled in June 1962 to age and study a batch of eleven SD2L diodes, from which a flight diode could be selected. SD2L diodes are double-diffused silicon junction diodes. They are operated reversed biased just beyond the knee of the Zener region. Measurements were made of noise output level, power spectrum, diode output impedance, age variations, and sensitivity of noise output to variations in diode current and ambient temperature. Of the eleven placed on test, seven were still on test May 1965. Two failed the first two months of test because their leads were overstressed during installation in the test fixture and two were withdrawn from test because their spectrum did not meet our needs. In general an individual diode's output remained constant at a given operating current and temperature over the three-year period. Since each diode exhibited a different response to operating current and to temperature, diodes are not interchangeable. The range of current for which output amplitude remains constant can be determined by viewing the output on a high frequency scope. A suitable diode does not exhibit spiked, ragged or erratic voltage fluctuations. Good noise output is represented on the scope by a symmetry with respect to the scope's zero baseline and appears to have a Gaussian amplitude distribution. The scope viewing technique was confirmed by comparison to a laboratory thermionic noise generator.

Figure 30 shows the flight diode rms noise output voltage variation with temperature and diode current. The data for this curve is the rms noise measured in a 3.5 kHz bandwidth centered at 1.225 MHz. Plots of the data taken at 0.75 MHz and 2.00 MHz have a similar shape and the noise output level is within ±0.5 db of the 1.225 MHz value in Figure 30 over the whole diode current range. An operating current of 528 microamperes was selected for use during flight because in that region the noise output is relatively insensitive to changes in temperature and diode current as Figure 30 shows. The flight diode has an effective output impedance of 140 ohms.

c. Noise Diode Circuit.—The flight circuit developed for use with the SD2L diode is shown in Figure 31. The circuit consists of noise diode D_1, emitter-follower Q_1, and the RC output attenuator network. The emitter-follower isolates the noise diode from the rest of the circuit. The output attenuator tailors the spectral distribution so that the desired calibration signal level is presented to each receiver. The attenuator, in addition, provides a 50 ohm match to the radiometer dummy antenna unbalanced-to-balanced input transformer. Noise diode current is monitored during flight by telemetering the voltage drop across R_3.

Since a small noise output temperature coefficient does exist, a small constant-temperature oven operating at 90°F ±3°F was designed for the complete noise generator circuit. The oven internal temperature is monitored during flight for reference purposes.

The flight unit was designed to provide an in-flight noise calibration level of 7.3×10^6 °K·Ω at 0.75 MHz, 2.8×10^7 °K·Ω at 1.225 MHz, and 7.6×10^7 °K·Ω at 2.00 MHz. These levels were selected to fall near the anticipated levels to be measured in free space.

It is important to recognize that the laboratory thermionic noise diode calibrations are used as the absolute standard. The in-flight solid-state diode serves to determine the magnitude of any change in the radiometer performance.

Once every 90 seconds during flight the noise generator is connected to the radiometer and turned on to perform a noise calibration. The radiometer noise calibration interval is shown in Figure 23 as occurring from the 55 to the 60-second time mark. For this five-second duration, the radiometer is connected to the dummy antenna. During the first 2-1/2 seconds no noise is present because the +130 volts is not applied to the noise generator. For the remaining 2-1/2 seconds of the calibration interval, +130 volts is applied and the noise signal is present. The first interval is referred to as "no noise," the second as "noise." The radiometer in-flight gain calibration is based on these two levels as discussed in Section III under Radiometer Prelight Calibration. The sample of analog telemetry record in Figure 79 shows the radiometer output level for the "no noise" and "noise" interval.

2. VCO Calibrator

Data processing is simplified and accuracy is greatly improved by feeding known DC levels through the complete telemetry system at regular intervals. This procedure makes it possible to determine voltage scale factors and offset levels which include effects from both the telemetry system and the data reduction equipment. By applying the known DC input levels at regular intervals the scale and offset factors may be recomputed, thereby eliminating drift effects in the complete system. Four levels are used so that errors due to nonlinearities may also be eliminated.

The four known DC levels which are applied to 8 of the VCO inputs once every 90 seconds are 0.000 volt, 1.530 volts, 3.059 volts, and 4.623 volts. Each level is applied for approximately 1/2 second, making the calibration interval 2 seconds long. The sample of analog telemetry record shown in Figure 79 contains a VCO calibration.

The VCO calibration interval occurs in the payload 90-second switching sequence as shown in Figure 23. The three radiometer channel VCO's are calibrated in the interval from 40 to 42 seconds. The two antenna impedance channels, the audio commutator channel, the Langmuir probe channel, and the solar aspect sensor channel are calibrated in the interval from 0 to 2 seconds.

The high and low frequency commutated channel VCO's are calibrated once per second as described in the telemetry section (Section II, Part K) of this report. The computer control channel VCO handles only 9 discrete DC voltage levels, which also serve as its calibration.

The VCO in-flight calibration relies on the accuracy and stability of the calibrating voltage source. Great care was taken in designing and temperature compensating the in-flight voltage references. Figure 32 is a schematic of the VCO calibrator unit which consists of a temperature compensated Zener diode followed by three voltage-divider emitter-follower configurations. This unit maintains the output levels ±3 mv as the temperature is varied between -10°C and +50°C. Construction and mounting details for the VCO calibrator are shown in Figure 33.

The transferring of the VCO inputs from the various data lines to the VCO calibration bus is accomplished by relays located on the "C" Deck VCO chassis. These relays, RY_1 through RY_5, shown in Figure 25, are controlled by the payload sequence timer.

3. Antenna Impedance Measuring Circuit Calibrator

The antenna impedance measuring circuit is calibrated in flight by pe-

riodically connecting it to a known impedance. The known impedance consists of a pair of series connected 120 pf capacitors whose common point is connected to ground. This configuration simulates the balanced antenna. The capacity of the Radio Astronomy antenna in free space will be near this value.

The calibration occurs once every 90 seconds between the 10- and 15-second mark as shown in Figure 23.

F. COMPUTER CONTROL

The major portion of the flight data reduction will be done on a digital computer. The payload contains a timer and programmer which automatically cycles the payload through the various measurement and calibration modes. The computer must be able to sense which of the nine modes the payload is in so it can select the proper routine to process the data. To accomplish this a computer control signal is generated aboard the payload by the opening and closing of various contacts on the Ledexes and relays. The resistive summing network for the computer control signal is shown in the upper right-hand corner of Figure 25. This DC level is impressed on the 2.3 kHz VCO and telemetered back along with the other data.

During the data processing operation, the DC computer control level is recovered and indicates the mode of payload operation. The levels were chosen to be a nominal 0.5 volt apart. Table I lists the DC levels and identifies the payload operational mode corresponding to each. Figure 79 is a sample of the analog telemetry record and shows the computer control channel output signal.

G. POWER SUPPLIES

1. Batteries

The primary power for all portions of this experiment is supplied by 33 Type HR-3 Yardney Silvercels. Ten cells are connected in series to form a nominal +14-volt battery and 23 are connected in series to form a nominal -34-volt battery. The +14-volt battery has a tap at approximately +12 volts for the antenna motors.

Each cell has a nominal rating of 3-ampere hours at 75°F which allows a minimum safety factor of 2 for the normal 30-minute rocket flight. The +14-volt battery has a somewhat greater safety factor because it is very lightly loaded except during antenna erection.

Because the trickle charge potential of a silver-zinc cell is 2.0 volts, the equipment operated from the battery packs must be capable of continuous operation at -46 volts on those units using the -34-volt pack, and +20 volts on the +14-volt pack.

These cells were protected from loss of electrolyte by vent plugs which were set at approximately 0.5 psia pressure differential. Thus, when the cells were placed in a hard vacuum, the electrolyte was still under 0.5 psia pressure, which was adequate to prevent appreciable loss of electrolyte. The battery container is lined with neoprene sheet, which holds the cells firmly and provides a degree of cushioning. A photograph showing the battery container structure is shown in Figure 34. Total weight of the battery pack is 8.94 pounds, of which the container weight is approximately 2.30 pounds.

2. DC-to-DC Converter

A -34-volt-in to +235-volt-out DC-to-DC converter is used in this experiment. The unit is shown schematically in Figure 35 and supplies 200 ma to the +130-volt and the +200-volt regulators. The converter is a conventional common emitter saturating core-type power multivibrator. The switching rate for the unit is approximately 3.5 kHz. Current input to the converter is 1.3 amperes. Careful attention was paid to filtering since this type of converter is capable of generating a considerable amount of pulse-type RF noise.

3. Regulators

The eight voltage regulators used fall into three categories: uncompensated Zener diode, Zener diode biased emitter-follower, and highly compensated series. One uncompensated Zener diode is used for regulation of the +35-volt supply to the antenna impedance sweep generator. Zener diode biased emitter-follower regulators are used for the transmitter -34-volt supply and the -34-volt supply to the +235-volt DC-to-DC converter. There are six highly compensated series regulators for (1) the radiometer filaments, (2) preamplifier B+, (3) receiver B+, (4) -23-volt bus, (5) +9-volt bus, and (6) +6.3-volt bus.

The regulators, shown in Figures 36, 37, and 38, are used to reduce the battery supply voltage variations and decouple converter noise from the main battery lines. The Zener diodes used in these regulators are selected to achieve the desired input voltage to their respective loads.

Filament and plate power for the three radiometers must be well regulated if stable operation is to be achieved. With a possible variation of 40% in the battery supply voltage, the use of regulators with high internal loop gain is required. Figure 39 shows the -25-volt, 1.5-ampere radiometer fila-

ment regulator. Transistors Q_1 and Q_2 are paralleled series passing elements. Resistors R_1 and R_2 also assist in dropping a portion of the input voltage, reducing the dissipation requirements on Q_1 and Q_2. Q_3 and Q_4 are cascaded emitter-followers providing sufficient current gain to drive the bases of Q_1 and Q_2. The error amplifier, Q_5, compares a fraction of the output voltage with the reference Zener diode (D_2) voltage, and amplifies this difference. Resistor R_{12} applies an error signal directly from the input to improve the compensation of input voltage variations. Temperature compensation is effected by adding a sufficient amount of positive temperature coefficient resistance to R_9. Typical performance of this regulator is as follows:

a. The output voltage is reduced by 1 mv for each 20 ma increase in current. This is an equivalent output impedance of 0.05 ohm. Full load current is 1.5 amperes.

b. The output voltage changes less than 6 mv for each 1-volt change in the input voltage.

c. For a constant input voltage, the output voltage changes less than 10 mv between 5°C and 50°C.

Both B+ regulators are very similar in design as shown in Figure 40. Both receive their input power from the +235-volt radiometer DC-to-DC converter which has a fairly constant output voltage because of its preregulator input. Transistor Q_1 is the series passing element driven by emitter-follower Q_2. Error amplifier Q_4 compares a fraction of the output voltage with the reference Zener diode (D_6) voltage and amplifies the difference. Additional voltage amplification is obtained from Q_3. Diode D_2 protects Q_1 from accidental over-voltage. A power Zener diode D_1 is used to drop 70 volts at the input of the +130-volt regulator only.

The amplifiers in each B+ regulator have the same operating voltages when referred to the positive polarity side of the regulator output. The error divider ratio and dropping resistors R_5 and R_6 for the Zener diodes have the values as indicated for the +130- and +200-volt operation. A load current of 70 ma may be drawn from each regulator. Temperature compensation is done with R_8 in the manner described for the -25-volt filament regulator.

Typical performance of this regulator type is as follows:

a. Less than 10 mv change in output occurs from no load to full load of 70 ma. This is an output impedance of 0.14 ohm.

b. The output voltage changes less than 0.5 mv per volt of input change.

c. For a constant input voltage, the output changes less than 50 mv between 5°C and 50°C.

The +9-volt regulator shown in Figure 41 is a low-voltage version of the B+ regulators and its electronic performance is similar. Its characteristics are as follows:

a. The output voltage varies less than 10 mv from no load to full load of 100 ma. Its output impedance is less than 0.1 ohm.

b. The output changes less than 1 mv per volt of input change for inputs from +13-volts to +19-volts.

c. For a constant input voltage, the output varies less than 10 mv between -10°C and +48°C.

The -23-volt regulator, whose schematic is shown in Figure 42 is also similar to the B+ regulators. Its characteristics are as follows:

a. The output voltage varies 0.01-volt from no load to a load current of 200 ma. Therefore, its output impedance at DC is less than 0.05 ohm.

b. The output changes less than 0.6 mv per volt of input change.

c. For a temperature change from -10°C to 50°C, with input voltage constant and a load current of 100 ma, the output changes 6 mv.

A photograph of this regulator showing circuit layout is shown in Figure 43.

The 6.3-volt regulator which powers the magnetometer electronics is also similar to the B+ regulators previously described. The schematic is shown in Figure 44. Its characteristics are as follows:

a. Output voltage varies 15 mv from no load to a full load current of 150 ma.

b. The output changes 15 mv as the input voltage varies from +13- to +20-volts.

c. For a constant input voltage, the output varies less than 22 mv between -10°C and +50°C.

H. ASPECT SENSORS

The relative angle between the earth's magnetic field and the radio astronomy antenna must be known for complete analysis and interpretation of the radiometer flight data. The strength of the earth's magnetic field may be

calculated[6] to within 1% for the flight trajectory. The relative orientation of the spin-stabilized payload and the earth's magnetic field vector must be measured during the flight.

The primary aspect system selected for the flight is a three-axis magnetometer capable of measuring the required angles to within ±3°. As a back-up system, a digital solar aspect sensor is included which measures the angle between the payload Z-axis and the sun once per payload revolution (one measurement every seventeen seconds).

1. Magnetic Aspect Sensor

The magnetic aspect sensor selected for this payload consists of three Schonstedt Instrument Company Type RAM-3 single-component magnetometers. Each RAM-3 consists of an electronics package and a field sensor which is mounted at the end of a two-foot length of cable. Each electronics package is 1.75 inches in diameter and 3.00 inches long. Each field sensor is 0.75 inch in diameter and 3.18 inches long. Each RAM-3 weighs 8 ounces.

Figure 2 shows the mounting of the three sensors and the three electronics packages on "E" Deck prior to the foam potting. Figure 45 gives the details of the interconnect wiring.

The electronics package is comprised of an input voltage regulator, oscillator, and phase-sensitive rectifier. The oscillator produces a current of approximately 5.0 kHz. This current is fed through the primary winding of the sensor to drive cyclically the highly permeable magnetic core of the sensor into saturation. The presence of a magnetic field along the axis of sensitivity (long axis) of the field sensor results in the generation of second-harmonic voltages in the split-secondary winding of the sensor.

The second-harmonic signal is fed back to the electronics unit where it is detected in a phase-sensitive half-wave rectifier circuit. For a condition of zero magnetic field on the sensor's axis of sensitivity, the output DC signal will be the nominal 2.4-volt bias level. For other field conditions, the signal will be less than or greater than the bias level depending upon the direction of the field with respect to the sensor axis. Calibration data is furnished by the manufacturer for each unit relating magnetic field along the sensor axis to output DC voltage. A nominal calibration curve is a straight line passing through +4.80 volts for a field of +600 milligauss and 0.00 volt for a field of -600 milligauss. Nominal linearity is 3% of full scale.

The three sensors are mounted in a phenolic fixture machined to assure that the three axes are mutually perpendicular. The fixture is oriented on "E" Deck of the payload with the X-axis parallel to the radio astronomy an-

tenna and the Z-axis parallel to the longitudinal axis of the payload. The Y-axis completes the right-hand system. Figure 46 identifies the rocket coordinate system and shows the relative orientation between the radio astronomy antenna, magnetometer axes, and the solar aspect sensor.

Each RAM-3 requires 35 ma from a +6.3-volt supply. One highly regulated and temperature compensated supply furnishes current to all units through three separate fuses (see Figure 44). The fuses are used so that all magnetometer data will not be lost if an overcurrent malfunction occurs in only one RAM-3.

In the construction and assembly of the payload, nonmagnetic materials are used where possible. This is done to reduce distortions in the earth's magnetic field at the sensor location. The payload main structure is made of magnesium; the external skin is hard aluminum; hardware consists of stainless steel nuts and bolts and nonmagnetic connectors. The relays and motors distort the field at the sensors slightly. The effect of this distortion was determined by using the earth's magnetic field in a preflight calibration of the magnetometer with the payload operating in the flight mode.

2. Solar Aspect Sensor

The solar aspect sensor selected for this payload is an Adcole Corporation Digital Solar Aspect System. This system measures the angle of incident sunlight with respect to a line perpendicular to the sensor face and expresses this angle as a digital number. In addition, the DC level of the output signal indicates the presence of the illuminated earth in the earth telescope field of view. The system is comprised of an electronics package designated as a Model 235D shift register and an optical sensor designated as a Model 135 solar sensor. The shift register measures 2x3-1/4x4-5/8 inches and weighs 2 pounds; the optical sensor occupies a volume of less than 3 cubic inches and weighs 4 ounces. Figure 2 shows the solar aspect system mounted in the payload structure. Note the three openings in the optical sensor. The long slit is used to determine the angle to the sun, the short slit is the command eye opening, and the round lens is the earth telescope.

The accuracy and resolution of the system are determined in the optical sensor. Light passing through the long slit on the top of a quartz block is screened by a gray-coded pattern on the bottom of the block to either illuminate or not illuminate each of seven photocells. The angle of incidence of sunlight determines which photocells are illuminated. The outputs from the seven cells constitute a seven-bit digital word. The gray-coded pattern is used so that angles differing by only one degree differ by only one bit in the digital output. This assures that only one bit changes at a time and eliminates the possibility of large angular errors due to a small error in transition synchronization. The bits are transferred in parallel to the shift

register and read out serially to the telemetry system. The gray-coded pattern and the seven photocells provide 2^7 or 128 digital words which allows a coverage of 127° in one degree increments. The angle of coverage is 63.5° each side of a line perpendicular to the sensor face. The sensor is oriented in the payload to give maximum coverage toward the tail by tilting 20.5° from the Z-axis (see Figure 47). The angle of coverage extends from ϕ = 174° (sensor output of -63.5°) to ϕ = 47° (sensor output of +63.5°).

The short slit in the sensor is part of the command eye which generates the read out trigger for the aspect sensor. This trigger causes the sun angle to be read out only when the incident rays are perpendicular to the long slit. The angle to the sun is therefore read out once per revolution of the payload and always at the same azimuth angle. Figure 47 shows the orientation of the half-plane the sun must be in to trigger the sensor. This half-plane passes through the Z-axis and is at an angle of 247° to the X-axis. This half-plane is actually a two-degree thick wedge determined by the command eye optics.

The earth telescope has a 1° conical field of view and is directed at an angle of ϕ = 120°45'. The sensor output reference level is 3.97 volts when the earth is not in the field of view of the earth telescope. This reference level drops to 1.40 volts when the illuminated earth comes into the field of view. Such a transition is shown in Figure 79 of the sample analog telemetry record; note that a deflection downward on this channel is an increase in voltage.

The output level corresponding to a binary "one" is 4.91 volts when the earth is not in view and 2.31 volts when the earth is in view. The corresponding levels for a binary "zero" are 3.11 volts for the earth not in view and 0.37 volt when the earth is in view.

The manufacturer furnishes a code table sheet which relates gray-code output to angle. The coded angles range from -63.5° to +63.5° in one-degree increments. The binary word indicated in Figure 79 for the angle between the sun and sensor is 11101010. The first seven bits indicate an angle of -25.5° in the gray-code (ϕ = 110.5° + 25.5° = 136°). The eighth bit is always a zero to signal the end of the word. The beginning of the first bit marks the point in time at which the angle was read. The shift out rate was chosen to be 3 bits per second or 2.7 seconds for all eight bits.

The solar aspect sensor data is assigned to the 7.35 kHz VCO telemetry channel.

I. LANGMUIR PROBE

1. Introduction

The Langmuir probe experiment consists of a cylindrical collector unit which is placed outside the payload and an electronic unit placed within the payload. A photograph of the two units is shown in Figure 48. The two units are connected through low pass filters provided in the probe mount. The current to the cylindrical collector is measured with a current detector as its potential is swept through a range of negative and positive values with respect to the payload body as shown in Figure 49. Each volt-ampere curve obtained during flight is later interpreted in terms of ionosphere electron temperature and density.

2. Cylindrical Collector Unit

The cylindrical collector unit consists of a collector electrode, a guard electrode, and a probe mount. The collector electrode is made of stainless steel and is about 9 inches long with a diameter of 0.022 inch. The guard electrode is made of stainless steel tubing (O.D. 0.065 inch and I.D. 0.042 inch). It is concentric with the collector electrode and insulated from it with Teflon tubing. The guard electrode is driven with the same voltage as the collector and serves a twofold purpose:

a. Places the collector beyond the sheath of the payload skin, and

b. helps to maintain a continuous sheath at the collector-guard boundary.

The collector and the guard electrodes are tied to a connector with a specially designed concentric spring arrangement that permits folding of the assembly to any desired position for stowing and deployment at nose cone ejection.

The probe mount provides space for two low pass filters, one for the collector, the other for the guard, and a connector for the collector and guard elements. The filter prevents the conduction of radio frequency interference, induced in the collector unit, to the electronic unit.

3. Electronic Unit

The electronic unit consists of positive and negative voltage regulators, a linear voltage (ΔV) sweep generator, a pair of dual range current detectors, and system logic to control the detector sensitivity and other functions. Figure 50 is the schematic diagram of the system and shows the interconnections between the units.

Since the system is not sensitive to input voltage change, a simple series regulator was sufficient to overcome the change of rocket battery voltage.

Positive -	Input voltage:	+16 to +20 volts
	Output voltage:	+13 volts
	Regulation:	±2%
Negative -	Input voltage:	-30 to -36 volts
	Output voltage:	-28 volts
	Regulation:	±2%

A unijunction-type ramp voltage generator[7] is used because of its simplicity; the schematic diagram is shown in Figure 51. The linearity requirement over the temperature range (0° to +50°C) is satisfied by temperature compensation with two thermistors. The desired negative starting voltage is obtained by a combination of a Zener diode and a diode. Positive voltage is determined by the unijunction[7] transistor ηV_{cc}, Figure 51.

Hi ΔV -	Magnitude:	(+) 4.8 volts (-) 3.21 volts
	Slope:	30.8 V/sec
	Linearity:	< ±1% from a best straight line
	Output impedance:	< 2KΩ
Lo ΔV -	Magnitude:	(+) 2.4 volts (-) 1.6 volts
	Slope:	15.4 V/sec

To fulfill the requirement of the Langmuir probe experiment (namely, floating input configuration as illustrated in Figure 49) a DC amplifier employing a ring modulator[8] was used, Figure 52. The detector utilizes the diode ring modulator, modulator driver, an AC (carrier) amplifier, and a demodulator. A current range of 0.02 to 6 microamperes was chosen to encompass the charged particle current range expected in this experiment. This current range was covered in four steps. Detector No. 1 measures 0.02 and 0.8 microampere full scale and Detector No. 2 measures 0.1 and 6 microampere full scale. This sensitivity arrangement permits a certain amount of useful data even if one of the two detectors fails.

The detector input impedance is dominated by a shunt resistance across the ring modulator. The driving frequency of the modulator is obtained by an astable multivibrator producing a 2 kHz square wave. To eliminate the carrier frequency, 2 kHz was chosen because the peak response of the modulator transformer near this frequency results in maximum sensitivity of the modulator. The frequency response of the detector is limited primarily by the low pass LC filter at the demodulator. The filter design is a compromise between a low carrier ripple component on the output and fast response to input current.

The detectors have the following characteristics:

Detector No. 1 -	Range:	0.02 and 0.8 μA full scale
	Input impedance:	< 120 KΩ 0.02 μA
		< 16 KΩ 0.8 μA
	Output:	0 to 5 volts
	Output impedance:	< 1.5 KΩ
Detector No. 2 -	Range:	0.1 and 6 μA full scale
	Input impedance:	< 27 KΩ for 0.1 μA
		< 3 KΩ for 6 μA
	Output:	0 to 5 volts
	Output impedance:	< 1.5 KΩ

The logic circuits were designed to carry out the following operations based on ΔV period, Figures 53 and 54.

a. Pulse amplifier—ΔV retrace is applied to the pulse amplifier and and amplified pulse is applied to flip-flop No. 1.

b. Hi-Lo ΔV—Hi-Lo ΔV switching is performed by relay 6 which is operated by flip-flop No. 1. Therefore the ΔV alternates between Hi and Lo ΔV. Flip-flop No. 1 drives flip-flop No. 2.

c. Range switch—Range 1 and range 2 of both detectors are determined by relays 3 and 4, operated by flip-flop No. 2; relay 3 for detector No. 1 and relay 4 for detector No. 2. To balance the input current, relay 3 is "on" when relay 4 is "off" and vice versa. Since flip-flop No. 1 drives flip-flop No. 2, a measurement of current with Hi and Lo ΔV is made in each range. Flip-flop No. 2 drives flip-flop No. 3.

d. Detector switch—Selection of detector for the collector current measurement is done by relay 2, input selection, and relay 5, output selection, both operated by flip-flop No. 3. Again to balance the input current, relays 2 and 5 are alternated. The change of detectors occurs after making a measurement with range 1 and range 2 of a detector.

e. Calibration—A Shockley diode timer with a free running period of about 50 seconds is synchronized by flip-flop No. 3. This insures that the calibration is synchronized with the ΔV. The timer triggers a 2.2-second monostable multivibrator which allows sufficient time to calibrate 4 ranges with Hi and Lo ΔV. Figure 55 shows the system output with a dummy resistance of 22 megohm.

4. Calibration

In general, it is difficult to ground calibrate a Langmuir probe since simulation of conditions found in the ionosphere is not possible. Therefore, an in-flight calibration of the current detectors is made by periodically (approximately every 50 seconds) disconnecting the detectors from the collector and substituting a known resistor (calibration resistor), appropriate in value for the sensitivity of the associated detectors. Calibration takes about 2.2 seconds to cover all four ranges with Hi and Lo ΔV. The accuracy of the detector calibration is limited by the knowledge of exact values of calibration resistors and the slope of the ΔV generator. Therefore, the calibration resistors are known to $\pm 1\%$ of their values and the total change of the ΔV slope is kept under $\pm 1\%$ from a best straight line over the temperature range 0° to 50°C.

The output of the ΔV generator is monitored through the commutator and the ΔV slope can be computed throughout the flight if it is required. Figure 56 shows typical detector calibration waveforms.

J. PREFLIGHT MONITOR SYSTEM

Preflight test point monitoring and remote control of the complete payload is accomplished via a twelve lead pull-off plug cable between the payload and a remote control box. The twelve leads and their functions are identified in Table II. Flight batteries can be monitored and charged, all payload equipment can be turned on and off and the payload checked for proper operation by use of the pull-off cable and the remote control box. This is a great convenience during the firing countdown because any operational delays can be managed without difficulty. Normally, the total payload power is supplied externally until just before rocket firing, at which time the system is switched to internal battery power and the pull-off plug is removed.

Three Ledex stepping switches designated "RECEIVER," "TRANSMITTER," and "MONITOR" in Figure 57 execute all remote control and monitor functions. These switches can be energized only by switched external power from the remote control box. The switches are stepped individually one step at a time by pressing one of the three push button switches located on the remote control box. The control box is connected via the pull-off cable and the payload interconnections shown in Figure 58. Both receiver and transmitter control Ledexes are wired as 6-position switches. They are used to apply power to the various portions of the payload. The monitor Ledex is wired as a 3-pole, 12-position switch which allows 36 test points to be remotely monitored. The monitored functions are tabulated in Table III.

The Ledex switches may be stepped in one direction only. The turn on sequence was carefully arranged so that certain sections of the payload could

be operated normally while other portions of the payload were still off. The turn on Ledexes can be stepped to any combination of their six positions and only those functions identified in Tables IV and V will have power applied. This feature greatly simplified payload check out by making it possible to operate the radiometers with the transmitter and timer off, etc.

Monitor Ledex outputs A, B, and C are connected to three voltmeters in the remote control box via the pull-off cable. Meter range resistors are located at the test point so the three meters are automatically on the proper range of 5 volts or 50 volts full scale. A manual polarity switch is provided. The meter readings for normal operations are known by the remote control operator and thus any possible malfunction can be noted and diagnosed. The monitor Ledex has a fourth output which is connected to a separate meter in the remote control box to indicate which monitor Ledex position has been selected. Additional switching was provided at the remote control box so that the panel meters A, B, and C could be disconnected and the output monitor lines switched to a digital voltmeter. This feature allows all monitor voltages to be read very accurately over a hard line.

Two other meters in the remote control box indicate the -34-volt and +14-volt external supply current to the payload at all times. This current is furnished by independently controllable power supplies external to the control box. A photograph of the remote control box is shown in Figure 59.

Nine test monitor points are thermistor signals indicating the temperature at various locations within the payload. It is possible to monitor any payload temperature rise during long operational holds in the rocket firing countdown. The temperature rise is caused by the dissipation of approximately 182 watts in the payload when the batteries are fully charged and all power is supplied externally. During flight the dissipation drops to approximately 160 watts. The payload normally has enough thermal capacity to limit the temperature rise to a satisfactory degree. However, the fiberglass nose cone is an excellent thermal insulator and full power operation prior to takeoff cannot be maintained indefinitely.

Prior to removal of the pull-off plug, it is mandatory that all control Ledexes be set in their proper positions. The receiver and transmitter Ledexes must be in position 6 and the monitor Ledex must be in position 12. A safety provision has been incorporated in the Ledex wiring circuit to prevent accidental incorrect positioning of the Ledexes. One switch section on each Ledex closes only when the Ledex is in the "flight" position. All three switch circuits are wired in series with a supply voltage to the monitor Ledex position 12. If the operator observes a -34-volt reading on the monitor output meter A, in position 12, he can be assured that all control Ledexes are properly set.

Diodes are placed in series with the two battery charging lines to prevent short circuits at the pull-off plug connector from discharging the battery pack. Placing a ground on either line at this connector merely reverse biases the diode and no current can flow.

K. TELEMETERING SYSTEM

1. General Operation

The telemetering system adopted for this experiment is a standard FM/FM system which conforms to IRIG specifications. The FM transmitter operates at 240.2 MHz with a power output of 2 watts, nominal. Eleven FM subcarrier channel signals are summed in a resistive network and constitute the transmitter modulation input. The transmitter RF output drives a turnstile antenna designed to have a near optimum radiation pattern for the expected rocket trajectory. Each of the telemetering subsections is described in detail below.

2. Subcarrier Oscillators

Eleven voltage controlled subcarrier oscillators (VCO) are used in this system. Table VI identifies the VCO model number, the IRIG bands used, the maximum intelligence frequency and the data assignments. The VCO's were purchased from the Electro Mechanical Research Corporation.

Five of the VCO's are mounted on "C" Deck and interconnected as shown in Figure 25. A photograph of the mounting structure is shown in Figure 60 prior to the foam potting operation. The remaining six VCO's are mounted on "E" Deck and their associated interconnect wiring is shown in Figure 61. Each VCO is designed to accept an input voltage of 0 to +5 volts, DC. The upper modulating frequency limit of each VCO is dependent on its output carrier center frequency. Modulation (i.e., deviation) linearity of the EMR Type 184C VCO is 0.1% or better, about the best straight line for ±7.5% deviation, and 0.25% for ±15% deviation. Modulation linearity for the EMR Type 213B VCO is 0.2% or better, about the best straight line for ±7.5% deviation. Input and output impedance is 500K ohms and 5K ohms, respectively, for all units. The output carrier level is adjustable from 0 to 2 volts rms for the 213B units and from 0 to 5 volts rms for the 184C units. Input power required is 4.5 ma at +9 volts regulated. Each VCO is separately fused so that a failure in one VCO will not affect the other ten.

All eleven VCO outputs are summed in a resistive network shown in Figures 25 and 61. This network is designed so that each VCO works into a 47K ohm load and the nominal resistance from the sum junction to ground is 5K

ohms. Subcarrier preemphasis is used to achieve equal signal-to-noise ratio for each channel at the telemetry receiver output. The subcarrier voltage levels for preemphasis were computed on the basis of having the transmitter deviation vary as the 3/2 power of the VCO center frequency. The minimum subcarrier level used was 40 millivolts rms which corresponds to a transmitter deviation of ±6.9 kHz. These levels were confirmed by dropout test measurements to insure that all data channels had equal signal-to-noise ratios.

3. Input Signal Limiting

Input voltage levels to the VCO's were limited to -0.5 to +5.5 volts DC by a signal limiting circuit for each VCO input to prevent a VCO from being deviated out of its frequency band and causing interference to an adjacent channel. Although all experiments are designed to have a signal output voltage in the 0- to +5-volt range, these limiting circuits are considered desirable safety features in the event that a portion of the payload should malfunction during flight. The limiting circuit consists of a series resistor followed by two biased silicon junction diodes as shown in Figures 25 and 61. The negative limit diode is biased at zero volts. The positive limit diode is biased at +5.0 volts derived from the +9-volt regulated supply.

4. Commutator

A 28-channel, 2-pole, 28 sample per second per pole, motor driven commutator is used to time-multiplex data onto the 14.5 kHz and 22 kHz subcarriers. The commutator is a Datametrics Type 914 employing break-before-make contacts and conforms to the IRIG standard[9] for automatic decommutation. The 56 additional data channels provided by the use of this commutator permit backup of all continuous channels against VCO failure; transmission of much operational data such as instrument temperature, battery condition, voltage levels, antenna deployment length, etc.; and provide the prime data channel for the 3-axis magnetometer. A photograph of the 1x3-9/32 x 3-17/32-inch, 11-ounce unit is shown in Figure 62. The motor draws a nominal 75 ma at 28 volts.

The commutator channel assignments are shown in Figure 63. The first 28 pins on J1 and J2 indicate the data function being sampled and the sampling order. Pin 1 is sampled first, then pin 2, etc. Each data channel is sampled for 16.5 milliseconds. A negative 0.25-volt pedestal of 9.5 milliseconds duration is used to separate data channels. The synchronization bar occurs between data channels Nos. 28 and 1. The synchronization bar has a duration of 49 milliseconds and is easily identified on the data records. The synchronization bar is also used as one point in the voltage calibration of the VCO since it is tied to the +4.623-volt calibration level. Commutator channels 1, 2, and 3 are tied to the other three voltage calibration levels and thus complete the four-step calibration of the commutated channels once every second. A sample of the commutated analog data record is shown in Figure 78.

Cross-strapping is employed on the 22 kHz VCO commutator section to provide 4 samples per second per axis for the magnetometer data and 2 samples per second for the antenna impedance backup data.

5. Transmitter

Telemetry signal strength data from our previous rocket-borne experiment[3] aboard a Journeyman D-8 vehicle fired from Wallops Island confirmed our calculations that 2 watts of radiated power would provide adequate signal strength during the flight. Calculations showed that for a rocket antenna with an isotropic radiation pattern, a ground station antenna with 15-db gain and a receiver with a noise figure of 4 db, the poorest signal-to-noise ratio would be approximately at apogee where the margin of safety would be 12.6 db. Calculations also showed that telemetering signals during the last 100 miles of altitude on the down leg of the trajectory would not be received because of horizon cutoff. It was therefore requested that the NASA Bermuda tracking station be operational so that the data obtained during the ionosphere bottom-side breakthrough could be recovered.

The telemetering transmitter selected for this payload is a Conic Corporation Model CTM-201, true FM transmitter, operating at 240.2 MHz. This solid state unit has a measured output of 2.8 watts into a 50-ohm load and a nominal carrier deviation of ±125 kHz for a 0.725-volt rms modulating signal. Its spurious output is at least 60 db down with respect to the carrier. It weighs 13 ounces and draws 550 milliamperes from a 28-volt supply. The 3-1/4 x 2-1/4 x 2-inch unit is shown in Figure 62. Since the transmitter requires an input voltage between -24 and -30 volts, an emitter-follower regulator is used between the battery pack and transmitter to maintain the supply voltage in this range. The regulator schematic is shown in Figure 38 and maintains an output voltage between -27.5 and -28.7 volts for input excursions between -32 and -45 volts.

6. Telemetering Antenna

Ideally, the telemetering antenna radiation pattern should be symmetrical about the payload spin axis, and have its major lobe directed to the rear of the vehicle. Since the protective fiberglass nose cone is ejected, the antenna must be mounted beneath the nose cone and should be capable of radiating during the powered portion of the flight when the nose cone is in place.

Before selecting the telemetering antenna, several basically different designs were constructed and radiation patterns were measured on a full size mock-up of the payload with the radio astronomy antennas in place. The design finally chosen is a modified turnstile antenna shown folded in Figure 2. A normal turnstile is simply a pair of dipoles positioned perpendicular

to each other and driven 90° out of phase. The modified turnstile shown here consists of 4 monopoles positioned every 90° around an 8-inch diameter cylinder. Each monopole is phased 90° from the adjoining monopole, with the phase increasing for each element counterclockwise as viewed from the tail of the rocket. This selection of electrical phasing produces right-hand circular polarization.

Each monopole is approximately $\lambda/4$ units long. The length is trimmed until the real part of the monopole impedance equals the 70 ohm impedance of the phasing harness. At the output of the summing junction, a single-stub matching cable is used to transform the impedance to 50 ohms. Figure 64(a), (b) illustrates details of the phasing network.

The monopoles are fabricated of 10 mil tempered beryllium copper strips, with a slight concavity perpendicular to the long dimension. This shape is similar to that used in flexible steel tape measuring rules. Therefore, the elements are sufficiently stiff to be self-erecting and to remain erected.

Nose cone ejection initiates telemetering antenna deployment by means of the assembly shown in Figure 65. When the nose cone is installed on the payload, the monopole tips are folded upward and secured under a phenolic plug. The plug is held in place temporarily by a long threaded rod. The rod projects through the central hole in the nose cone ejection spring assembly as the nose cone is lowered in place over the payload. In this position the monopole tips are pressed against contacts on the inner surface of the plug support. The 4 contacts connect 1500 ohm terminating resistors to the ends of the monopoles so that the transmitter remains terminated with 50 ohms ±20% when the telemetering antenna is undeployed. In this position the radiation pattern is not ideal, but it is adequate for the initial portion of the flight. After the ejection spring assembly is cocked and seated properly on top of the phenolic plug, the long threaded rod must be unscrewed and removed. During nose cone ejection, the spring loaded pheolic plug is ejected. As soon as the nose cone clears the top of the payload, the telemetering monopoles spring into their stable position which is in a plane perpendicular to the payload spin axis. Release of the phenolic plug also actuates a switch which signals nose cone ejection via the low frequency commutated channel of the telemetry system.

Measured radiation patterns obtained from a full-scale model of the payload with radio astronomy antennas deployed are shown in Figures 66 and 67. Since the antenna test range used was less than ideal, the patterns and magnitudes shown are probably not precisely correct. Enough work was done with various antennas, however, to provide reasonable confidence in the results. On each polar pattern, the 0 db reference corresponds to the maximum signal received from a $\lambda/2$ dipole antenna transmitting an equal amount of power. As viewed from the ground, the transmitted signal is right-hand circularly polarized which complies with the standard polarization of most ground station helical antennas.

7. Equipment Temperature Monitor

The various sections of the payload are designed to be as insensitive as possible to temperature variation. However, for completeness the preflight calibration of the payload includes equipment temperature at various locations as a variable and these same temperatures are monitored during flight.

The temperature at each of eight locations in the payload is measured once per second and relayed to ground via the 14.5 kHz VCO commutated channel. The thermistor locations and commutator data channels are identified in Figure 63. Each YSI precision thermistor (Part Number 44005) is connected in series with a 14.02K ohm resistor to the +9-volt regulated bus. This combination forms a voltage divider, the ratio of which varies as the resistance of the thermistor varies. A typical thermistor has a resistance of 3,000 ohms at 25°C, 2,417 ohms at 30°C and 1,959 ohms at 35°C. The voltage at the junction of the resistor and thermistor is the telemetered data. A preflight calibration curve was prepared relating temperature to telemetered voltage.

The equipment temperature is expected to increase monotonically during flight. The temperature at liftoff is determined by the length of time the payload is operated at full power prior to launch and the ambient temperature at the launch site.

L. MECHANICAL DETAILS OF STRUCTURE

Figure 68 is a scale drawing of the instrumentation rack structure. It is fabricated of magnesium plates and hollow tube vertical members, most of which are heliarc welded in place. One post between the "B" and "C" Deck is removable and the "D" Deck is completely bolted in place. This construction technique requires that all mounting holes in Decks "A" and "B" be completed before welding. Additions or modifications are difficult, but not impossible because the space between plates A, B, and C does permit the entry and use of hand tools and right angle electric drills.

A 0.042-inch thick aluminum outer skin is bolted to each deck with 24 flat-head screws per deck. This type construction is very stiff.

Placement of subassemblies is determined by consideration of electrical, mechanical, accessibility, thermal, and vehicle spin and balance requirements. The placement of major subassemblies is shown in Figure 2 where the outer aluminum skin has been removed for clarity. In the final configuration, only 0.88 pound of lead had to be added to comply with the 1 ounce-inch static and 20 ounce-inch squared dynamic balance limits for the Argo D-8 vehicle.

M. DECK LAYOUT AND INTERCONNECT WIRING

Deck location and interconnections of all subsections of the payload are shown in Figure 58. The "A" Deck shown at the top of Figure 58 is the base of the instrumentation rack. It is mounted on top of the drum-shaped extension tube. The extension section in turn is bolted to the thrust face of the fourth-stage rocket motor. The extension section contains batteries and timers used to actuate the nose cone release and vehicle despin mechanisms. A plan view of the location of all major assemblies is shown to the left of the interconnections for each deck. Each terminal shown in a box is accessible for disconnect or check. The designation on the lines to each terminal refers to the destination of that line. There are two main vertical cable runs with branches at each deck. Coaxial cables are shown only at their termination points. Extensive use is made of barrier strip type terminals. Although this adds slightly to the overall payload weight, the problems of testing, interference tracing, calibration and trouble shooting are greatly reduced. Wiring used throughout is silver plated, high strand count, with spiral wrapped Teflon insulation.

III. PAYLOAD PREFLIGHT CALIBRATION

A. SUMMARY

Since precise measurement of the absolute cosmic noise background temperature is desired, many preflight calibrations and measurments are required to document system performance under normal and abnormal conditions. The primary preflight calibrations consist of measuring the radiometer output for various inputs from the laboratory standard noise generator (temperature limited thermionic diode) and are used to interpret the flight data. The other measurements are intended to aid in monitoring performance and recovering as much usable information as possible if a malfunction such as a change in supply voltage or ambient temperature occurs in the system during flight. The following is a typical list of preflight calibrations and measurements, some of which are described in detail later in this section:

1. Measure insertion loss and input impedance of flight dummy antenna matching transformer at 0.75, 1.225, and 2.00 MHz.

2. Measure the value of flight radiometer dummy antenna C_A capacitors.

3. Measure stray (base) capacity and resistance to ground of the DeHavilland antennas and associated wiring. Include correction for change in stray capacitance caused by antenna deployment during flight.

4. Measure and adjust flight radiometer dummy antenna shunt capacitors to match Item 3 above.

5. Measure radiometer dummy antenna-preamplifier voltage transfer function versus antenna C_A, R_A, and ambient temperature at 0.75, 1.225, and 2.00 MHz.

6. Calibrate antenna impedance measurement circuit for various combinations of R_A and X_A. Let R_A range from 0 to 1,000 ohms. Let X_A range from negative values corresponding to 108 pf to positive values corresponding to 1 millihenry.

7. Determine temperature coefficient and supply voltage sensitivity of Item 6 above.

8. Noise calibrate each radiometer through the flight radiometer dummy antenna.

9. Determine temperature coefficient of Item 8 above.

10. Measure each radiometer noise bandwidth.

11. CW calibrate each radiometer through rocket dummy antenna.

12. Repeat Item 8 and vary filament voltage by ±2-1/2% and ±5%.

13. Repeat Item 8 and vary +200 volt B+ voltage by ±10%.

14. Repeat Item 8 and vary +130 volt B+ voltage by ±5% and ±10%.

15. Calibrate thermistor circuits.

16. Measure the flight noise generator output level at the three radiometer frequencies.

17. Confirm the calibration of the solar aspect sensor.

18. Calibrate the magnetic aspect sensor with payload operating.

19. Measure linearity of the eleven telemetering subcarrier oscillators.

20. Calibrate the antenna length sensor.

21. Measure the absolute value of the in-flight telemetering calibrator voltage.

22. Measure preamplifier noise parameters (G_o, B_o, R_n, and F_m).

23. Measure spurious responses of radiometers.

24. Measure each radiometer center frequency, local oscillator frequency and IF frequency.

25. Determine the voltage divider ratio for the following telemetry inputs:

    (a) -34 volt TM/monitor

    (b) +14 volt TM/monitor

    (c) +130 volt TM/monitor

    (d) +200 volt TM/monitor

    (e) -25.2 volt TM/monitor

(f) -23 volt TM/monitor

(g) +9 volt TM/monitor

(h) +12 volt TM/monitor

(i) noise generator current

(j) +6.3 volt TM/monitor

26. Accurately measure the following voltage levels:

(a) calibration level No. 2, i.e., 1.530 volts

(b) calibration level No. 3, i.e., 3.059 volts

(c) calibration level No. 4, i.e., 4.623 volts

(d) oscillator No. 1 (0.75 MHz) output TM monitor

(e) oscillator No. 2 (1.225 MHz) output TM monitor

(f) magnetometer bias

(g) +130 volt supply

(h) +200 volt supply

(i) -25.2 volt filament supply

(j) -23 volt supply

(k) +9 volt supply

(l) +12 volt antenna power supply

(m) +6.3 volt supply

(n) pedestal voltage (commutator)

27. Calibrate Langmuir probe.

28. Measure the value of the in-flight antenna Z calibrating capacitor.

29. Measure the plug-in capacitors and resistors used in the calibration of the antenna impedance system.

30. Calibrate the noise diode current monitor circuit.

B. RADIOMETER PREFLIGHT CALIBRATION

1. General Operation

The calibration curve for the radiometer shifts slightly if either supply voltages or ambient temperature is changed. This shift may be thought of as occurring from an overall gain-bandwidth change in the radiometer plus a DC offset in the zero signal output level of the receiver. The magnitude of the shift is easily measured by applying a known noise signal level to the input and monitoring the output. A new response curve may then be simply generated from the preflight reference curve by making proper allowance for the gain-bandwidth change, and the DC shift. Calibrations are made with "white" noise, so that changes in either gain and/or bandwidth will be accounted for without needing to know which has changed.

2. Laboratory Measurements

All laboratory preflight radiometer response calibrations are performed with a wideband random noise generator designed and built in this laboratory. The noise generator circuit shown in Figure 69 uses a temperature limited thermionic diode as a noise source followed by a stable wideband amplifier. Amplifier gain is measured and adjusted if necessary with accurate step attenuators before each calibration is undertaken. This is done at each of the three radiometer operating frequencies. The resultant accurately known noise energy is controlled by cascaded step attenuators which feed the rocket dummy antenna input. This calibration scheme thus requires only a constant output noise generator and stable, accurate step attenuators. Since the diode current can be measured with high precision and all other measurements require only the use of passive attenuators, it is believed that a minimum amount of systematic calibration uncertainty is introduced.

The calibrations are performed by coupling the laboratory noise generator output into the preamplifier via a dummy antenna unit shown schematically in Figure 9. The dummy antenna contains a transformer to match the single-ended noise signal to the balanced input of the preamplifier. The dummy antenna was designed to accept plug-in capacitors so that various values of antenna capacitance, C_A (source reactance), can be used during calibration. This same dummy antenna is flown and is used to inject the in-flight noise calibration level. The dummy antenna also contains capacitors to simulate the base (stray) capacitance in the antenna circuit. Figure 10(a) is a picture of the antenna switch box showing the radiometer dummy antenna on the left side.

During laboratory calibration, many values of source impedance are inserted in the dummy antenna to simulate the impedance changes which occur when the antenna is immersed in the ionosphere.

Considerable data are also taken for many combinations of supply voltage and ambient temperature. These additional data are used to check the validity of the gain-bandwidth correction procedure described below.

3. Gain-Bandwidth Correction

During flight, a dummy antenna simulating the nominal free space antenna impedance is connected to the preamplifier input. The receiver output is then recorded: (1) with the dummy antenna passive ("no noise"); (2) with a known amount of noise injected from a reference noise source. The changes in these recorded receiver outputs, compared with their values measured during laboratory calibration, permit correction for changes in radiometer gain-bandwidth characteristics.

The antenna is represented by an impedance R_A+jX_A together with an imaginary generator, $\overline{V}_A$ as shown in Figure 70. For the purpose of these calculations, antenna base capacity, C_B, is assumed to be part of the radiometer and is included in X_L. This generator includes the signal induced in the antenna by incident waves plus the effects of noise in the receiver, which is otherwise regarded as noise-free. Thus:

$$\overline{V}_A^2 = 4k(T_A+T_R)R_A B \qquad (1)$$

where

T_A = antenna temperature

T_R = equivalent receiver noise temperature.

For given radiometer conditions, the output, e_o, is a function purely of the equivalent voltage $\overline{V}_L$ developed at the input terminals, regardless of the antenna impedance. The voltage $\overline{V}_L^2$ is related to $\overline{V}_A^2$ by an expression involving the antenna impedance:

$$\overline{V}_L^2 = \alpha_o^2 \overline{V}_A^2 \qquad (2)$$

where

$$\alpha_o^2 = \frac{R_L^2 + X_L^2}{(R_A+R_L)^2 + (X_A+X_L)^2} \qquad (3)$$

The antenna impedance affects two quantities which contribute to $\overline{V}_L^2$: (i) the voltage transfer factor α_o; (ii) the receiver temperature, T_R, which is included in the voltage $\overline{V}_A$. Thus, the receiver output is purely a function of the quantity U, where

$$U \equiv \alpha_o^2(T_A R_A + T_R R_A) \quad . \tag{4}$$

This has been verified experimentally for many different source impedances. A typical reference curve of e_o vs. U is shown in Figure 71.

The outputs e_{o_1} and e_{o_2} corresponding to "no noise" and "noise" conditions of the dummy antenna are used as the reference receiver outputs for comparison with the in-flight calibration outputs. Note that the input U_1 under "no noise" conditions is not zero, but represents the effects of receiver noise only.

By a lengthy series of laboratory measurements it is found that if the radiometer response curve changes, for example due to changes in supply voltages or in environmental temperature, a simple procedure will correct for this over wide ranges of the input quantity U. It is found that the new response curve may be derived from the reference curve by means of successive shifts horizontally and vertically. These correspond respectively to a change in overall "gain" (since the scale is logarithmic) and a DC shift. These changes may be denoted by:

$$\Delta \mathcal{G}/\mathcal{G}_o = \text{fractional gain change}$$

$$\Delta V = \text{DC shift in } e_o$$

During the actual flight, two points on the response curve are given once every 90 seconds by the gain calibration procedure, so that the two parameters $\Delta \mathcal{G}/\mathcal{G}_o$ and ΔV may be deduced and the complete response curve is determined. A computer program has been developed to carry out this procedure, and it converts any output reading, e_o, into the equivalent input, U. Actual curves of radiometer output vs. the function U are shown in Figures 72, 73, and 74.

To obtain $T_A R_A$ from this value of U by a solution of (4), it is necessary to carry out the calculation:

$$T_A R_A = \frac{U}{\alpha^2} - T_A R_A \tag{5}$$

Both α_o^2 and $T_R R_A$ depend on the antenna impedance, which is measured frequently in flight. α_o^2 also depends on the radiometer input impedance R_L+jX_L [Eq. (3)]. This impedance is measured accurately in the laboratory, and, for a given antenna impedance, α_o^2 can be calculated to within a few millibels (1 millibel = 10^{-3} bel = 10^{-2} decibel).

$T_R R_A$ is obtained from the noise parameters, also measured accurately in the laboratory:

$$T_R = T_m + \frac{T_o R_n}{G_A}\left[(G_A-G_o)^2 + (B_A-B_o)^2\right] \qquad (6)$$

where

$$G_A = \frac{R_A}{R_A^2+X_A^2} = \text{antenna conductance}$$

$$B_A = \frac{-X_A}{R_A^2+X_A^2} = \text{antenna susceptance}$$

$$T_o = 290°K$$

T_m, R_n, G_o, B_o are the noise parameters.[4] By means of (6) we can calculate T_R to an accuracy of a few millibels (while T_R is dependent on R_A, it should be pointed out that when $R_A \ll X_A$ and $G_A \ll G_o$, which is the case of greatest interest to us, the product $T_R R_A$ is almost independent of R_A and so can be estimated accurately without accurate knowledge of R_A). Thus, for antenna temperatures comparable to receiver noise temperature, we can solve (5) to yield $T_A R_A$ accurate to about 5 millibels (about 1.3%). For most of our measurements, in fact, $T_A \gg T_R$, so the correction for receiver noise is small.

4. Tests of Gain-Bandwidth Correction Procedure

Many laboratory tests were made with deliberately varied supply voltages and environmental temperatures. The effective antenna temperature was supplied by means of a controlled, accurately known, variable noise generator driving the dummy antenna and e_o was measured over a wide range of $T_A R_A$. The noise generator circuit is shown in Figure 69. From the values of e_{o_1} and e_{o_2} under test conditions, $\Delta\mathcal{G}/\mathcal{G}_o$ and ΔV were calculated. α_o^2 and $T_R R_A$ were calculated from (3) and (6) using the known value of source impedance, R_A+jX_A. The value of $T_A R_A$ for each e_o was then estimated using the correction procedure described above applied to the standard reference response curve, and this estimate was compared with the accurately known, true value of $T_A R_A$.

Under certain laboratory test conditions, values $\Delta G/G_o$ as high as 2.4 and ΔV greater than 0.8 volt occur. We can estimate the value of $T_A R_A$ within 10 millibels (2.5%) in the range of 3×10^5 to 10^7 °K·Ω even in this extreme case (the range of $T_A R_A$ of special interest to us is approximately 10^6 to 10^7 °K·Ω). For less extreme changes in the radiometer, the range of $T_A R_A$ over which we can correct to this accuracy is much greater.

The actual in-flight performance showed relatively minor changes from laboratory calibration, and corrections should be very accurate.

C. PREFLIGHT ANTENNA IMPEDANCE MEASURING CIRCUIT CALIBRATION

The antenna impedance measuring circuit is calibrated in the laboratory by measuring its output waveforms when accurately known calibration impedances are connected to the input. By analyzing the variations in the output waveforms as the calibrating impedance is varied, a complete electrical equivalent circuit is determined for the antenna impedance measuring circuit. The waveform analysis is performed on an IBM 7090 computer using a least square error curve fitting technique. The computer is also used for flight data reduction to solve for the value of impedance present at the input terminals, given the equation based on this equivalent circuit and the measured output waveforms.

The preflight calibration is done at several controlled ambient temperatures and supply voltages so that their effect on elements in the equivalent circuit may be determined.

The calibration resistors and capacitors are mounted on separate plug-in units to facilitate changing the value of resistance or reactance during calibration. As shown in Figure 8, the calibrating impedances are balanced in relation to ground to simulate the actual antenna impedance. Ten reactance plug-in units and eight resistance plug-in units are used in all combinations to produce eighty values of calibrating impedance. Inductive reactance as well as capacitive reactance is used. Values for R are between 0 and 500 ohms. Values for C are between 0 and 215 pf. The plug-in boards with inductors on them are to simulate a negative antenna capacitance.

The output waveforms were recorded on magnetic tape during calibration along with various housekeeping functions. These tapes were then digitized and put in the proper format for computer processing.

Proper interpretation of the antenna impedance measurement during flight requires that proper allowance be made for the antenna base impedance (stray capacitance to ground). This base impedance was accurately measured during the preflight calibration.

D. ANTENNA LENGTH SENSOR CALIBRATION

The antenna length sensors are calibrated by deploying each antenna element in a calibrated track. As the tip of the antenna element reaches a length mark, the voltage out of the length sensor is recorded. The curve relating output voltage to antenna length is then drawn.

E. SOLAR ASPECT SENSOR CALIBRATION

The solar aspect sensor output is digital. The preflight calibration consists of orientating the sensor at known angles to the sun and checking the readout with that stated by the manufacturer. The complete field of view of 128° in 1° increments was checked and confirmed. The accuracy of the instrument at transition for a one bit change in the digital output is ±0.25°. Resolution is 1°.

F. MAGNETOMETER CALIBRATION

The magnetic aspect sensor is required to measure the angle between the radio astronomy antenna and the earth's magnetic field to ±3°.

The manufacturer of the magnetic aspect sensor supplied a complete calibration curve for each axis. Since the payload alters the magnetic field at the sensor location, it is necessary to determine two correction factors for each axis. These factors consist of a shift in the calibration curve due to a residual magnetic field and a multiplicative scale factor related to field distortion.

These factors were determined by placing the complete operating payload at a location where the earth's magnetic field was accurately known. Using a nonmagnetic fixture, the payload was then positioned in 108 known orientations. The magnetometer output was recorded for each orientation. A least square error technique (a program for the IBM 7090 computer) was then used to determine the two correction factors for each axis.

G. SALT MINE SELF-INTERFERENCE CHECKS

Laboratory testing the radiometers for self-interference is difficult, if not impossible, because the radio astronomy measurement frequencies are subject to a high level of man-made interference. Two of the measurement frequencies fall in the AM broadcast band; other interference is caused by automobile ignition, diathermy machines and other such equipment. During flight the ionosphere acts as a shield to prevent earth noise at these frequencies from interfering with the instrument. The length of the extended radio

astronomy antennas (71.5 feet tip-to-tip) precludes the use of a screen room, so other radio quiet locations were investigated.

Interference measurements made in sections of the International Salt Mine, 1200 feet under Detroit, Michigan, showed that the mine is very quiet in the portion of the radio frequency spectrum used and makes an excellent "screen room." The portions of the mine that contain no power lines or telephone cables proved to be the quietest, and therefore most suitable for our use. The International Salt Mine Company was most cooperative and allowed us free access to the mine for self-interference checks on the payload.

During testing, battery powered test equipment was used exclusively. The tests measured both conducted and radiated noise from the payload with the antenna completely extended. Power was applied to selected portions of the payload to identify contributions to the total noise level by specific unit, i.e., voltage regulators, DC-DC converters, commutator motor, and solar aspect sensor.

In all, three trips were made to the salt mine to evaluate the effectiveness of corrective filtering actions. Self-interference was reduced to an insignificant level.

IV. THE UNIVERSITY OF MICHIGAN TELEMETERING GROUND STATION

A complete telemetering ground station has been assembled for this experiment. It provides a means to perform preflight system checks and postflight data reduction. This station is used as a backup ground station for in-flight data recording with real time readout if required. A photograph of the telemetering ground station is shown in Figure 75. The tape recorder rack contains the main items of the FM/FM telemetering station. Below the Ampex Model CP-100 tape recorder is a Nems-Clarke Model 1432 phase lock FM receiver. Below it is a bank of six EMR Model 167-01 phase lock subcarrier discriminators. An interconnect and control panel is below the discriminators, followed by a Nems-Clarke Model 200-3 spectrum display unit for the FM receiver. The bottom panel contains an EMR Model 101-A crystal reference oscillator with mixer amplifiers for the tape speed compensation system. To the left of the rack is a CEC Model 5-124 direct recording oscillograph with seven galvanometers for quick readout information. A Tektronix Model 533 oscilloscope for waveform monitoring completes the telemetering ground station.

For telemetry reception and recording, the ground station is arranged as shown in Figure 76. In general, this is typical of a high precision system with extra features added to optimize its performance for this application. Following signal capture by the right-hand helical antenna with a gain of 20 db, the signal is amplified by a 33 db gain, 5 db noise figure preamplifier at the antenna site. The high gain antenna and preamplifier are required for flight data acquisition only. The amplified signal enters the receiver and is demodulated. The resulting composite subcarrier signal is fed to a mixer amplifier where a precision 100 kHz sine wave is added to the subcarriers. Introduction of the 100 kHz signal provides a reference frequency for the tape speed compensation channel which is used during tape playback. The mixer output goes to two direct channels on the 7-channel tape recorder. The direct channels have a frequency response from 200 Hz to 100 kHz at a tape speed of 30 inches per second. This speed allows approximately 34 minutes of uninterrupted recording time. Two channels are used to preclude the loss of data if one channel fails during recording. From the receiver, the signal also goes to the subcarrier discriminators. Each discriminator has an input band-pass filter to select the appropriate channel as shown. The discriminator output is a replica of the corresponding payload telemetering input voltage and is recorded on the direct readout recording oscillograph. Provisions are also made to record the discriminated output on the FM channels of the tape recorder which have a frequency response from 0 to 10 kHz.

The receiver signal strength information is displayed on a meter at the antenna location so that the operator can manually track the payload by posi-

tioning for maximum signal strength. Provisions are made to record signal strength on an FM tape channel.

Voice comments describing the test conditions under which the data were taken are recorded on a separate track and are a great aid in locating specific sections of data on the tape.

The overall circuit for the telemetering ground station is shown in Figure 77 when used during flight as a backup ground station. Note that a second receiving channel along with a left-hand helical antenna has been added to assure acquisition of the best possible data even if the payload were to tumble during flight.

Not shown is the circuit used for automatic three-step calibration of the direct (FM) channels of the tape recorder. Calibration of the FM channels is desirable because these channels do not have playback tape speed compensation. Any drift caused by speed variation cannot be separated from a signal level change without resort to a calibration procedure such as this. Since the discriminators' outputs vary from -2.5 volts to +2.5 volts for 0 to +5-volt variations in the rocket payload, -2.5, 0, and +2.5-volt calibration levels are programmed automatically for two seconds once every two minutes by a ground station FM channel calibrator unit. In addition to the automatic calibration sequence, a manual switch allows additional calibrations to be made at any other time. This switch does not affect the automatic two-minute calibration cycle.

The tape recorder and discriminators are also used for tape playback. As Figure 77 indicates, the cable patch panel is arranged to transfer the played-back composite signal containing the 100 kHz reference signal from the signal delay line into the discriminators for demodulation. In this mode, the normal tuning units for channel 6 discriminator are removed and 100 kHz units are substituted. If there are any tape speed variations they cause a steady-state offset or fluctuation in the 100 kHz discriminator output. This error signal is inserted at the proper point in each of the other discriminators. Cancellation of output variations due to tape speed changes is thus accomplished. The composite signal to the 100 kHz channel does not pass through the signal delay unit. In this way, the proper time delay between the tape speed error signal and the other discriminator outputs is maintained. When properly adjusted, this technique produces a reduction of a least 100:1 in tape recorder flutter and wow compared to an uncompensated system.

Figures 78 and 79 show a section of a typical oscillograph recording of the discriminator outputs. Each oscillograph trace corresponds to the input of a VCO, except for reference traces at the top and bottom and a 36-bit serial decimal time code trace derived from the National Bureau of Standards WWV Time signal. The in-flight four-step VCO calibration sequence used in

conjunction with the reference traces provides a means of determining the actual voltages represented by the various traces. Event timing may be determined from the vertical "1-second" lines or the 36-bit time code.

The oscillograph records provide a visual means of checking payload operations, provides corroborative information for computer-digital reduction of the data and provides prime data for the solar aspect channel. Final precise data reduction is done from the flight magnetic tape, via an analog-to-digital converter and an IBM 7090 Computer.

V. DATA FORMATING EQUIPMENT

Information collected by the 11.03 rocket experiment is prepared for scientific study and analysis by a process of data reduction. A detailed discussion of the data processing procedures and the results of the scientific analysis will be given in a separate document. The following discussion is concerned with only the preliminary steps in the data processing and the special data logging equipment used to prepare the telemetry data for computer input.

The telemetry data recorded during the rocket flight by the ground station tape recorder is digitized and rerecorded on computer compatible magnetic tape by the data formating equipment. The digital tapes are then available for entry of the payload information into a digital computer for processing. The equipment consists of: a Scientific Data Systems Model MU31-1 Multiplexer and Model AD20-14 Analog-to-Digital Converter; an Ampex Model TM4113-D Digital Tape Handling System; and special sequence and control circuitry assembled from Computer Control Company 1 MHz logic modules. A photograph of the data logger and ground station is shown in Figure 80.

The SDS Model MU31-1 Multiplexer has 16 input channels. The maximum switching rate is 15 kHz. The multiplexer is connected for the digitizing of the 11.03 rocket data so that channel 0 is sampled 2500 times per second, channel 1 is sampled 1250 times per second, channels 2 through 7 are each sampled 156 times per second and channels 8 through 15 are each sampled 39 times per second.

The SDS Model AD20-14 Analog-to-Digital Converter provides digital samples with a resolution of 13 bits plus sign. It has a conversion rate of 13,300 samples per second. The analog-to-digital converter also includes sample and hold circuitry which provides a sample aperture of less than 1 microsecond.

The TM4113-D Tape Handling System is designed to read and write tapes that are compatible with the IBM 7090 Computer. It can be operated at tape densities of either 200 or 556 characters per inch and tape speeds of either 30 or 60 inches per second. It uses 2400-foot reels of 1/2 inch magnetic tape. A 2400-foot reel of tape provides a recording period of about 16 minutes at low speed.

The data formater is used with the telemetry ground station. Figure 81 is a block diagram showing the connections of major components. The telemetry tapes are played back through the ground station and the analog signals from the discriminators routed to the various inputs of the multiplexer. The multiplexer inputs are sampled in a fixed sequence but not all channels

are sampled at the same rate. The sampling rate of each channel is selected so there will be sufficient digital samples to preserve the intelligence of the associated analog signal. The gain of the discriminators is adjusted to provide an output signal amplitude of +8 volts to -8 volts. The data formater converts these to digital samples with a resolution of more than 1 part in 8000. Gain and offset of the ground station and data formater electronics are not significant in the data analysis because all data can be rescaled using the in-flight VCO calibration voltages.

A special feature of the data formater provides a means of synchronizing the data sample times with the 100 kHz tape speed compensation signal and introducing range time into the computer format records. The 100 kHz signal is used as the basic sampling frequency source. The relative timing of samples with respect to one another can be determined with the same accuracy as the frequency of the original clock signal. The accuracy is independent of the ground station tape recorder speed changes and/or the digital tape recorder speed variations. The 100 kHz signal is routed to the control logic via a special tracking multivibrator circuit. If any "drop-outs" of the 100 kHz clock signal are encountered, the multivibrator will continue to supply clock signals within 2 or 3 percent of 100 kHz.

Range time is put on the digital magnetic tape records essentially unprocessed. The IRIG format is decoded by a special computer program as one step in the computer data processing.

Two passes of the telemetry tapes are required to digitize the recorded information. The digital tape recorder is operated at a speed of 30 inches per second and data are recorded with a density of 556 tape characters per inch. This corresponds to a sample density of more than 185 analog samples per inch. Approximately 2 reels of digital tape are obtained from each pass of each reel of telemetry tape. The sampling frequency of the data logger could be doubled by changing to a digital tape recorder speed of 60 inches per second, but this also doubles the ratio of digital-to-telemetry tapes, and is not necessary to preserve the intelligence of the analog signals.

VI. PAYLOAD ENVIRONMENTAL TEST REQUIREMENTS

It is standard practice to subject rocket payloads to a series of rigorous tests to determine functional reliability of all components and construction techniques. The flight unit is subjected to tests which demonstrate the ability of the design to meet all performance requirements without harmful degradation at the expected flight levels.

The required test facilities available at GSFC and the tests prescribed by NASA for The University of Michigan Radio Astronomy Observatory Cosmic Noise Rocket Payload designated NASA 11.03 are itemized in the Appendix.

VII. VEHICLE DESCRIPTION AND PREDICTED PERFORMANCE

The Argo D-8 vehicle shown in Figure 3 is a four-stage solid propellant sounding rocket designed to be fired from a zero length launcher. The first three stages are fin stabilized and the fourth-stage is spin stabilized. The maximum spin rate is 7 revolutions per second. With a total payload weight of 140 pounds, the predicted peak altitude is approximately 994 nautical miles for an 80° launch angle. The vehicle staging consists of a first-stage Sergeant with two Recruit booster rockets attached to the sides. The booster rockets give a high initial acceleration to build up the velocity immediately after release from the launcher. Each Recruit burns for 1.8 seconds and has a thrust of 38,000 pounds. The second-stage is a Lance which ignites after a 10-second first-stage coast interval. The third-stage is another Lance rocket. Its fins are canted so that at burnout the vehicle spin rate is increased to approximately 7 rps for fourth-stage spin stabilization. The fourth-stage is an Altair 6 which ignites after a 13-second third-stage coast interval. The fourth-stage remains attached to the payload throughout the flight. At 180 seconds the nose cone is spring ejected and a "yo-yo" despin mechanism is deployed to despin the vehicle to 0.54 rps. The payload is further despun by the erection of the radio astronomy antenna. The antenna starts deploying at 184 seconds and erection is complete at 294 seconds, at which time the payload spin rate is 0.059 rps.

Table VII presents a summary of the rocket predicted performance, and sequence of events.

APPENDIX. ENVIRONMENTAL TESTS

The following is a description of the environmental test program required by NASA for the flight model payload. The launch vehicle was an Argo D-8 (Journeyman).

A. TEST FACILITIES

1. General

The apparatus used in conducting tests shall be capable of producing and maintaining the test conditions required, with the equipment under test installed in/on the apparatus and operating or nonoperating as required. Changes in test apparatus conditions may be the maximum permitted by the test apparatus, but shall not exceed the applicable equipment specification requirements.

2. Volume

The volume of the test facilities shall be such that the bulk of the equipment under test shall not interfere with the generation and maintenance of test.

3. Heat Source

The heat source of the test facilities shall be so located that radiant heat shall not fall directly on the equipment under test, except where application of radiant heat is one of the test conditions.

4. Standard Conditions for Test Area

Normally checkout will be conducted at room-ambient conditions. Reversion to standard conditions will be required only in the case of equipment malfunction or unresolved questionable operation. For this condition, standard conditions are defined as follows:

a. Temperature 25 ±3°C (77° ±5°F)

b. Relative humidity: 55% or less

c. Barometric pressure: local ambient

5. Measurements

All measurements shall be made with instruments whose accuracy conforms to acceptable laboratory standards, and which are appropriate for measurement of the environmental condition concerned. If tests are conducted outside of GSFC facilities, the accuracy of the instruments and test equipment shall be verified before test, after test, and periodically as required by GSFC.

6. Tolerances

The maximum allowable tolerances on test conditions shall be as follows:

a. Temperature ±2°C (3.6°F)

b. Vibration amplitude: ±10%

c. Vibration frequency: ±2%

d. Additional tolerances: additional tolerance shall be as specified.

7. Vacuum Gauge

The vacuum shall be indicated by a vacuum gauge, the sensing element of which is located within the chamber test space. The gauge shall measure the vacuum as it exists at the payload.

B. TEST SEQUENCE

1. Dynamic Balance

Although not an environmental test, balancing is necessary for a spin stabilized payload and shall be performed prior to exposure to environmental tests. Balancing is chosen as the first operation so that the adhesion and effect of the balance weights on payload operation may be evaluated during the course of the tests.

The payload, while nonoperative, shall be balanced about the thrust axis in accordance with the following:

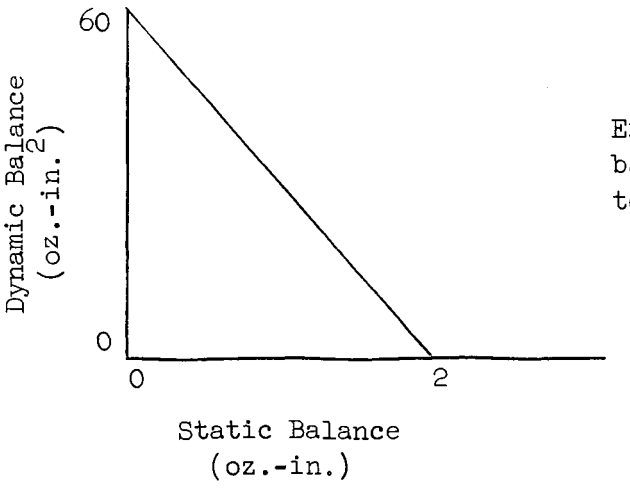

Envelope of acceptable payload balance restraints in relation to C.G. of payload

The payload and the fourth stage shall be balanced as a composite unit upon completion of all environmental tests.

2. Spin Test

The spin test will demonstrate the ability of the electronics and payload structure to withstand the spin forces experienced during flight.

Before exposure to spin, the payload shall be visually examined and functionally tested to assure correct performance.

3. Thermal Vacuum Test

This test will demonstrate the ability of the electronics and payload structure to withstand both flight temperatures and pressure.

Test Procedure.—Before exposure to thermal vacuum visually examine and functionally test the payload to assure correct performance.

With the payload in the nonoperative condition slowly pump the chamber down to 10^{-4} mm Hg and let the payload outgas. Back fill the chamber with dry nitrogen.

With the payload in the flight operative condition, pump the chamber down rapidly (to 10^{-4} mm Hg) and hold for 30 minutes. During the test maintain the control thermistor located on the payload skin at 100°F. Fill the chamber with dry nitrogen and return to atmospheric pressure.

After exposure to the thermal vacuum, visually examine and functionally test the payload to assure correct performance.

4. Vibration Tests

a. Sinusoidal Swept Frequency Test.—The vibration tests given herein are intended to provide assurance that the payload will survive the expected flight environment and are applicable to the complete payload in its powered flight configuration. The vibration tests are based principally on the excitations generated by use of the Altair 6 rocket motor. The vibration excitation shall be applied at the interstage connection between the final stage and the payload. In establishing the test levels some allowance has been made for excitation generated by earlier stages, aerodynamic disturbances and handling transporation effects. The resonance test is required because of unique resonant burning observed in the fourth-stage rocket motor.

Before exposure to vibration, the payload shall be visually examined and functionally tested to assure correct performance.

The payload, while in operational condition normal to powered flight, shall be exposed to the following vibration levels:

Flight Unit: Sinusoidal Swept Frequency Test Schedule

Direction	Frequency Range, cps	Test Duration, ≃ Min	Acceleration g, 0-to-peak
Thrust (Z-Z axis)	10-50	0.6	1.5
	50-500	0.8	7.0
	500-2000	0.5	14.0
	2000-3000	0.1	36.0
		Total 2.0	
Lateral A (X-X axis)	10-50	0.6	0.6
	50-500	0.8	1.4
	500-2000	0.5	2.8
	2000-3000	0.1	11.0
		Total 2.0	
Lateral B (Y-Y axis)	10-50	0.6	0.6
	50-500	0.8	1.4
	500-2000	0.5	2.8
	2000-3000	0.1	11.0
		Total 2.0	

Sweep Rate: 4 octaves/minute

Flight Unit: Random Motion Vibration Test Schedule

Direction	Frequency Band, cps	Spectral Density, g^2/cps	g-rms
Thrust axis	20-2000	.03	7.7
Transverse axes	20-2000	.03	7.7

Duration: 2 minutes each direction
Total time: 6 minutes

Control accelerometer response shall be equalized with peak-notch filterization such that the specified PSD values are within ±3 db everywhere in the frequency band. The filter roll-off characteristic above 2000 Hz shall be at a rate of 40 db/octave or greater.

b. Combustion Resonance Test.—The apparent weight of the flight payload may be measured at 600 Hz. The amplitude values given below are based on an apparent weight of 7 pounds at this frequency. Correction of the amplitude in inverse proportion to the actual apparent weight should be made,

but in no case shall the amplitudes be greater than those given. An alternate method may be substituted wherein vibration force is programmed into the payload between 550 and 650 Hz at ±400 pound force thrust direction and ±67 pound force transverse direction if a suitable force control is employed.

Flight Unit: Combustion Resonance Vibration Test Schedule

Direction	Frequency, Hz	Acceleration, g 0-to-peak	Test Duration, sec
Thrust axis	550-650	33.0	15
Transverse axes	550-650	9.5	15*
	Sweep rate 1 octave/minute		

*15 seconds each axis.

After exposure to vibration, the payload shall be visually examined and functionally tested to assure correct performance.

REFERENCES

1. "Test Directive for Wallops Model G4-2018 (Goddard Model Journeyman 11.03 UR)," 1965, Ralph D. Welsh, Jr., Project Engineer.

2. Extensible Rigid Antennas Maximum De-Spin Bending Moment and Centrifugal Force During Extension From a Rotating Satellite, The DeHavilland Aircraft of Canada, Limited, Report Number DHC-SP-TN 150.

3. Schulte, H. F., H. W. Estry, R. L. Miller, and J. W. Kuiper, Instrumentation for Measurement of Cosmic Noise at 0.75, 1.225, and 2.00 Mc/s From a Rocket, NASA CR-228, May 1965.

4. "IRE Standards on Methods of Measuring Noise in Linear Twoports, 1959," and "Representation of Noise in Linear Twoports," Proc. IRE, 48, No. 1, January 1960.

5. Solitron Sounvister Diode Type SD2L, Manufactured by Solitron Devices, Norwood, New Jersey.

6. Finch, H. F. and B. R. Leaton, "The Earth's Magnetic Field—Epoch 1955.0," Royal Astronomical Society Geophysical Supplement, 7, 314, 1957.

7. G. E. Transistor Manual, General Electric Company, Sixth Edition, p. 196, 1962.

8. Brace, L. H., "Transistorized Circuits for Use in Space Research Instrumentation," The University of Michigan, Space Physics Research Laboratory, Report No. 02816-1-3-S, October 1959.

9. Telemetry Standards, IRIG Document No. 106-60, Revised June 1962.

10. "Flight Plan for Argo D-8 NASA 11.03 UR," John W. Townsend,Jr., Assistant Director, NASA Goddard Space Flight Center, March 15, 1965.

TABLE I

COMPUTER CONTROL LEVELS AND CORRESPONDING PAYLOAD MODE

Voltage Level	Payload Mode
0.5	Ant. Z cal. 750 kHz
1.0	Ant. Z meas. 750 kHz
1.5	Ant. Z cal. 1225 kHz
2.0	Ant. Z meas. 1225 kHz
2.5	Radiometer $T_A R_A$
3.0	Radiometer no noise cal.
4.0	Radiometer noise cal.
4.5	Radiometer VCO cal.
5.0	General VCO cal.

TABLE II

PULL-OFF PLUG LEAD IDENTIFICATION

Wire to	Deck Designation	Interface Jack	Lead Function	Pull-Off Plug	Remote Control Box Plug
B70	A50	A	+14V BATT CH INPUT	1	A
MB28	A51	B	RCV LEDEX COIL	2	B
MB15	A52	C	XMITTER LEDEX COIL	3	C
MB17	A53	D	MONITOR LEDEX COIL	4	D
MB24	A54	E	MONITOR OUTPUT NO. A	5	E
MB25	A55	F	MONITOR OUTPUT NO. B	6	F
MB19	A56	G	MONITOR LEDEX POSITION	7	G
MB51	A57	H	SIGNAL GND	8	H
A71	(A48)	I	ANTENNA PWR SQUIB SW INPUT	---	---
MB20	A58	J	+12V TO LEDEX POSI IND	9	J
MB26	A59	K	MONITOR OUTPUT NO. C	10	K
MB128	A60	L	PWR GND	11	L
B69	A61	M	-34V BATT CH INPUT	12	M
A67	(A49)	N	ANTENNA PWR SQUIB SW OUTPUT	---	N

				NO CONNECTION	P

				NO CONNECTION	R
				NO CONNECTION	S

TABLE III

MONITOR LEDEX TEST POINT POSITIONS

Monitor Meter A			Monitor Meter B			Monitor Meter C		
Ledex Position	Test Point	Full Scale	Ledex Position	Test Point	Full Scale	Ledex Position	Test Point	Full Scale
1A	-34V battery	-50V	1B	+14 battery	+50V	1C	+9V to VCO's	+10V
2A	Fil. -25.2V supply	-50V	2B	Mag. 6.3V supply	+10V	2C	Mag. bias	+5V
3A	Ant. Z ckt. -23V supply	-50V	3B	Sweep voltage ant. Z	+5V	3C	Envelope output ant. Z	+5V
4A	+200V to preamp.	-500V	4B	+130 to RCV	+500V	4C	Temp. no. 7	+5V
5A	RCV no. 1 e_o	+5V	5B	RCV no. 2 e_o	+5V	5C	RCV no. 3 e_o	+5V
6A	Temp. no. 1	+5V	6B	Temp. no. 2	+5V	6C	Temp. no. 3	+5V
7A	Temp. no. 4	+5V	7B	Temp. no. 5	+5V	7C	Temp. no. 6	+5V
8A	Cal. level no. 2 (+1.530V)	+5V	8B	Cal. level no. 4 (+4.623V)	+5V	8C	Computer control	+5V
9A	Mag. X-axis	+5V	9B	Mag. Y-axis	+5V	9C	Mag. Z-axis	+5V
10A	Langmuir probe monitor no. 1 PIN 6	+5V	10B	Asp. sens. monitor	+5V	10C	Langmuir probe monitor no. 2 PIN 3	+5V
11A	Receiver Ledex position	+10V	11B	Transmitter Ledex position	+10V	11C	Temp. no. 8	+5V
12A	-34V master on interlock	-50V	12B	Main board mon. (spare)	+5V	12C	Temp. no. 10	+5V

TABLE IV

CIRCUITS ENERGIZED BY THE RECEIVER TURN ON LEDEX

Switch Position	Circuits Energized
1	All power off
2	A B C D E
3	A B C D E F
4	A B C D E F G
5	A B C D E F G H J
6	A - C D E F G H J K

Designation	Circuit and Connection
A	-34V to receiver filament preregulator
B	-34V to noise diode oven
C	+14V to +9V regulator and timer
D	-34V to antenna Z circuit
E	+9V to antenna Z VCO driver (connected directly to +9V reg.)
F	-34V to receiver converter preregulator (+130V and +200V)
G	+200V to preamp.
H	+14V to transfer relay
J	-34V supply to timer
K	Master on interlock connection

TABLE V

CIRCUITS ENERGIZED BY THE TRANSMITTER TURN ON LEDEX

Switch Position	Circuits Energized
1	All power off
2	L
3	L M N
4	L M N P
5	L M N P Q
6	L M N P Q R S

Designation	Circuit and Connection
L	+9V regulator to VCO's and 5V limiter circuit
M	-34V to transmitter regulator
N	-34V to commutator motor
P	14V to magnetometer reg.
Q	-34V and +14V to Langmuir Probe
R	+14V to aspect sensor
S	Master on interlock connection

TABLE VI

VCO ASSIGNMENTS

IRIG Channel No.	Center Frequency, cps	Frequency Deviation, %	Maximum Intelligence Frequency, (MI=5) cps	EMR Model No.	Nominal Carrier at Sum Junction Monitor, mv rms	Data Assignment
7	2300	± 7.5	35	213B	40	Computer control level
8	3000	± 7.5	45	213B	40	750 kHz receiver output
9	3900	± 7.5	59	213B	40	1225 kHz receiver output
10	5400	± 7.5	81	213B	40	2000 kHz receiver output
11	7350	± 7.5	110	184C	40	Solar aspect sensor output
12	10500	± 7.5	160	184C	40	Langmuir probe output
13	14500	± 7.5	220	184C	42	28-channel commutator, LF
14	22000	± 7.5	330	184C	60	28-channel commutator, HF
15	30000	± 7.5	450	213B	100	Sweep voltage, antenna Z circuit
16	40000	± 7.5	600	213B	115	Envelope output, antenna Z circuit
E	70000	±15.0	2100	184C	175	3-channel commutator, receiver audio

TABLE VII

PREDICTED VEHICLE PERFORMANCE BASED ON A 140-POUND GROSS[1] PAYLOAD WEIGHT AND AN 80-DEGREE LAUNCH ANGLE

Event	Time (+sec)	Velocity (ft/sec)	Altitude (ft)	Horizontal Range (N.M.)	Flight Path Angle (deg)
Recruits burnout	1.8	472	475	.01	79.7
First-stage (Sergeant) burnout	27.5	2,870	42,745	2.23	69.9
First-stage separation	35.0	2,417	61,081	3.42	68.1
Second-stage (Lance) ignition	37.5	2,321	66,561	3.79	67.4
Second-stage burnout and third-stage (Lance) ignition	43.9	4,461	86,476	5.19	66.0
Third-stage burnout	50.3	8,944	124,855	8.04	65.4
Fourth-stage ignition	63.0	8,532	225,194	15.73	64.4
Heat-shield release	67.0	8,926	257,000	18.21	64.2
Fourth-stage burnout	104.9	17,109	670,733	52.24	62.4
Apogee	865.3	5,800	6,037,862	728.43	----
Impact	1,667.9	18,290	0	1,460.56	----

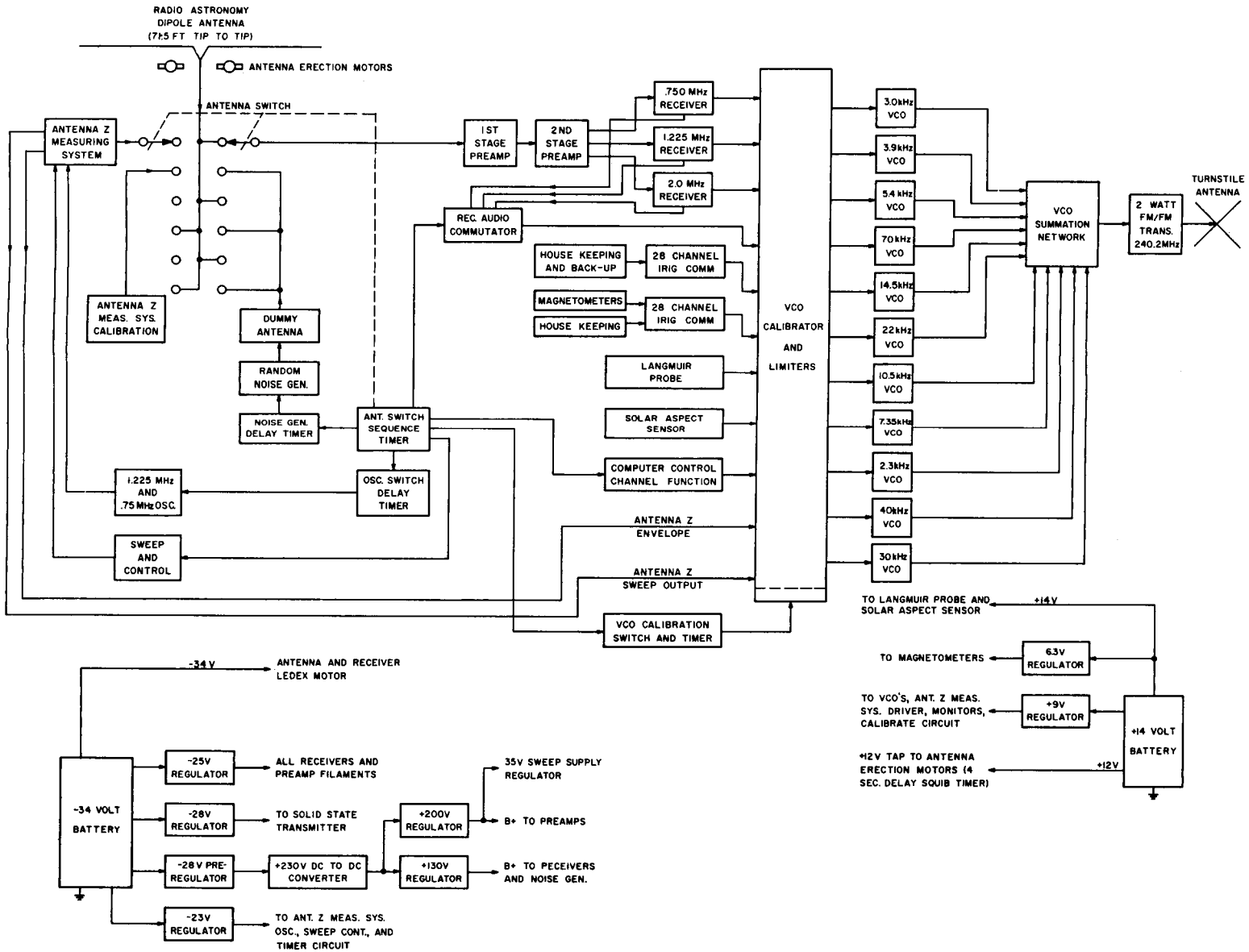

Figure 1. Payload block diagram.

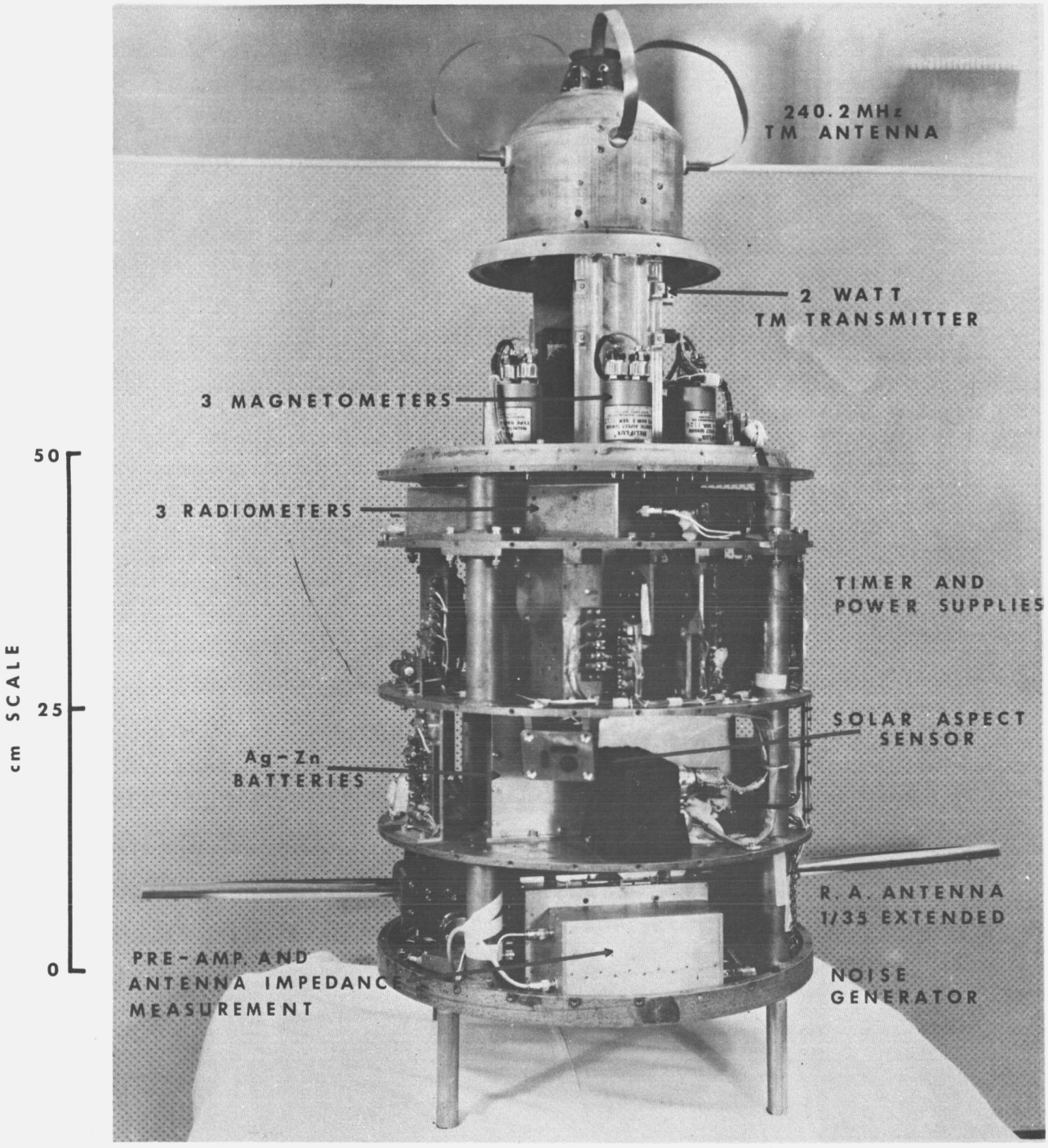

Figure 2. Payload except skin, nose cone, and extension section.

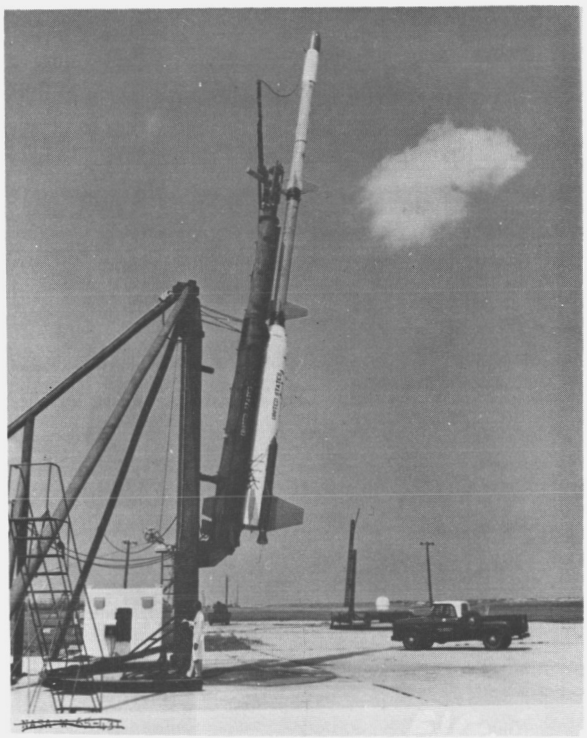

Figure 3. Rocket with payload on launch pad.

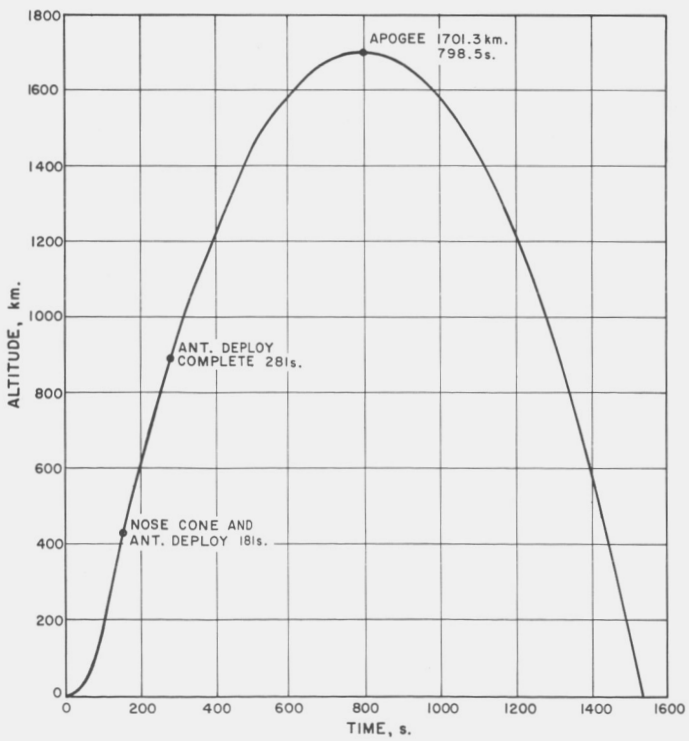

Figure 4. NASA 11.03 UR Trajectory.

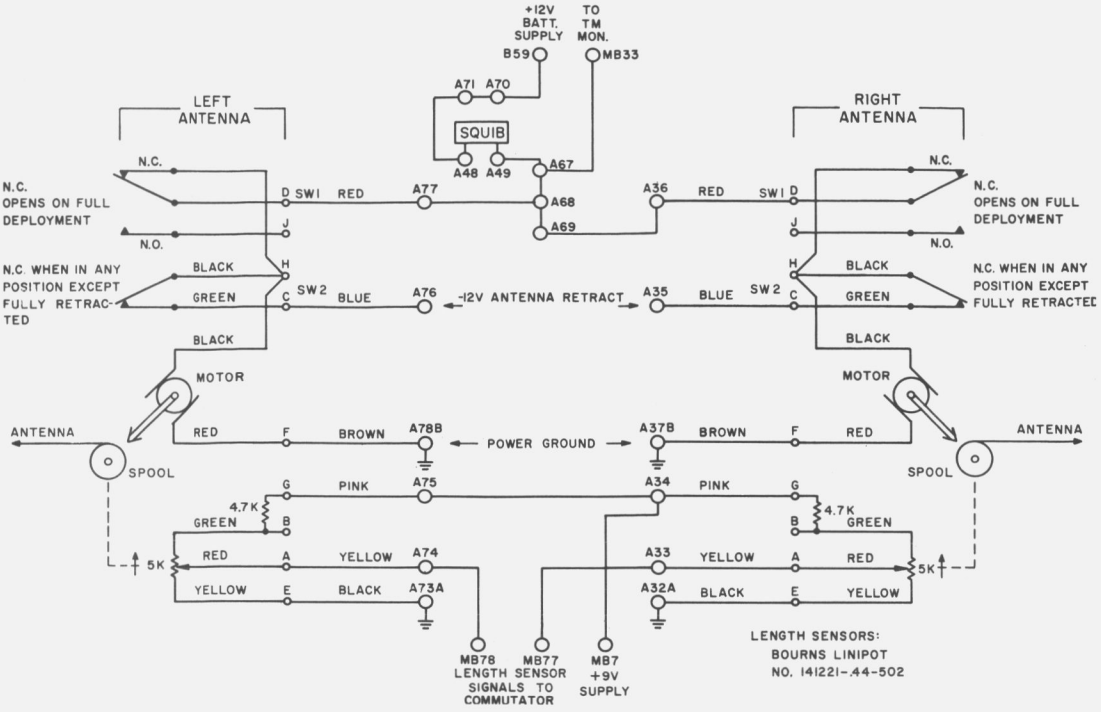

Figure 5. Antenna interconnect wiring.

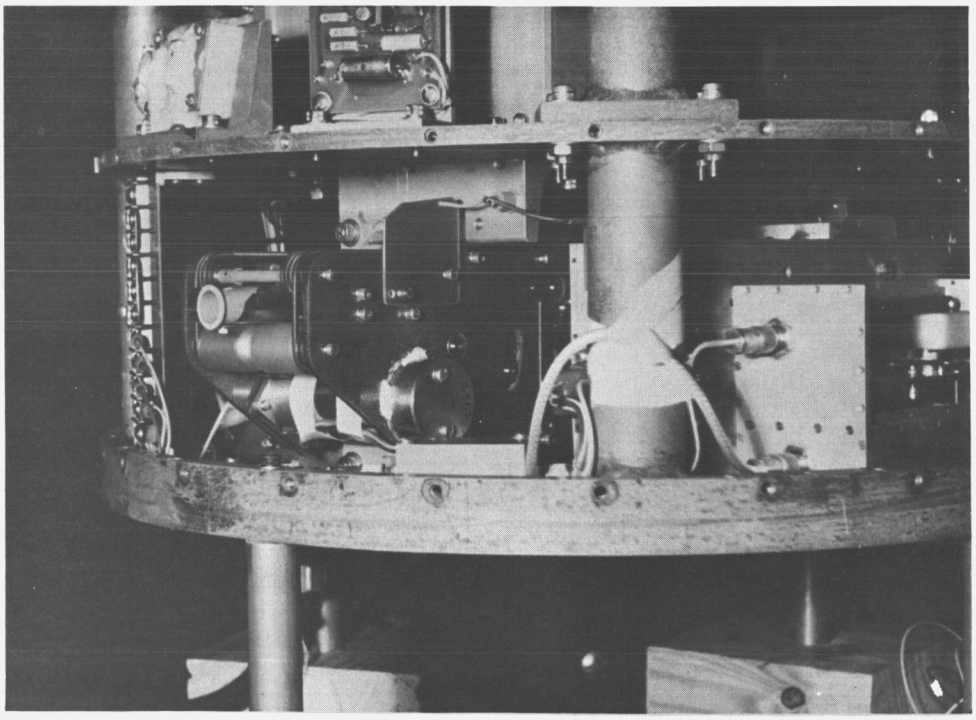

Figure 6. Left antenna deployment unit.

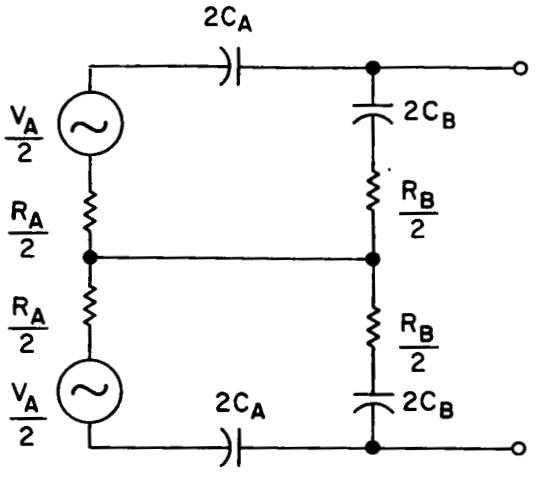

BALANCED DIPOLE ANTENNA
EQUIVALENT CIRCUIT

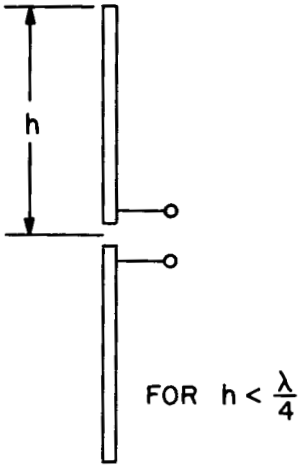

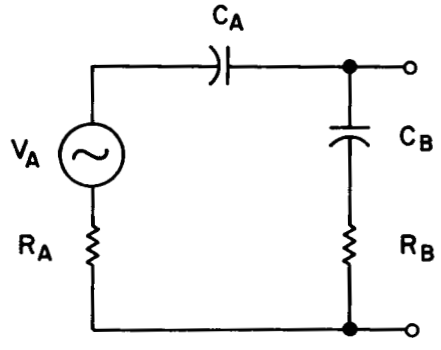

UNBALANCED EQUIVALENT DIPOLE
ANTENNA CIRCUIT

C_A = ANTENNA CAPACITANCE
R_A = RADIATION RESISTANCE
C_B = EQUIVALENT STRAY CAPACITANCE
R_B = EQUIVALENT LOSS RESISTANCE
$V_A^2 = 4k\ T_A\ R_A\ \Delta f$

Figure 7. Equivalent circuit of radio astronomy antenna.

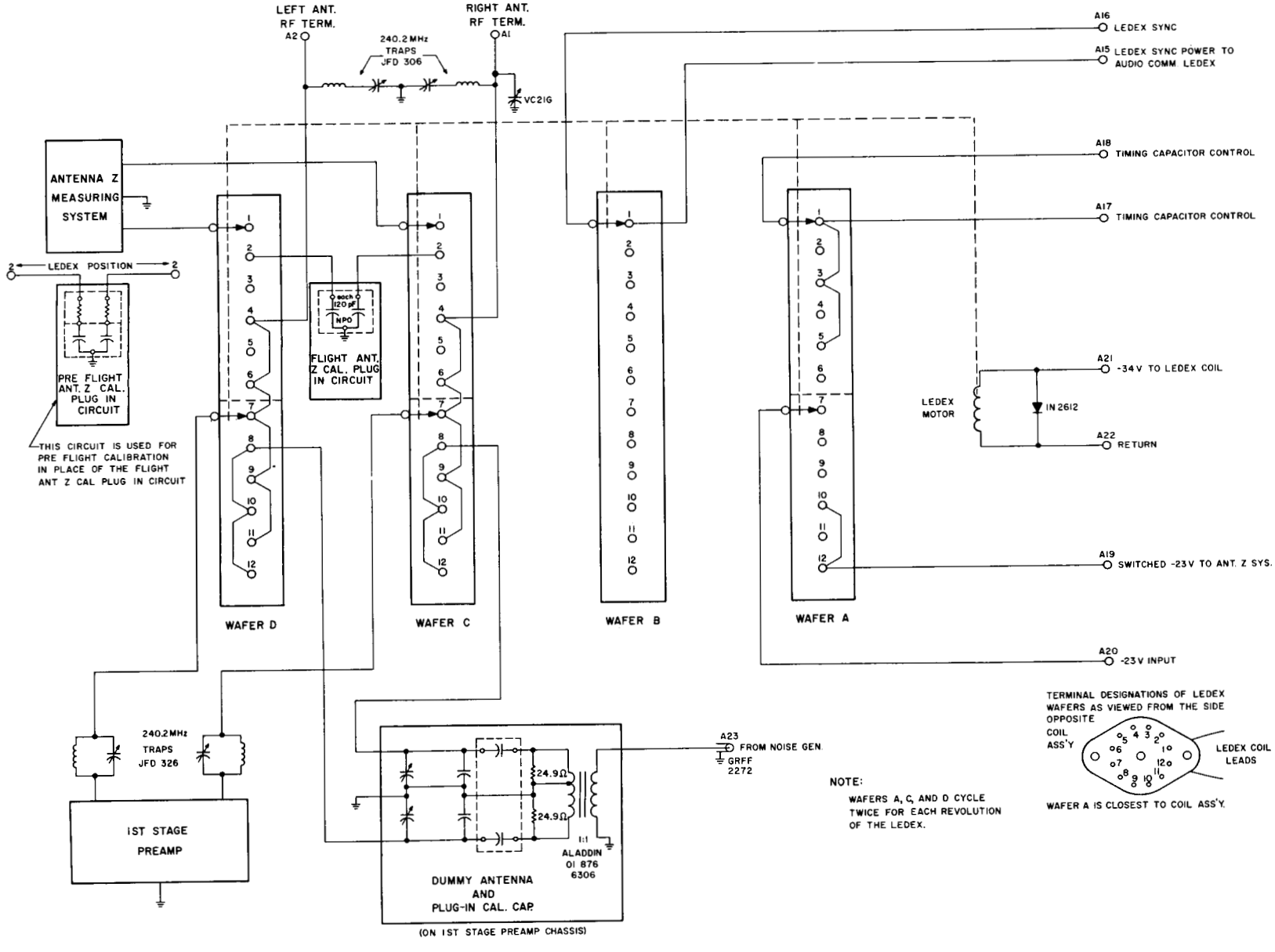

Figure 8. Antenna switching circuit.

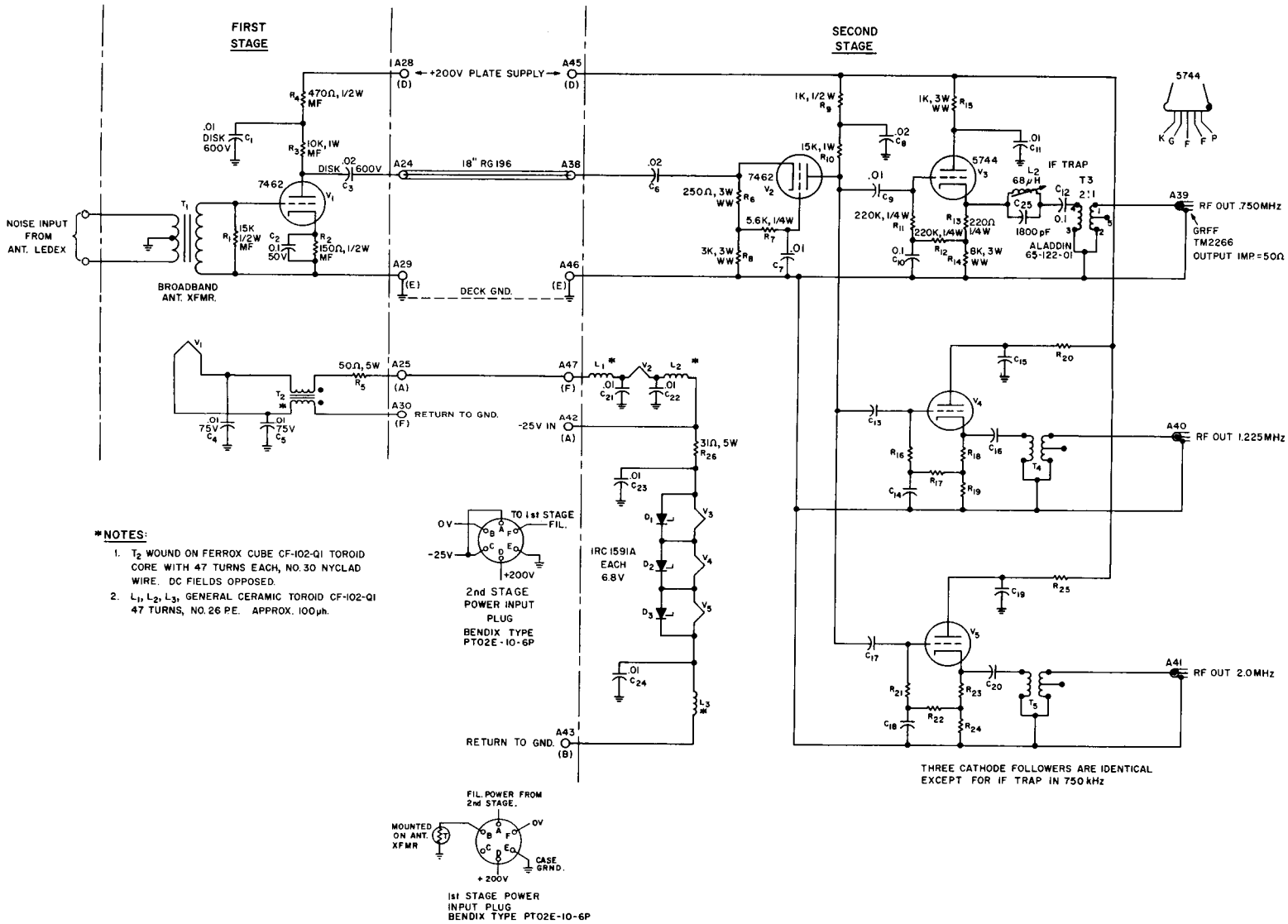

Figure 9. Radiometer preamplifier circuit.

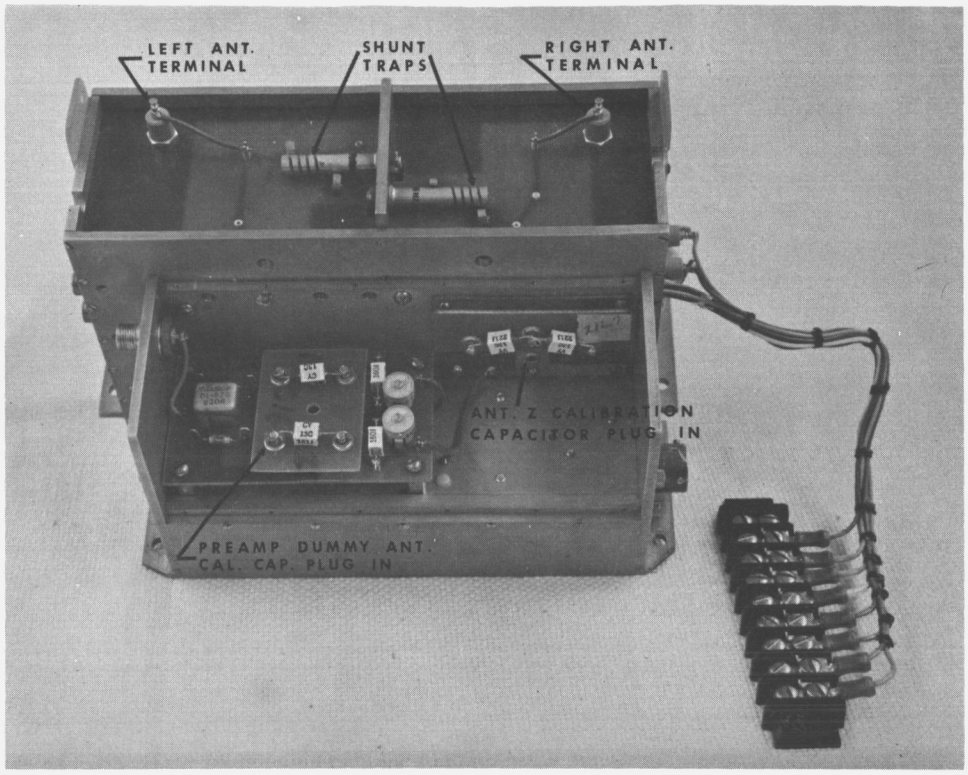

(a)

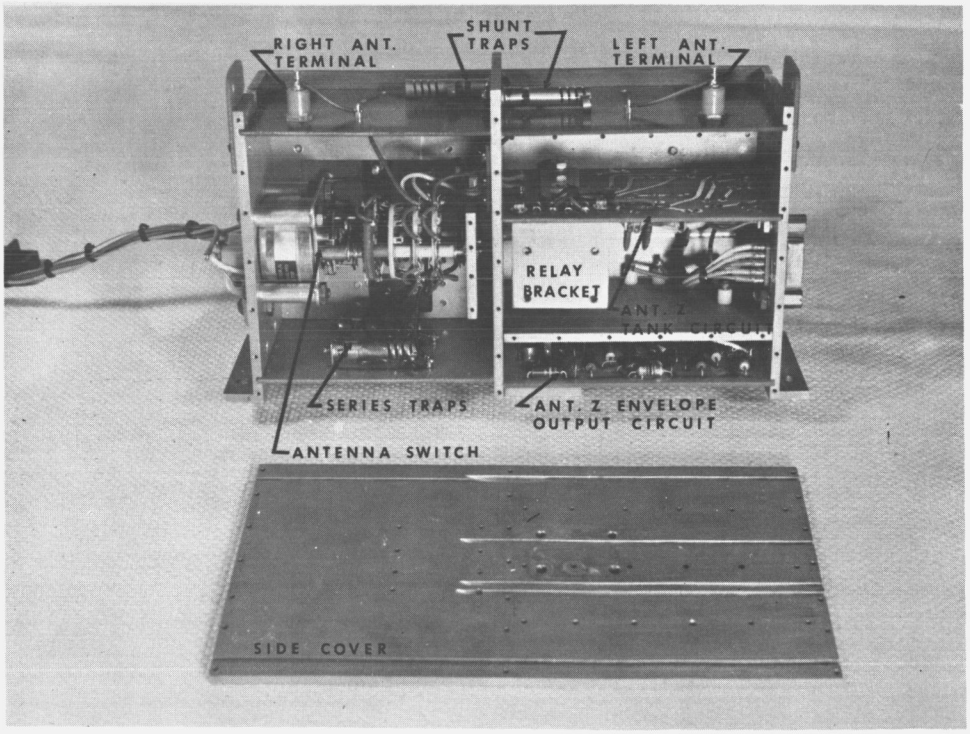

(b)

Figure 10. Preamplifier first stage.

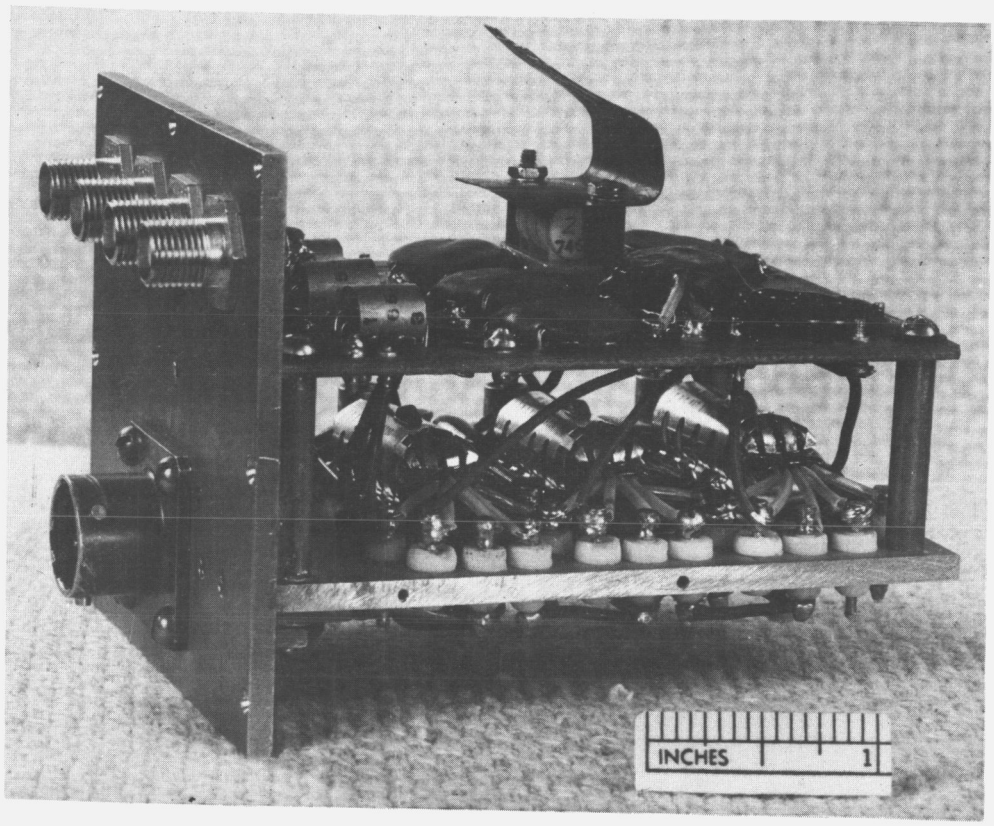

Figure 11. Preamplifier second stage.

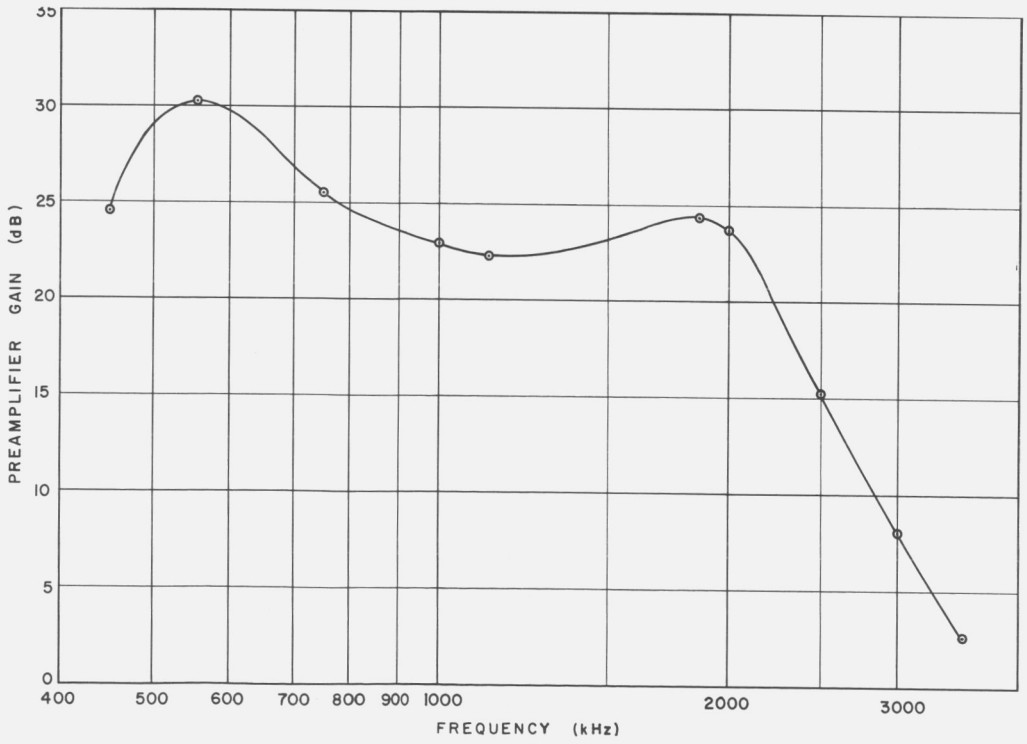

Figure 12. Prototype preamplifier gain vs. frequency (C_A = 51.3 pf).

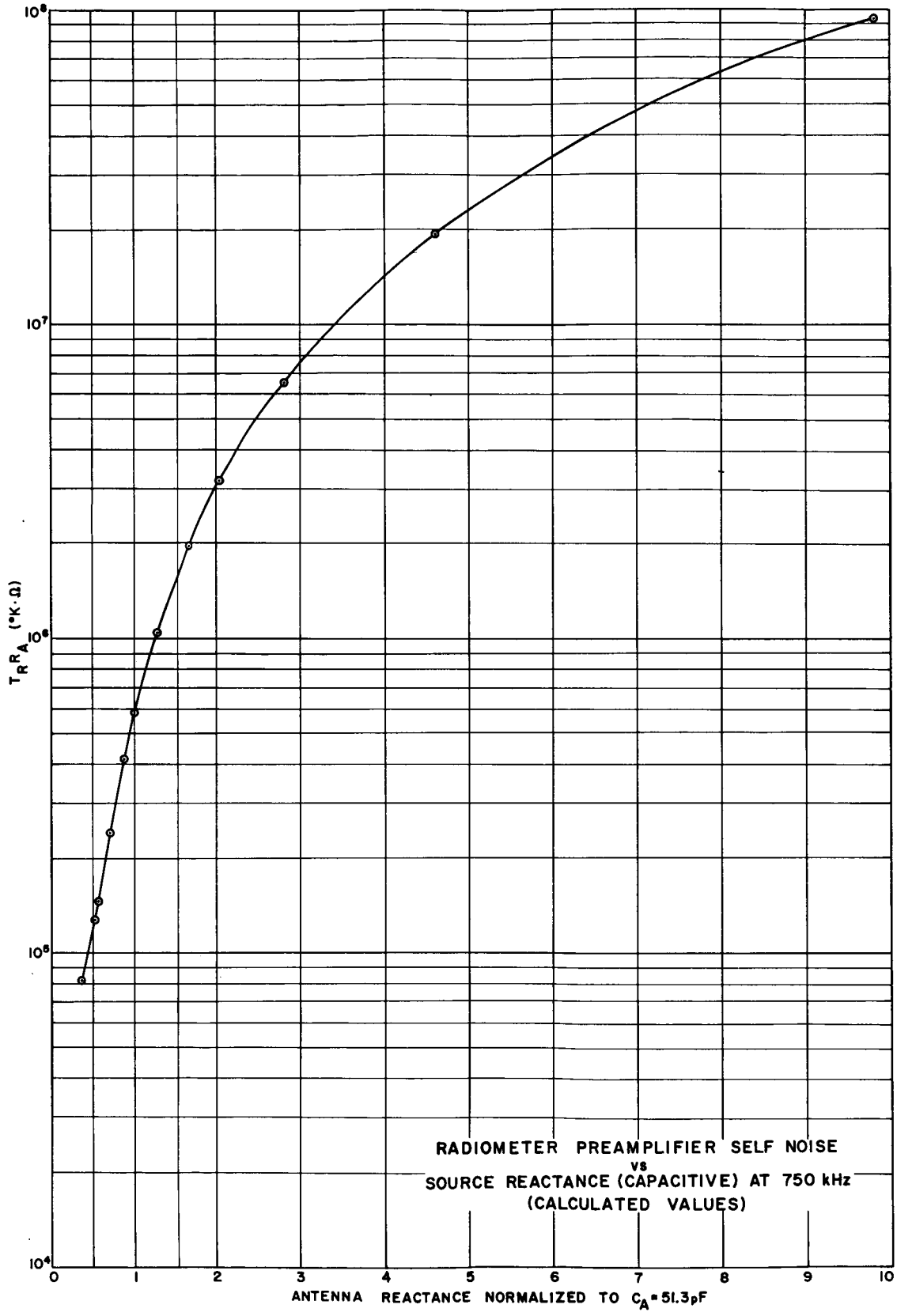

Figure 13. Radiometer preamplifier self noise vs. source reactance.

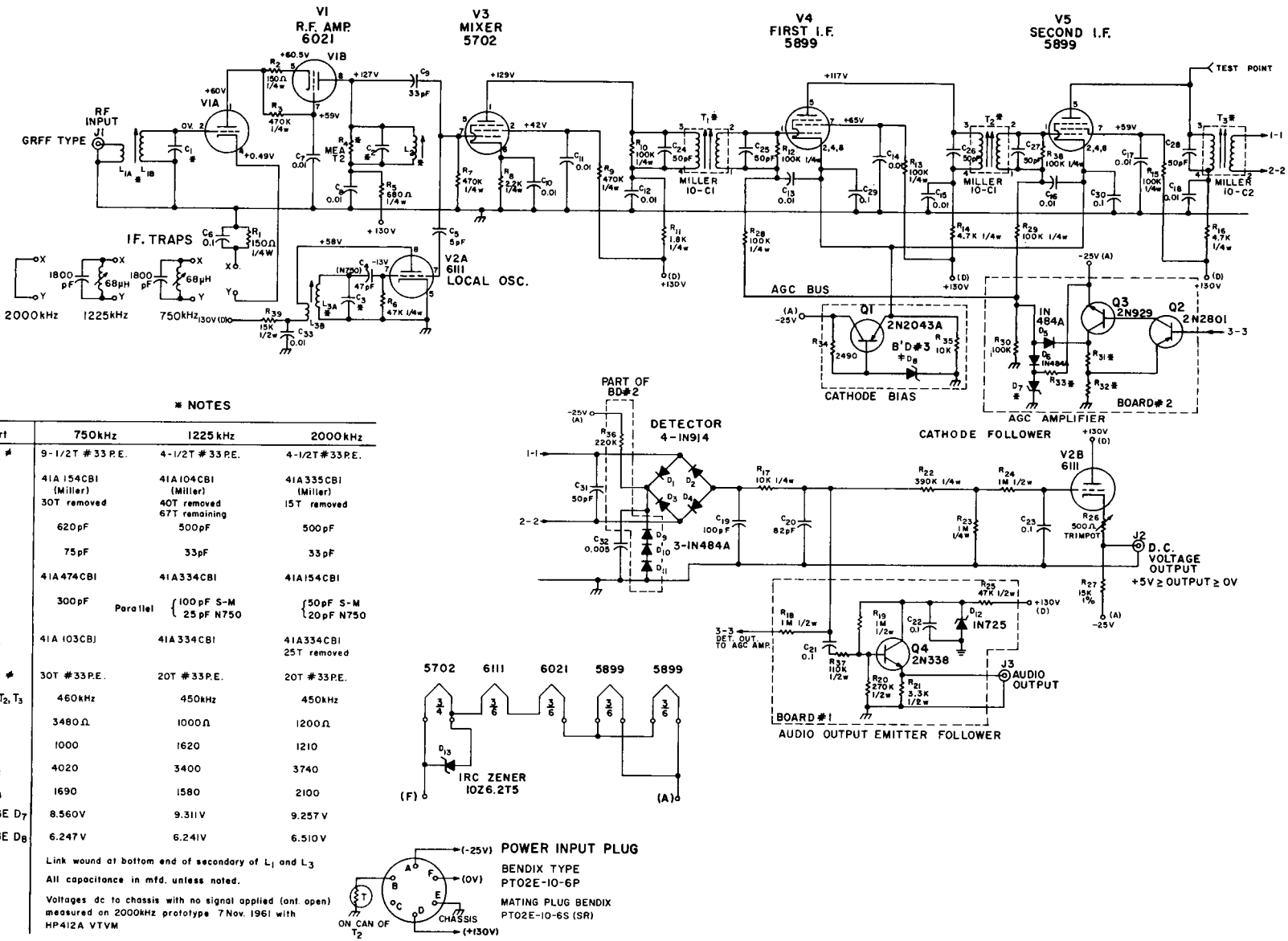

* NOTES

Part	750kHz	1225 kHz	2000kHz
L_{1A} ≠	9-1/2T #33 P.E.	4-1/2T #33 P.E.	4-1/2T #33 P.E.
L_{1B}	41A154CBI (Miller) 30T removed	41A104CBI (Miller) 40T removed 67T remaining	41A335CBI (Miller) 15T removed
C_1	620pF	500pF	500pF
C_2	75pF	33pF	33pF
L_2	41A474CBI	41A334CBI	41A154CBI
C_3	300pF Parallel {100pF S-M 25pF N750		{50pF S-M 20pF N750
L_{3A}	41A103CBI	41A334CBI	41A334CBI 25T removed
L_{3B} ≠	30T #33 P.E.	20T #33 P.E.	20T #33 P.E.
T_1, T_2, T_3	460kHz	450kHz	450kHz
R_4	3480Ω	1000Ω	1200Ω
R_{31}	1000	1620	1210
R_{32}	4020	3400	3740
R_{33}	1690	1580	2100
VOLTAGE D_7	8.560V	9.311V	9.257V
VOLTAGE D_8	6.247V	6.241V	6.510V

≠ Link wound at bottom end of secondary of L_1 and L_3

All capacitance in mfd. unless noted.

Voltages dc to chassis with no signal applied (ant. open) measured on 2000kHz prototype 7 Nov. 1961 with HP412A VTVM

Figure 14. Receiver circuit.

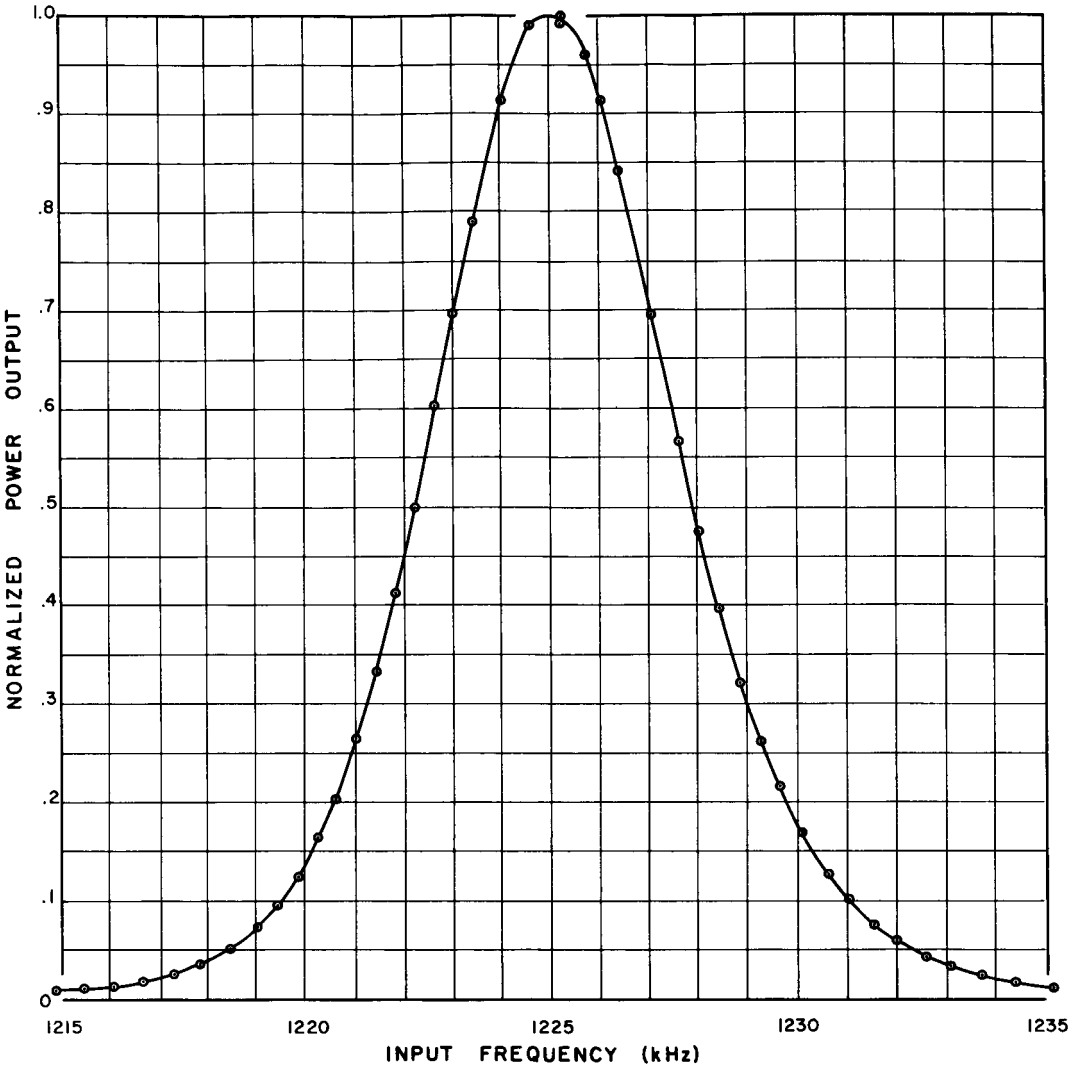

Figure 15. 1225 kHz receiver power bandwidth.

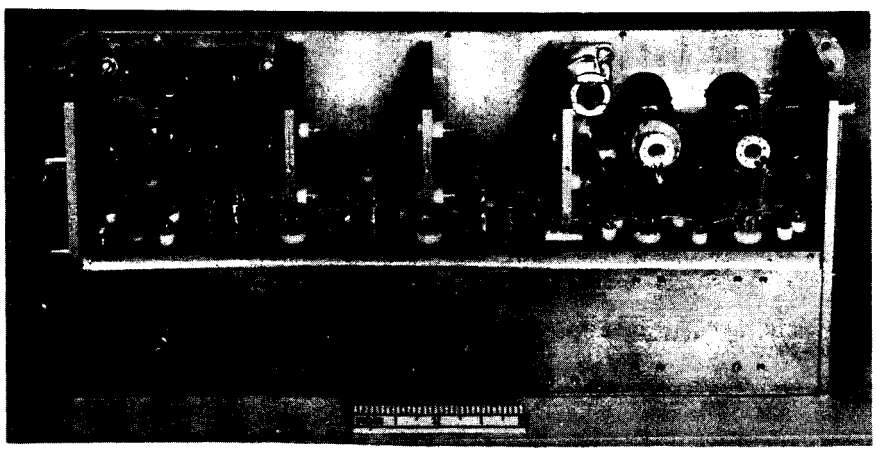

Figure 16. Receiver construction.

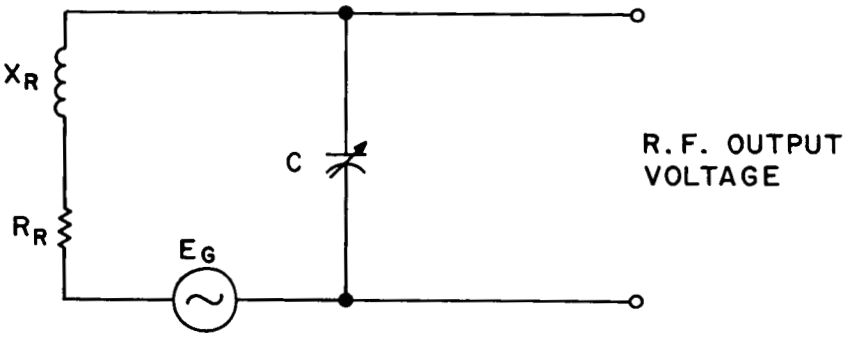

(a) SIMPLIFIED SERIES RESONANT CIRCUIT

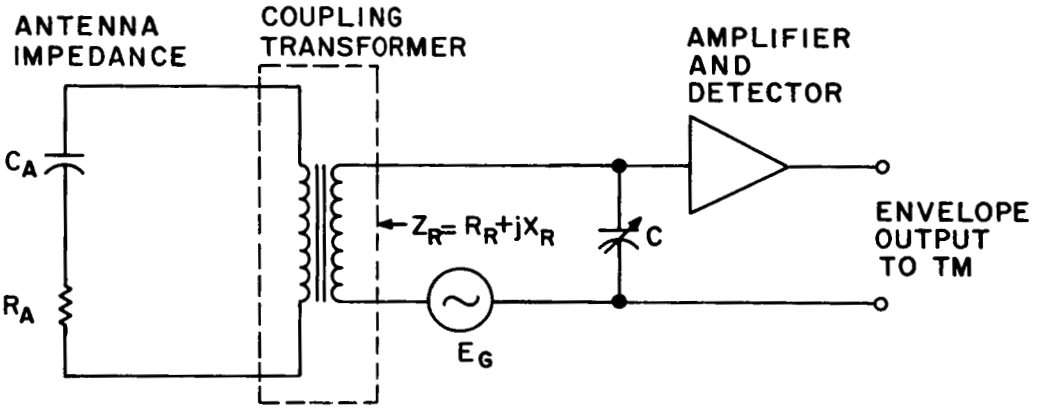

(b) SIMPLIFIED SCHEMATIC DIAGRAM OF THE ANTENNA IMPEDANCE MEASURING CIRCUIT

Figure 17. Simplified antenna impedance measurement circuit.

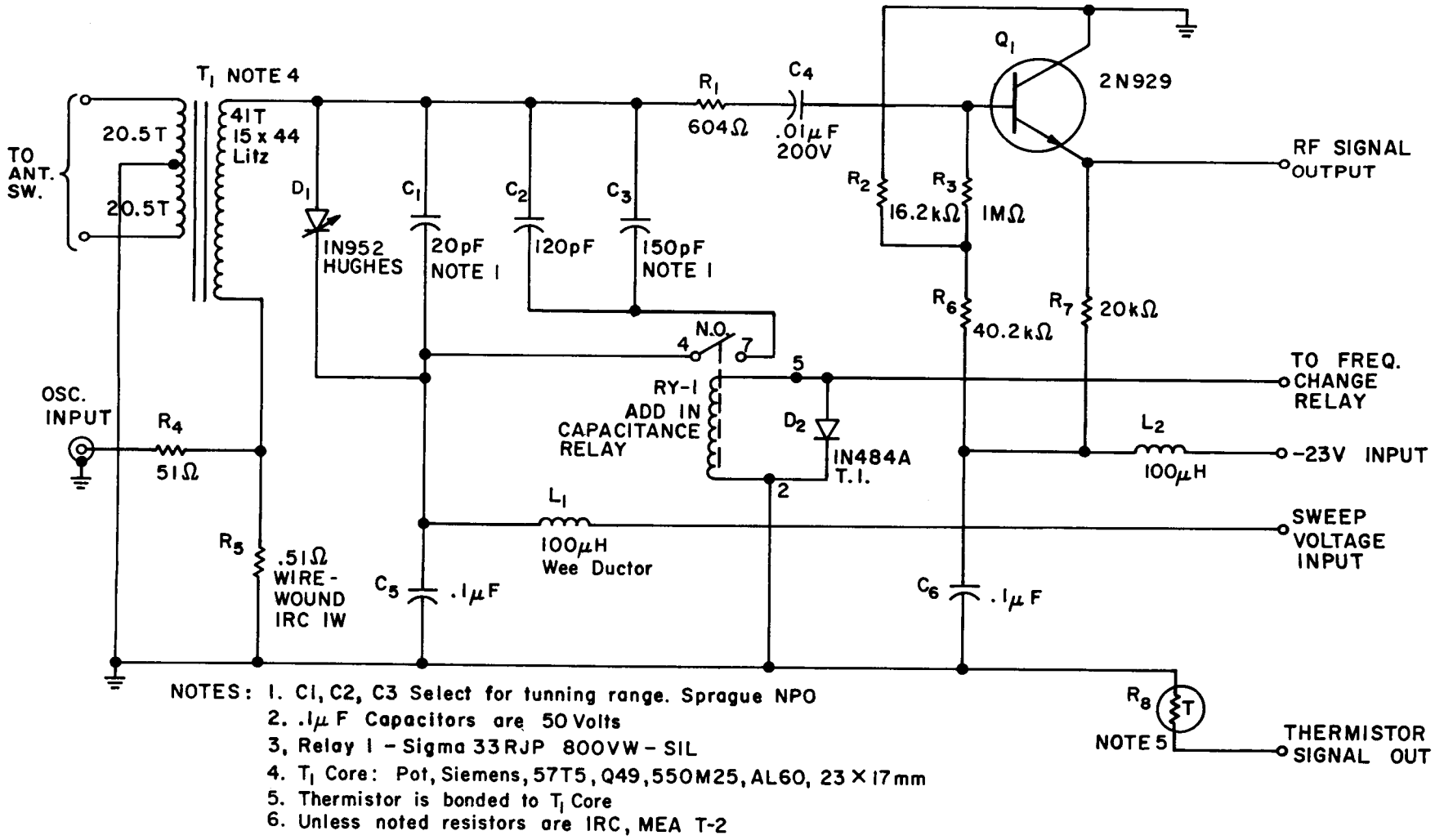

NOTES:
1. C1, C2, C3 Select for tunning range. Sprague NPO
2. .1μF Capacitors are 50 Volts
3. Relay 1 - Sigma 33RJP 800VW - SIL
4. T_1 Core: Pot, Siemens, 57T5, Q49, 550M25, AL60, 23 X 17mm
5. Thermistor is bonded to T_1 Core
6. Unless noted resistors are IRC, MEA T-2

Figure 18. Antenna impedance tank board circuit.

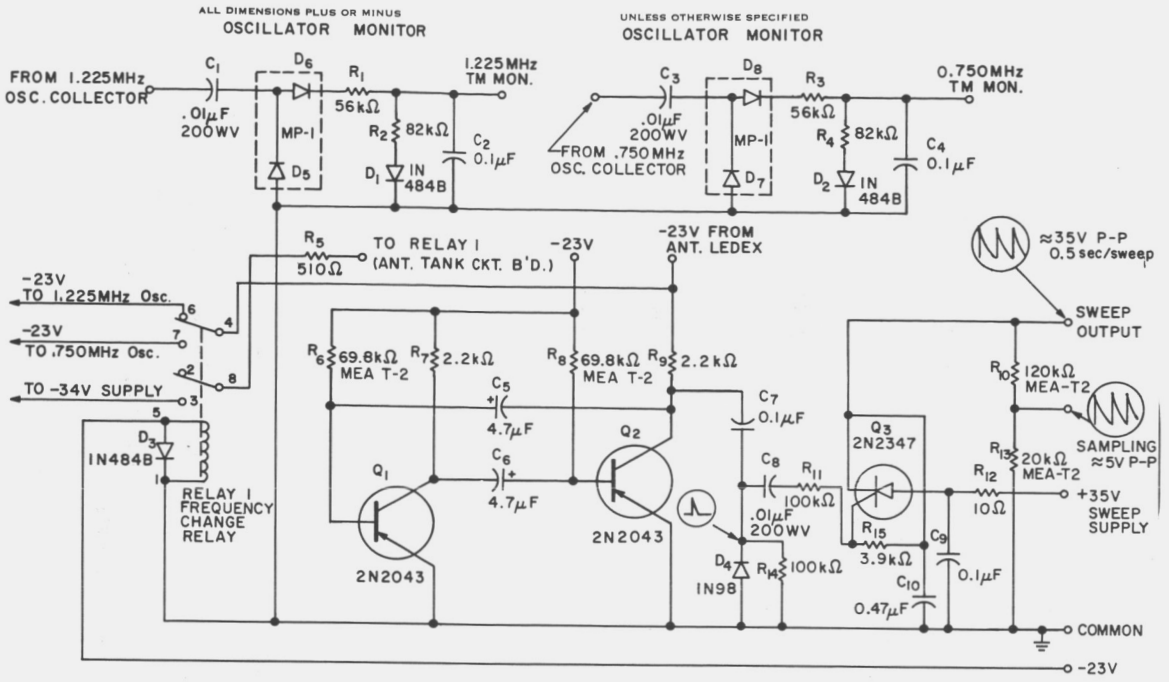

NOTES: 1. ALL RESISTORS 1/2W, MOLDED CARBON UNLESS OTHERWISE INDICATED.

2. ALL CAPACITORS 50WV, UNLESS NOTED.

Figure 19. Sweep generator board.

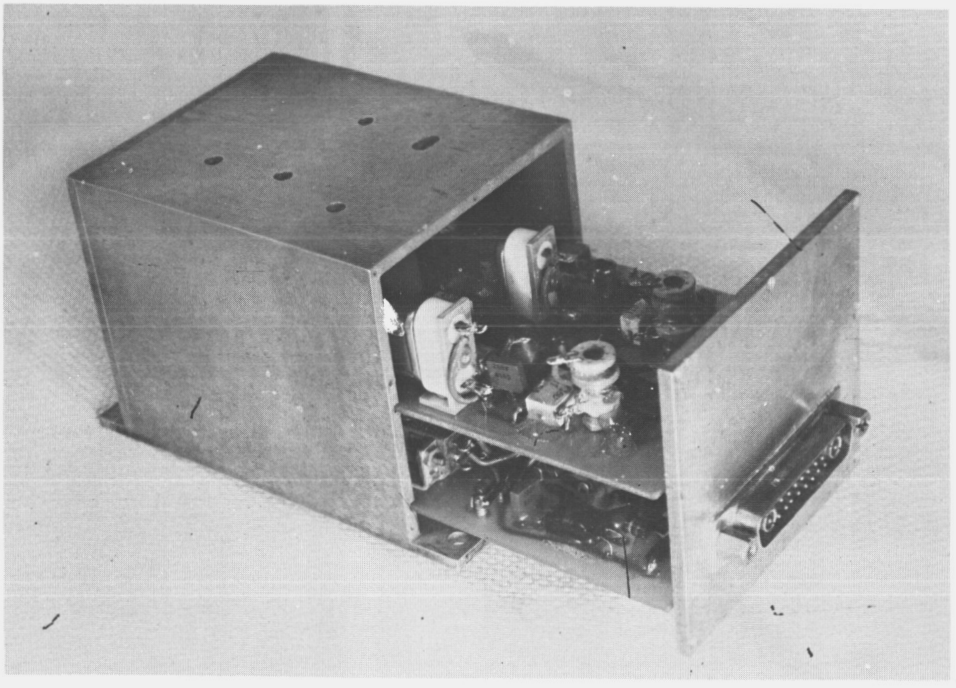

Figure 20. Sweep generator housing.

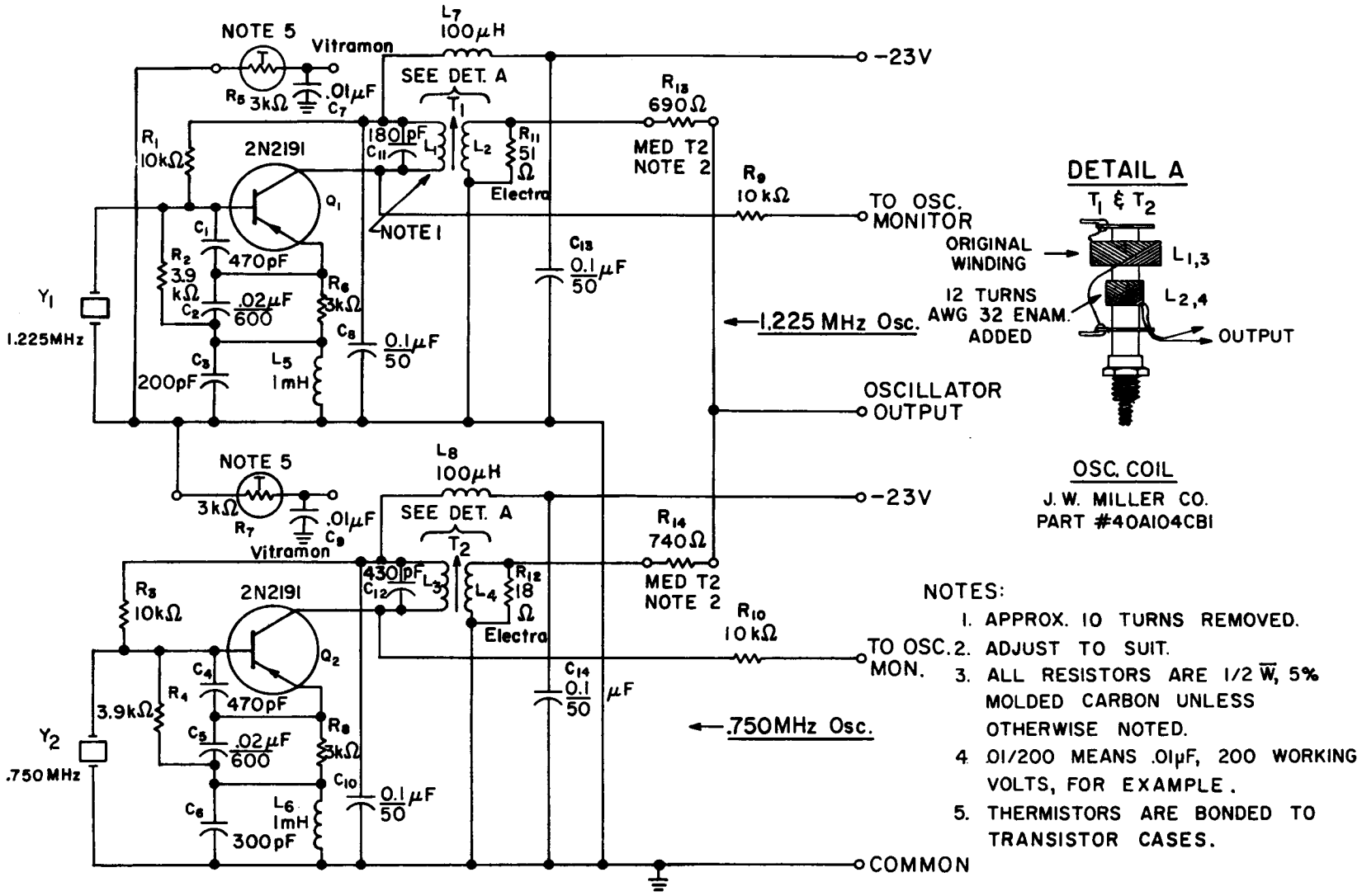

Figure 21. Oscillator board.

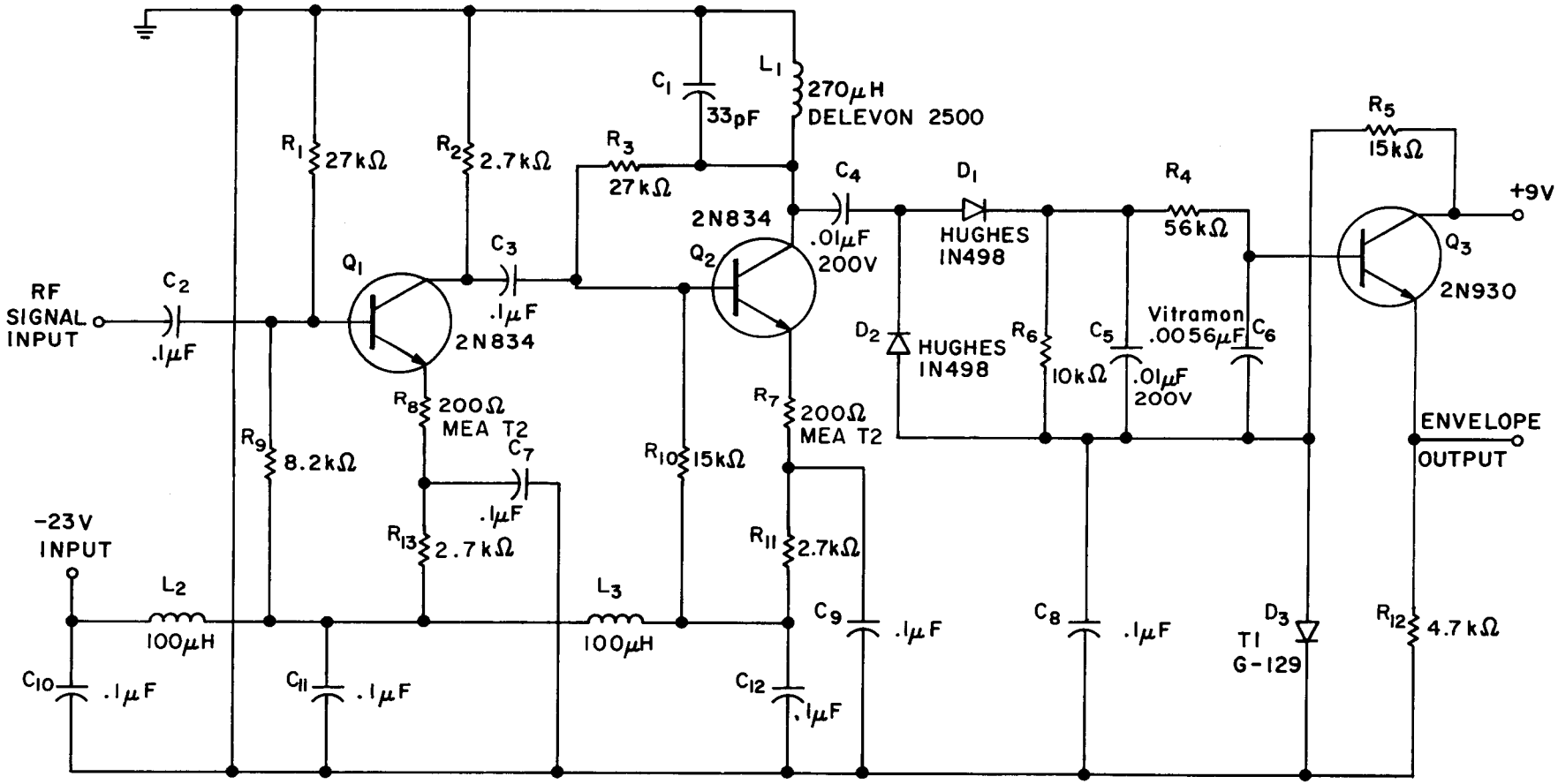

NOTES: 1. Unless noted capacitors to have 50V rating
2. .1 F capacitors are Aerovox manuf. type CR89W104AM
3. L2, and L3 Nytronics choke (Wee-Wee ductors)

Figure 22. Antenna impedance amplifier.

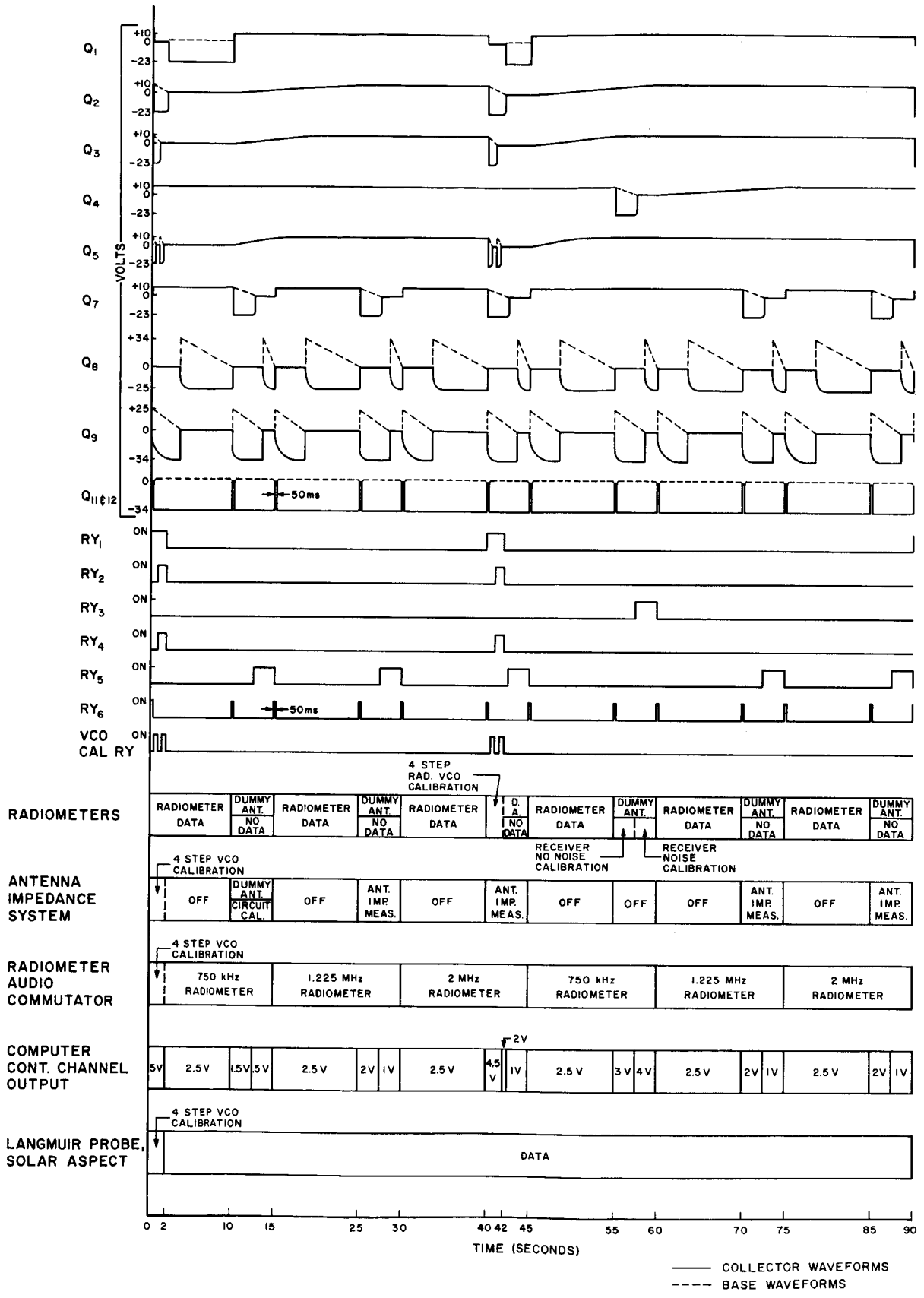

Figure 23. Timing circuit waveforms.

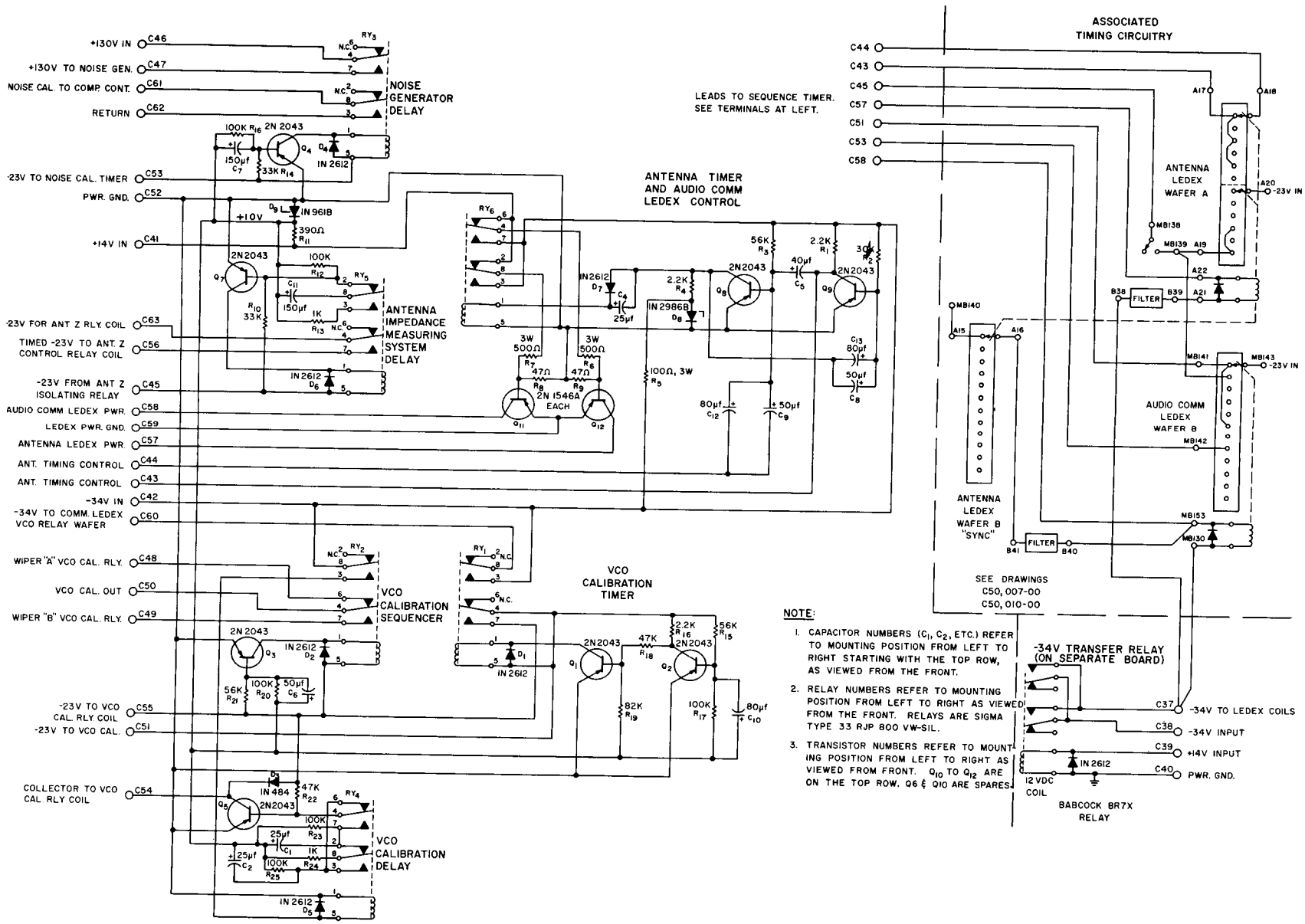

Figure 24. Rocket sequence timer.

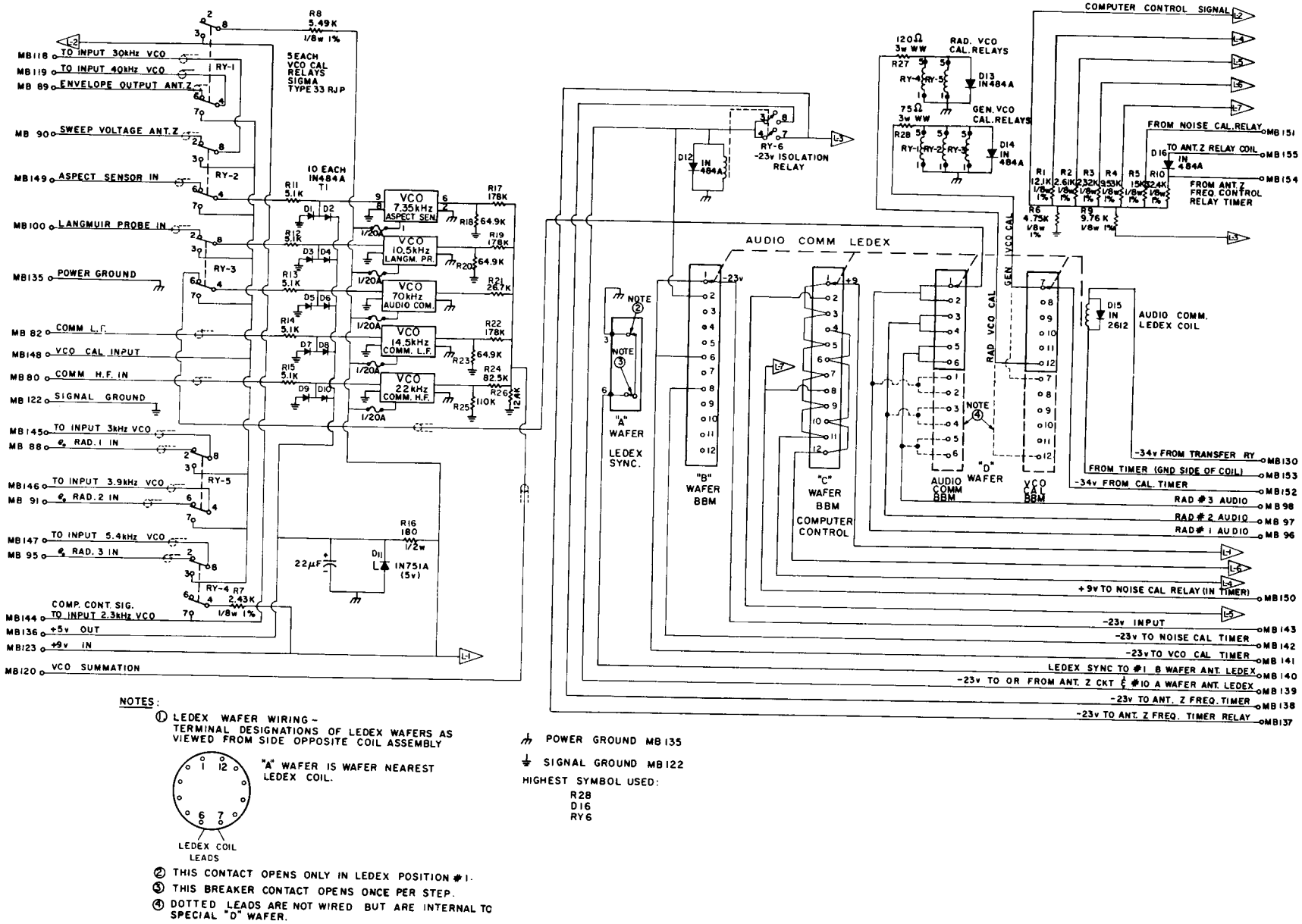

NOTES:

① LEDEX WAFER WIRING - TERMINAL DESIGNATIONS OF LEDEX WAFERS AS VIEWED FROM SIDE OPPOSITE COIL ASSEMBLY

"A" WAFER IS WAFER NEAREST LEDEX COIL.

② THIS CONTACT OPENS ONLY IN LEDEX POSITION #1.

③ THIS BREAKER CONTACT OPENS ONCE PER STEP.

④ DOTTED LEADS ARE NOT WIRED BUT ARE INTERNAL TO SPECIAL "D" WAFER.

⏚ POWER GROUND MB135

⏚ SIGNAL GROUND MB122

HIGHEST SYMBOL USED:
R28
D16
RY6

Figure 25. VCO chassis "C" Deck.

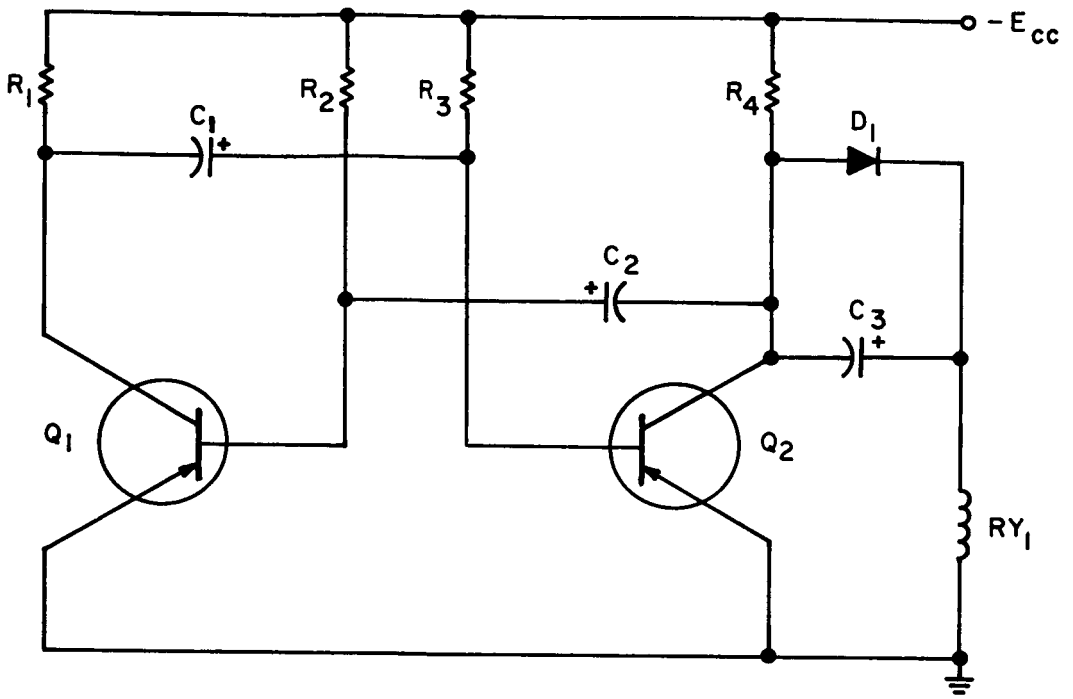

Figure 26. Basic antenna timer.

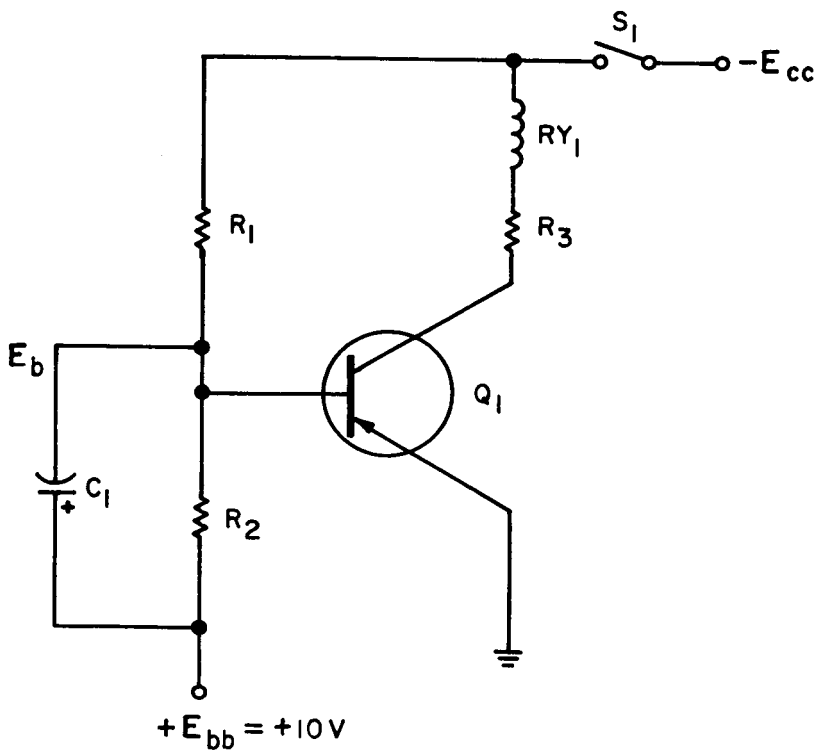

Figure 27. Basic delay on.

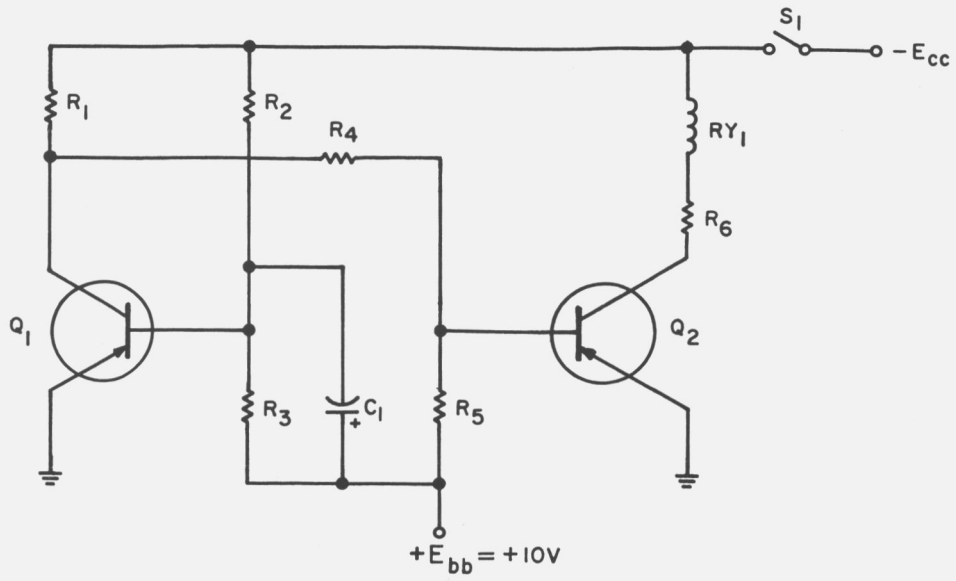

Figure 28. Basic delay off.

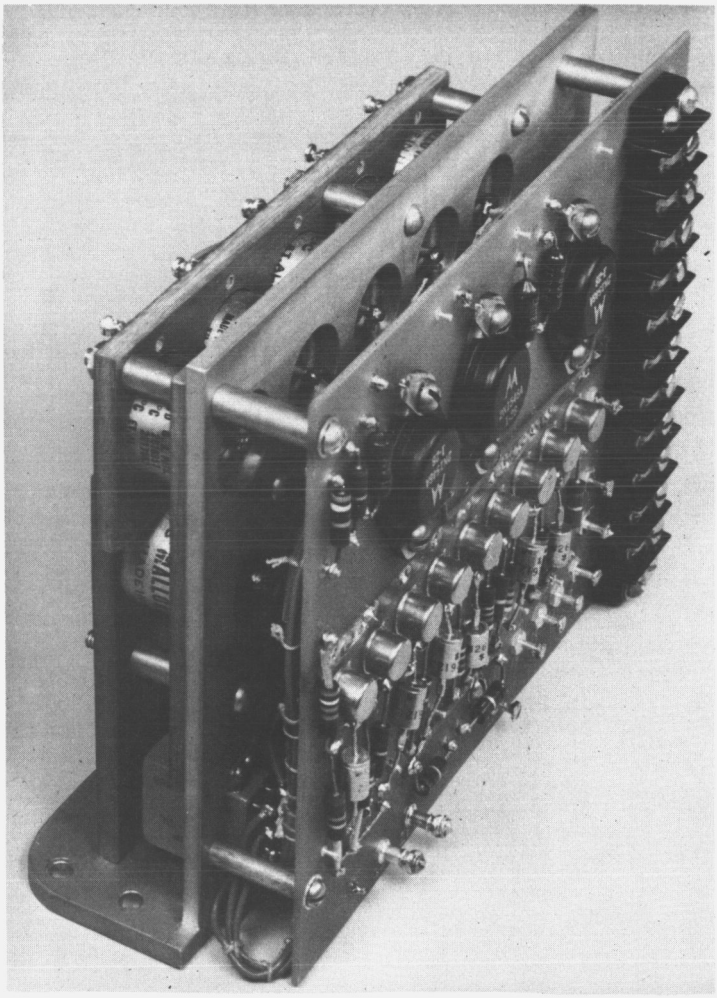

Figure 29. Timer subassembly.

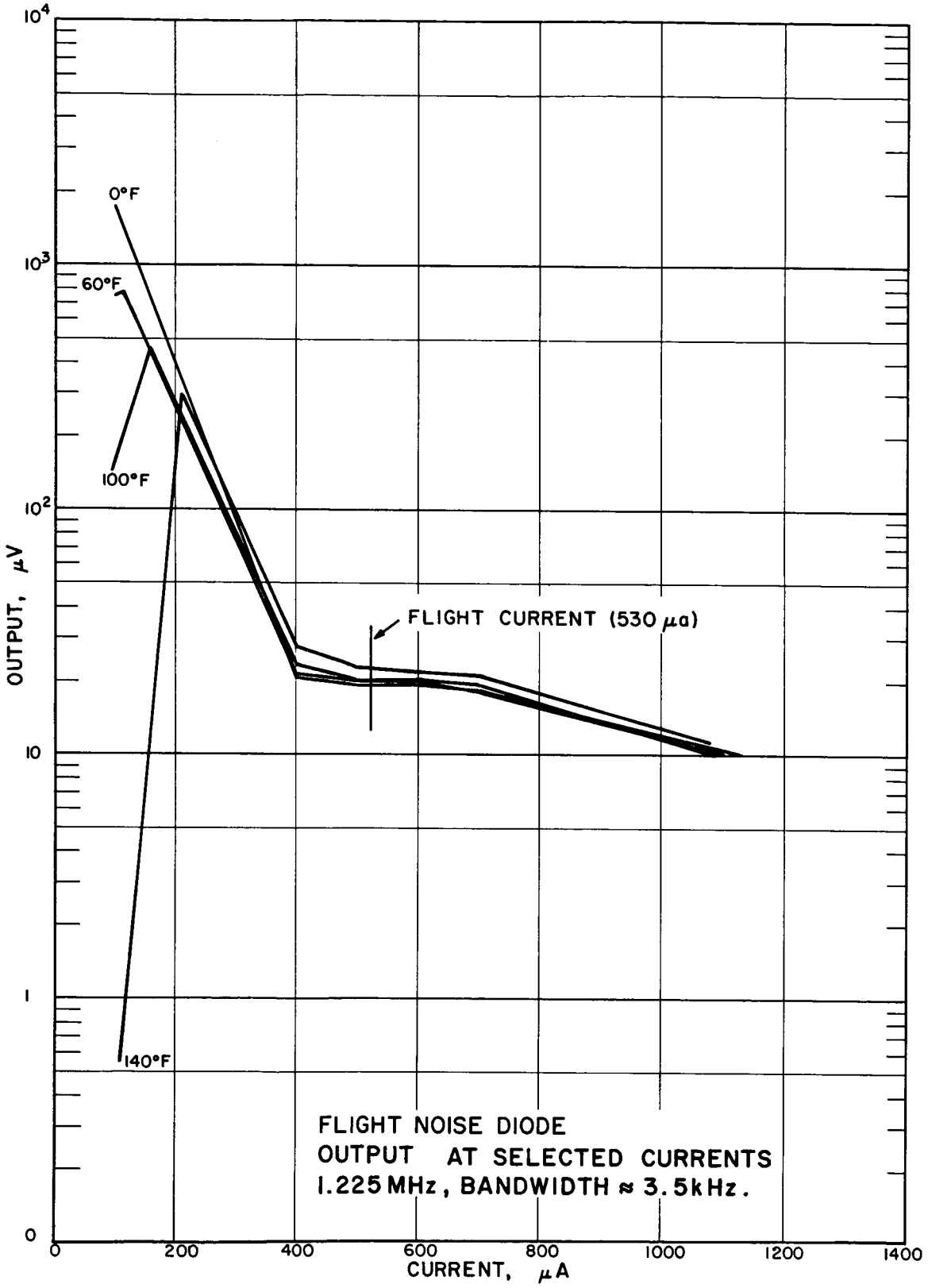
10^4
10^3
10^2
10
1
0
OUTPUT, μV
0°F
60°F
100°F
140°F
FLIGHT CURRENT (530 μa)
FLIGHT NOISE DIODE
OUTPUT AT SELECTED CURRENTS
1.225 MHz, BANDWIDTH ≈ 3.5 kHz.
0
200
400
600
800
1000
1200
1400
CURRENT, μA

Figure 30

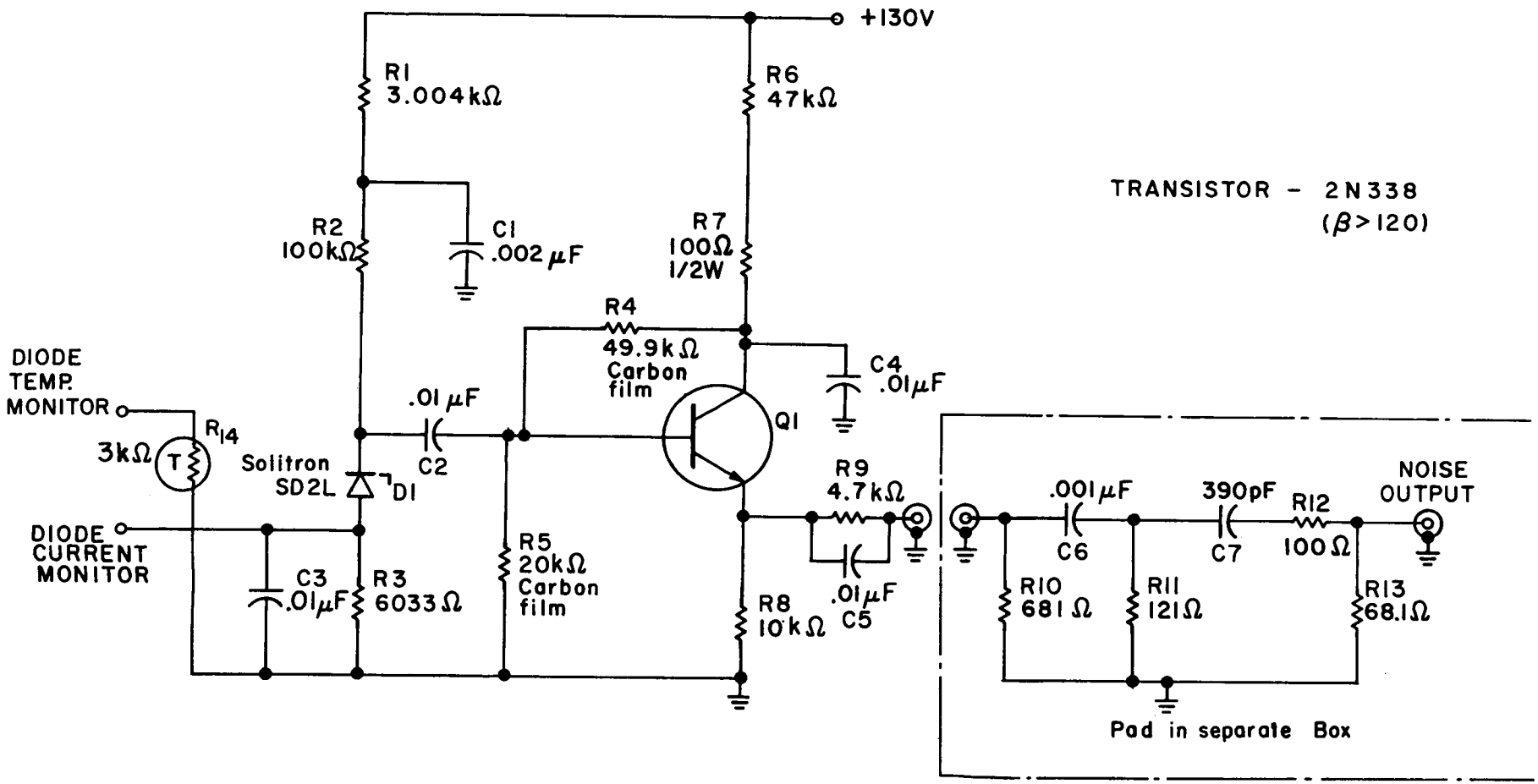

Figure 31. 11.03 noise generator circuit.

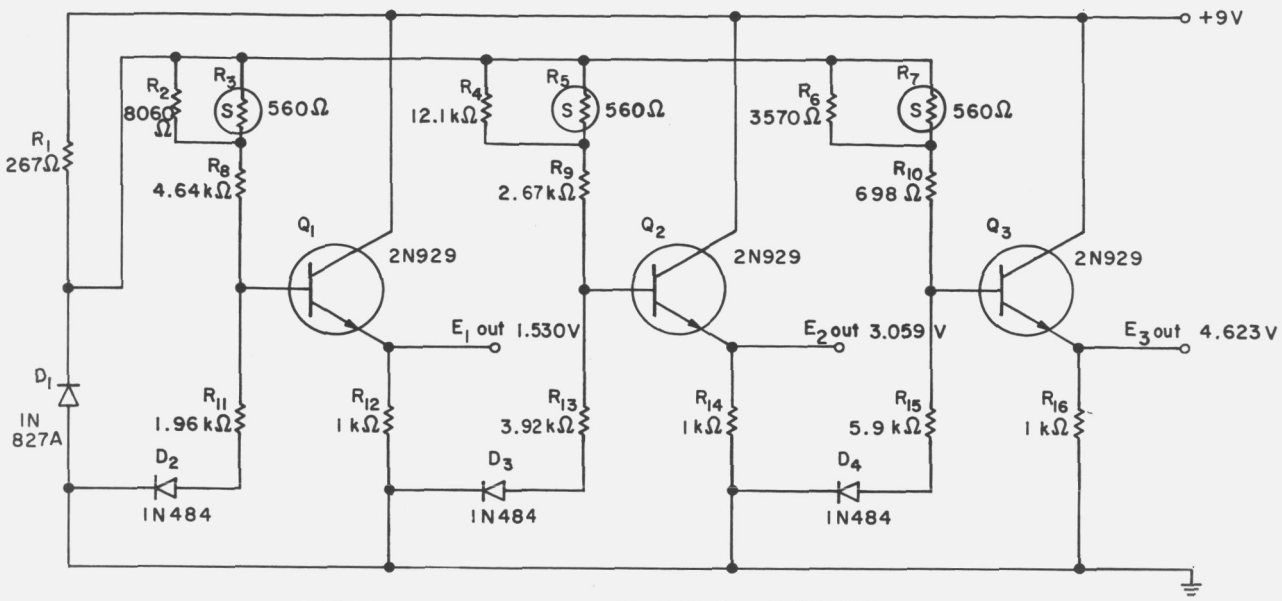

Figure 32. VCO calibrator.

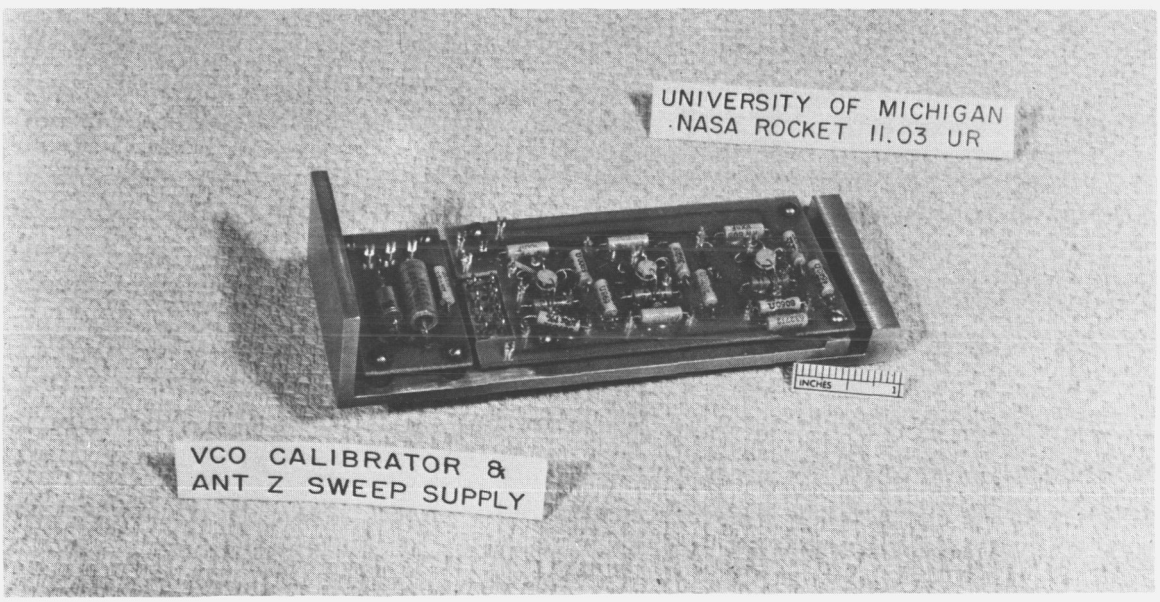

Figure 33. VCO calibrator and antenna Z sweep supply.

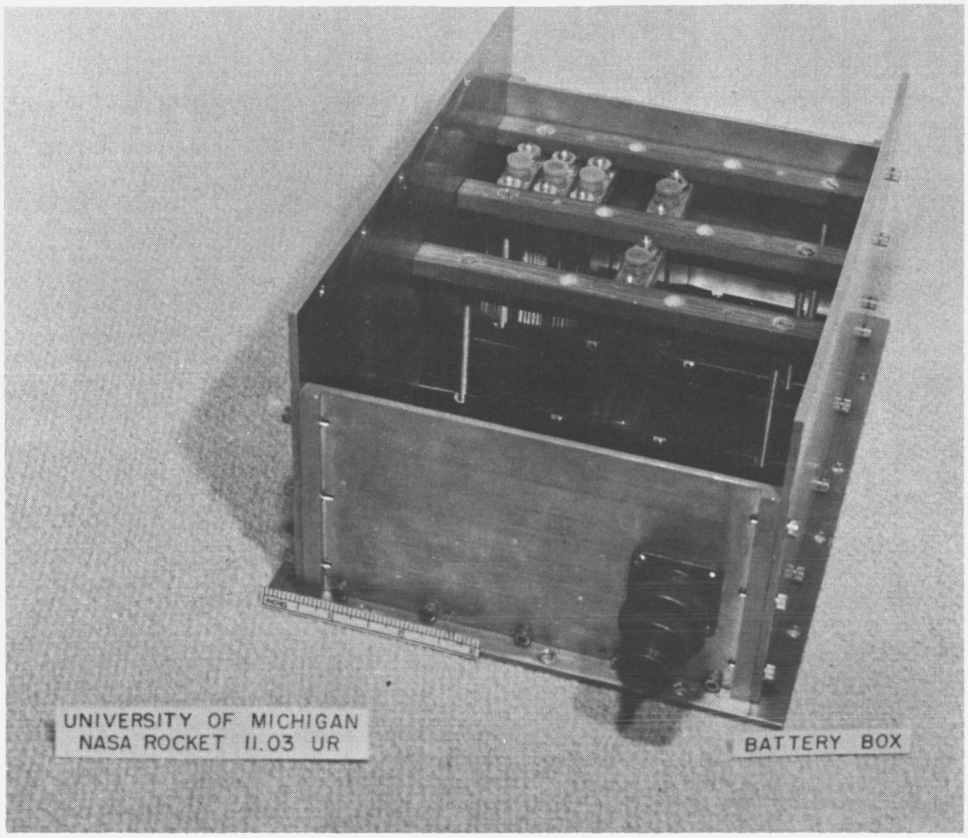

Figure 34. Battery box.

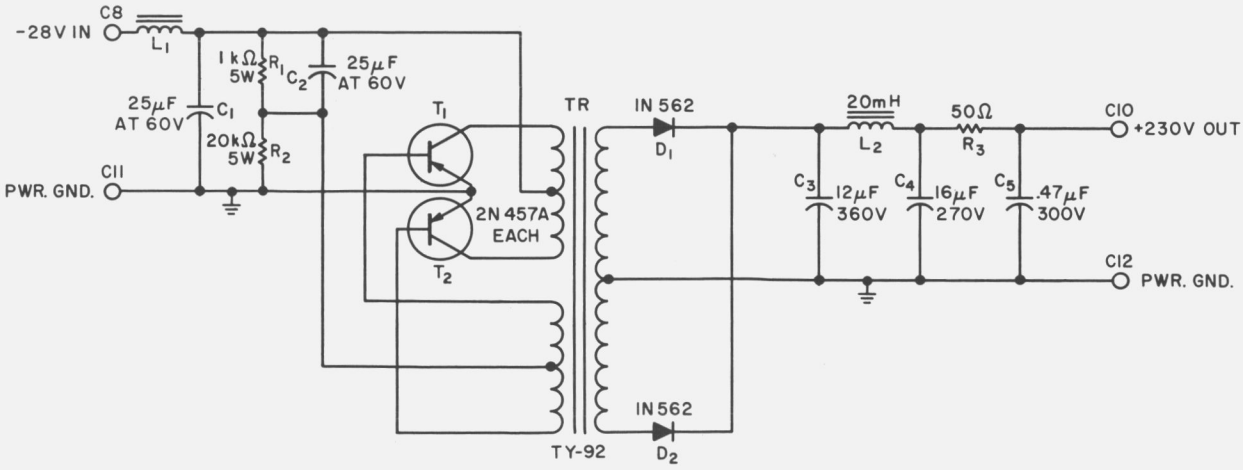

Figure 35. Receiver DC-to-DC converter.

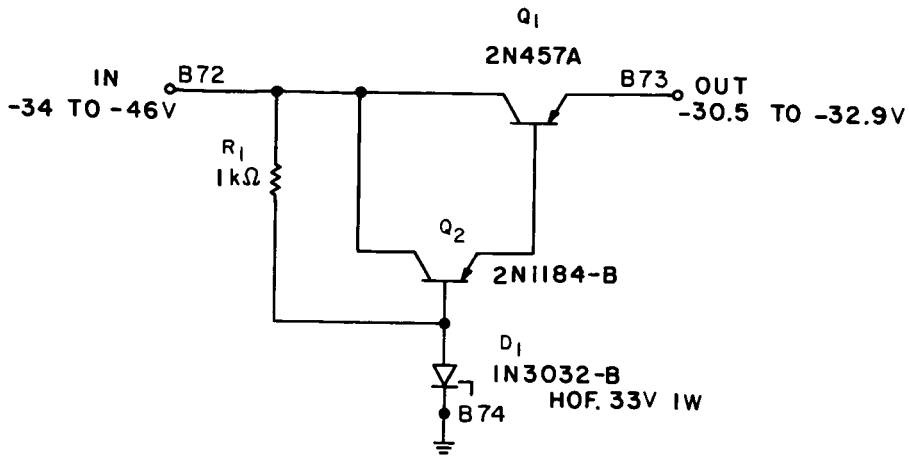

Figure 36. Filament preregulator.

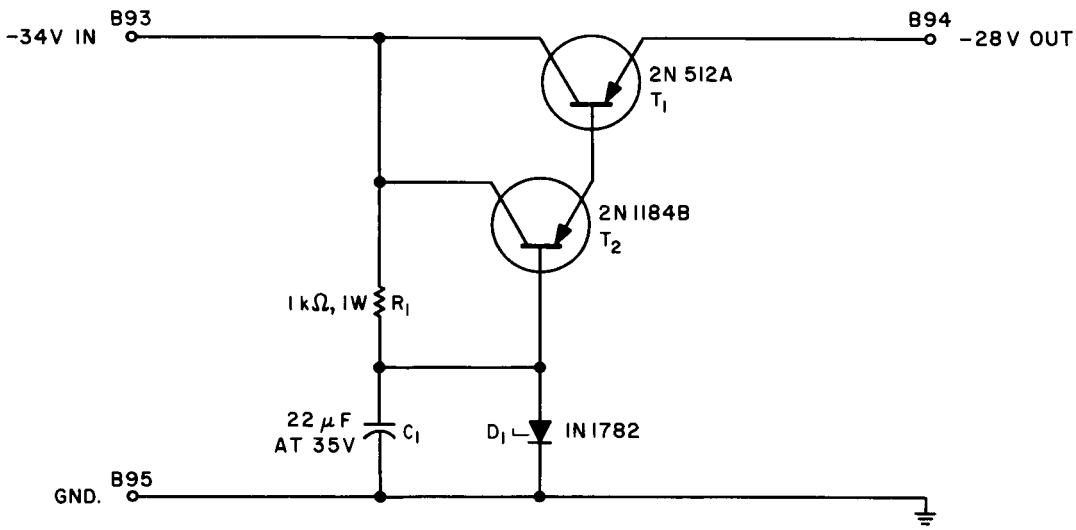

Figure 37. Receiver converter preregulator.

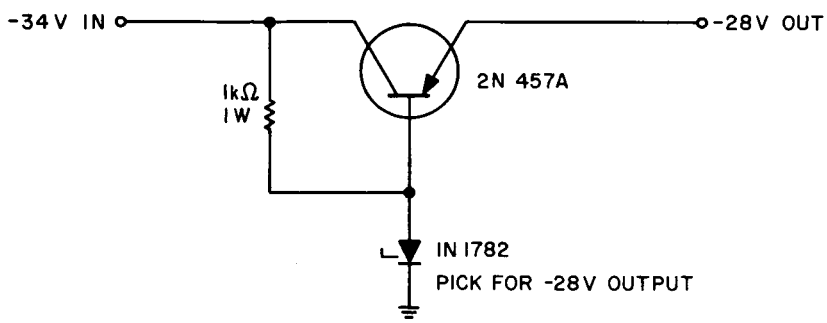

Figure 38. -28 volt regulator.

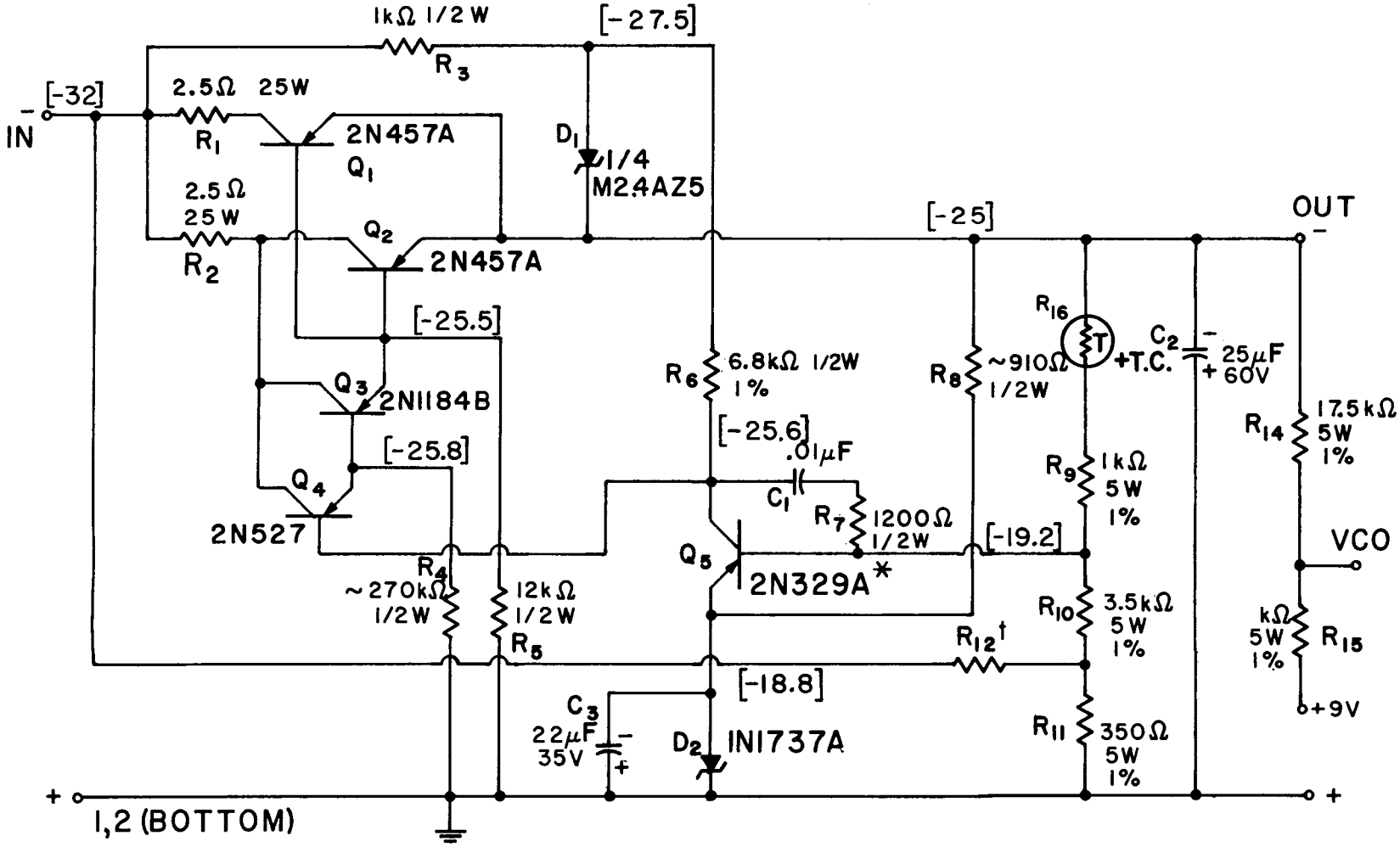

VOLTAGES AT 1 AMP. LOAD

*PICK β >70; I_{CO} LOW

† PICK TO REDUCE ΔV_{OUT} TO MIN. WHEN ΔV_{IN} CHANGED (SELECT ≈30-60kΩ 1/2W)

Figure 39. -25 volt regulator.

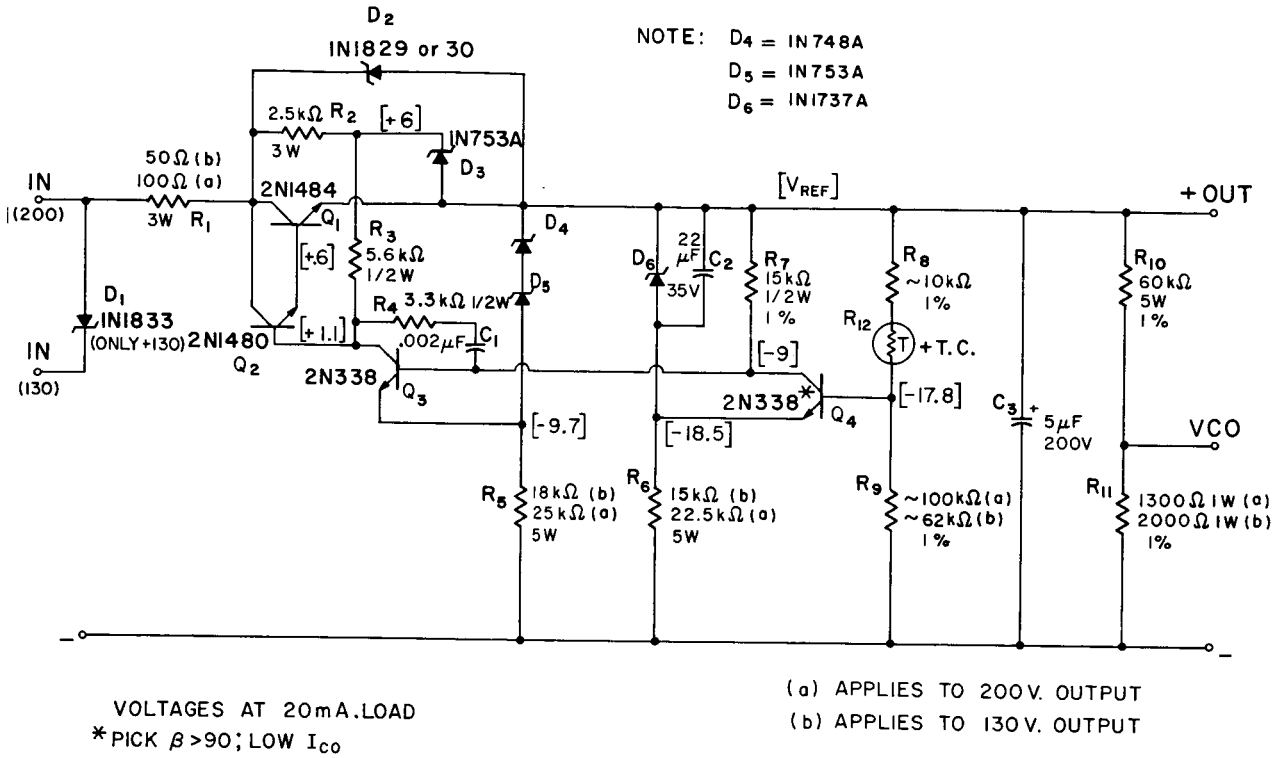

Figure 40. B+ regulators.

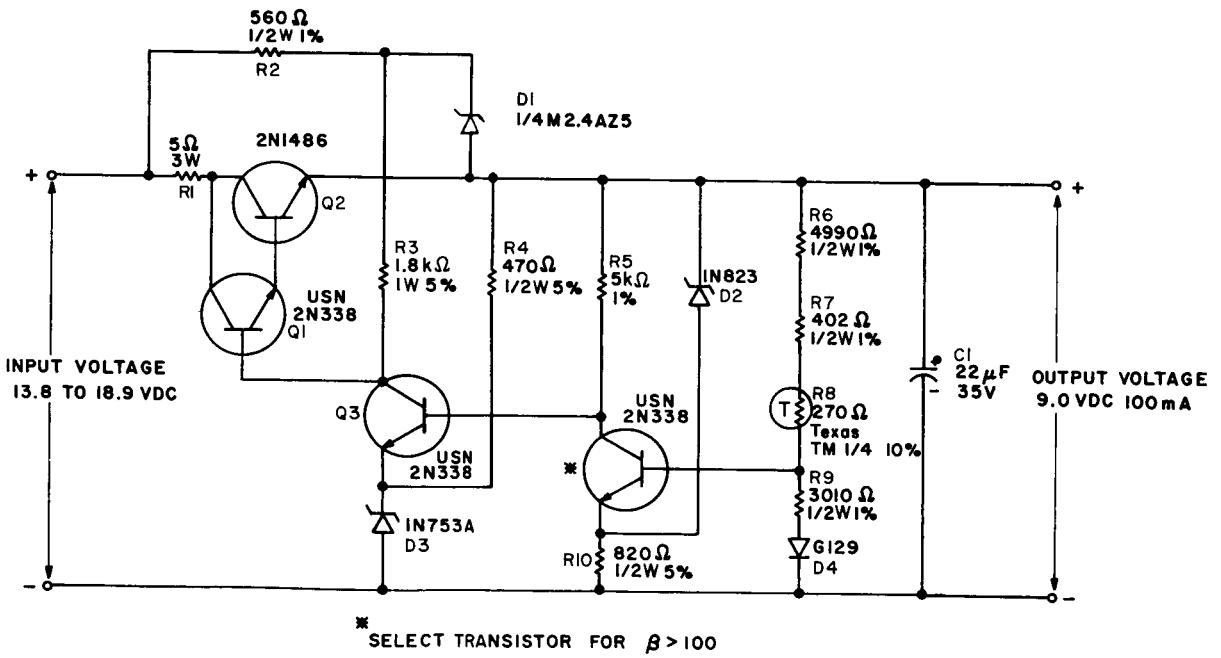

Figure 41. 9 volt regulator.

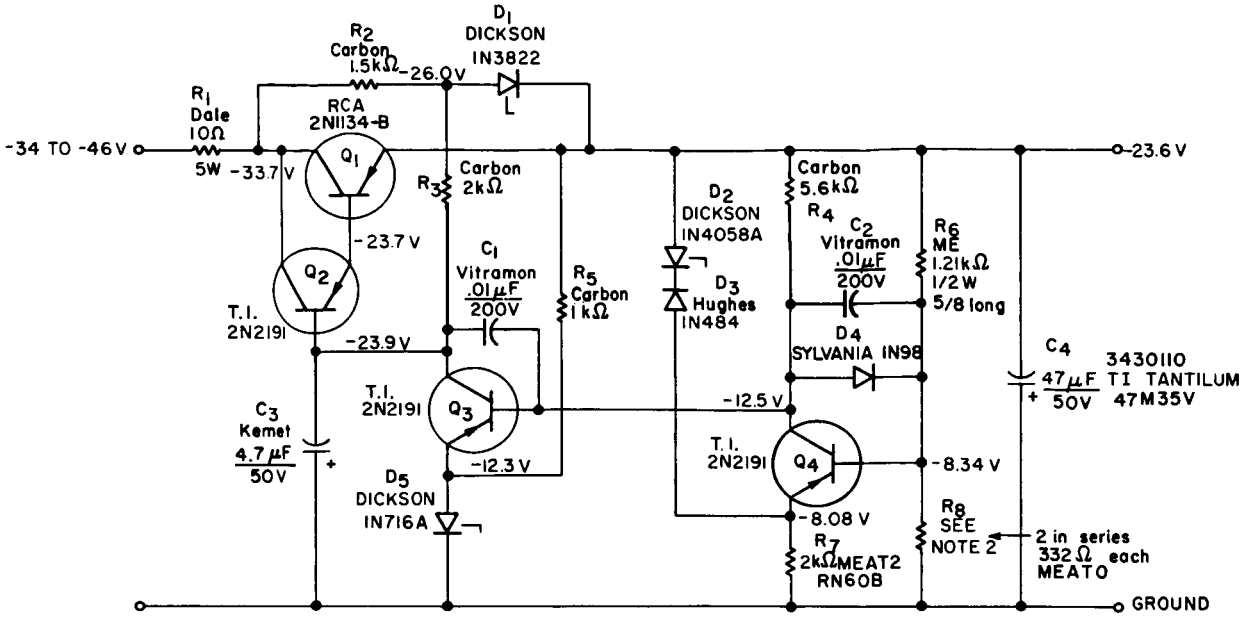

NOTES:

1. SAMPLING RESISTORS AND THE EMITTER RESISTOR OF 1st. VOLTAGE AMP. (1.21K, #700, & 2K) ARE METAL FILM MEA T2. ALL OTHERS ARE 1/2 WATT CARBON UNLESS SPECIFIED.
2. ADJUST FOR -23V OUTPUT (APPROX. 700Ω)
3. VOLTAGES MEASURED WITH 34 V. INPUT USING HP-405-CR
4. ALL VOLTAGES MEASURED WITH RESPECT TO GROUND

Figure 42. -23 volt regulator.

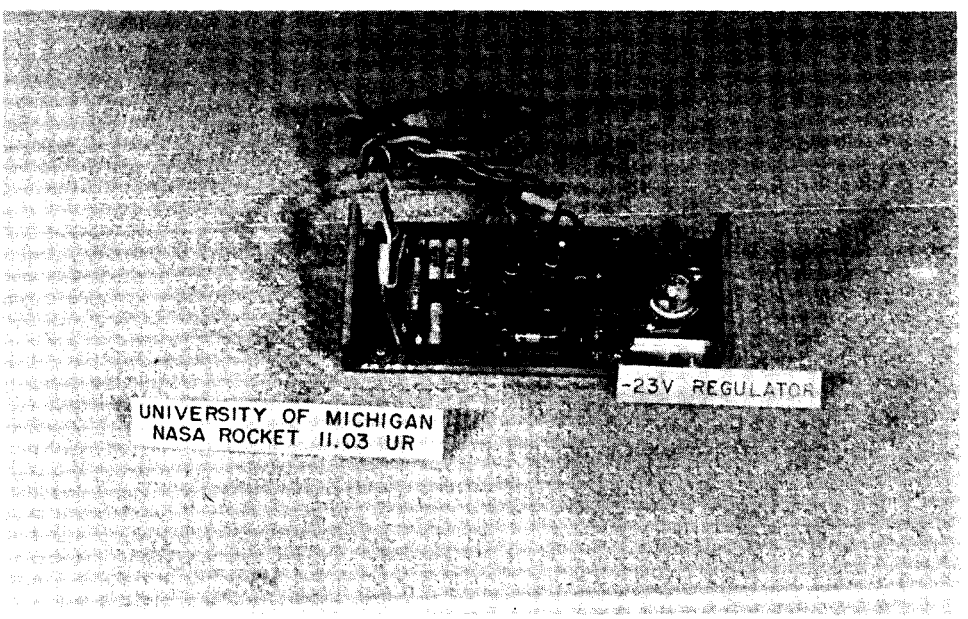

Figure 43. -23 volt regulator.

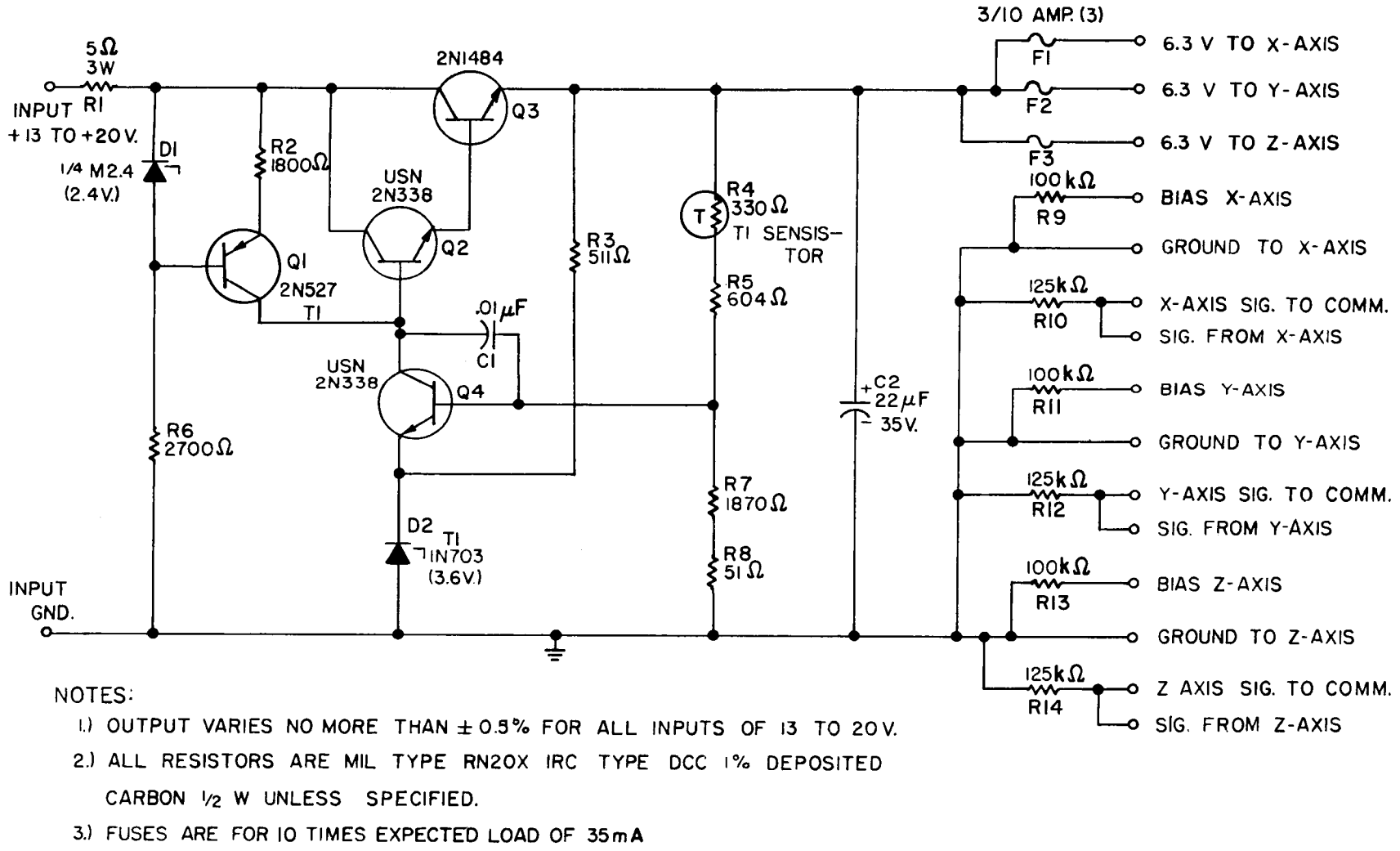

NOTES:

1.) OUTPUT VARIES NO MORE THAN ± 0.5% FOR ALL INPUTS OF 13 TO 20 V.

2.) ALL RESISTORS ARE MIL TYPE RN20X IRC TYPE DCC 1% DEPOSITED CARBON 1/2 W UNLESS SPECIFIED.

3.) FUSES ARE FOR 10 TIMES EXPECTED LOAD OF 35mA

Figure 44. 6.3 volt regulator.

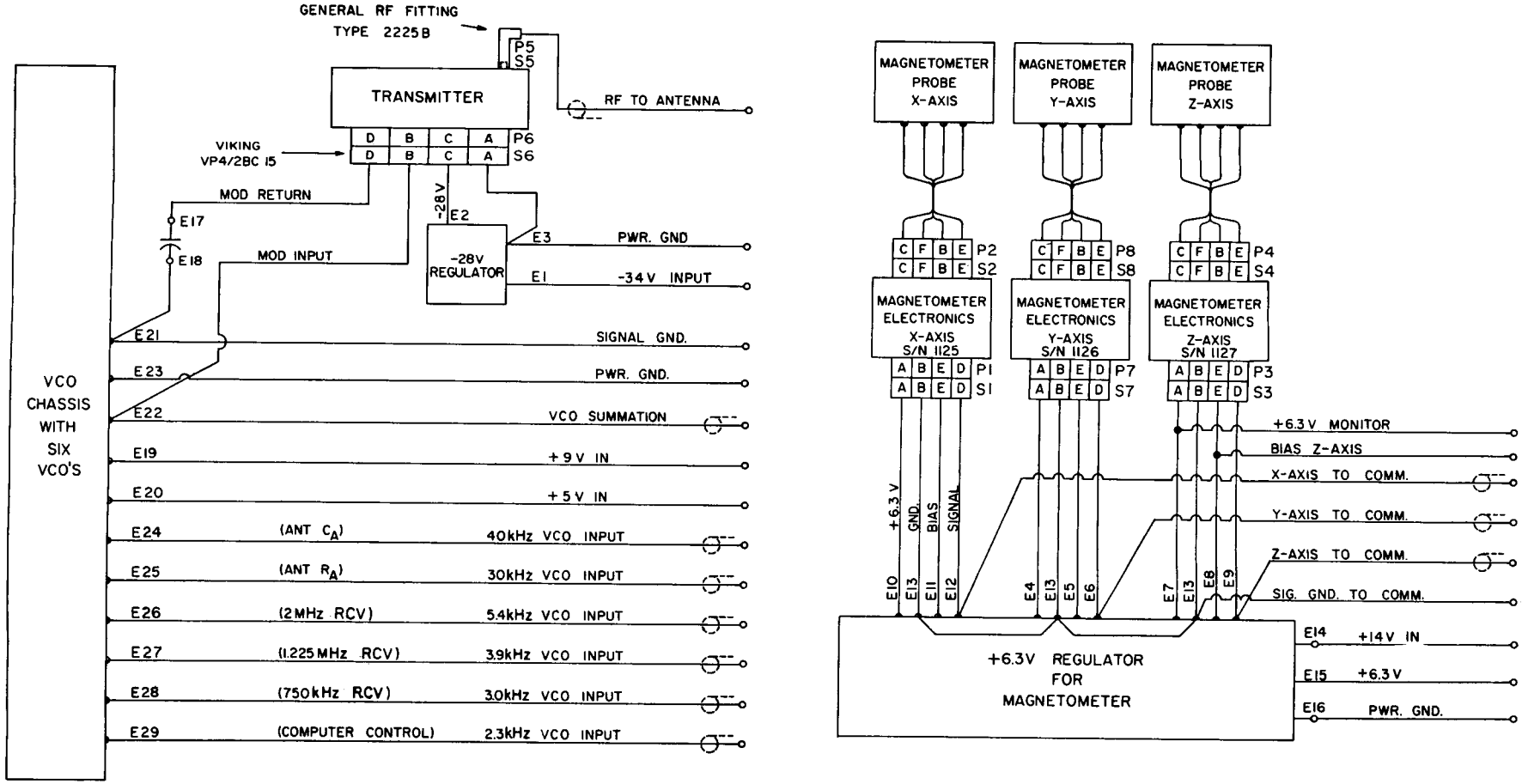

Figure 45. Interconnect wiring "E" Deck.

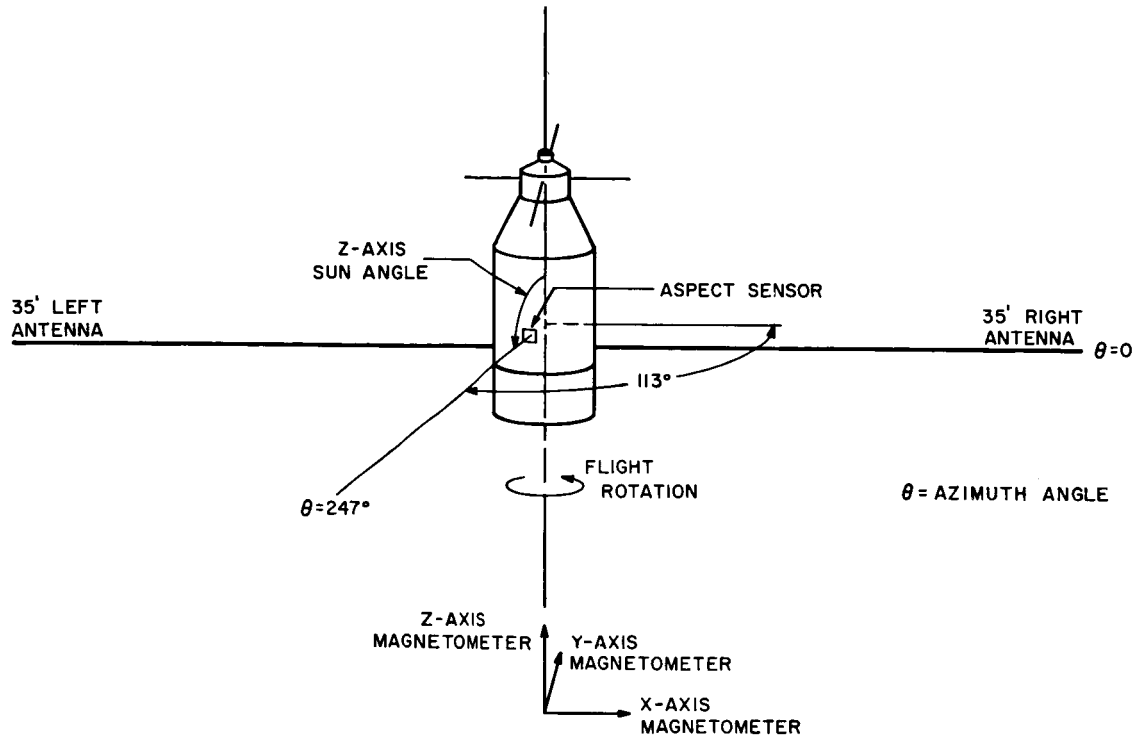

Figure 46. Rocket coordinate system.

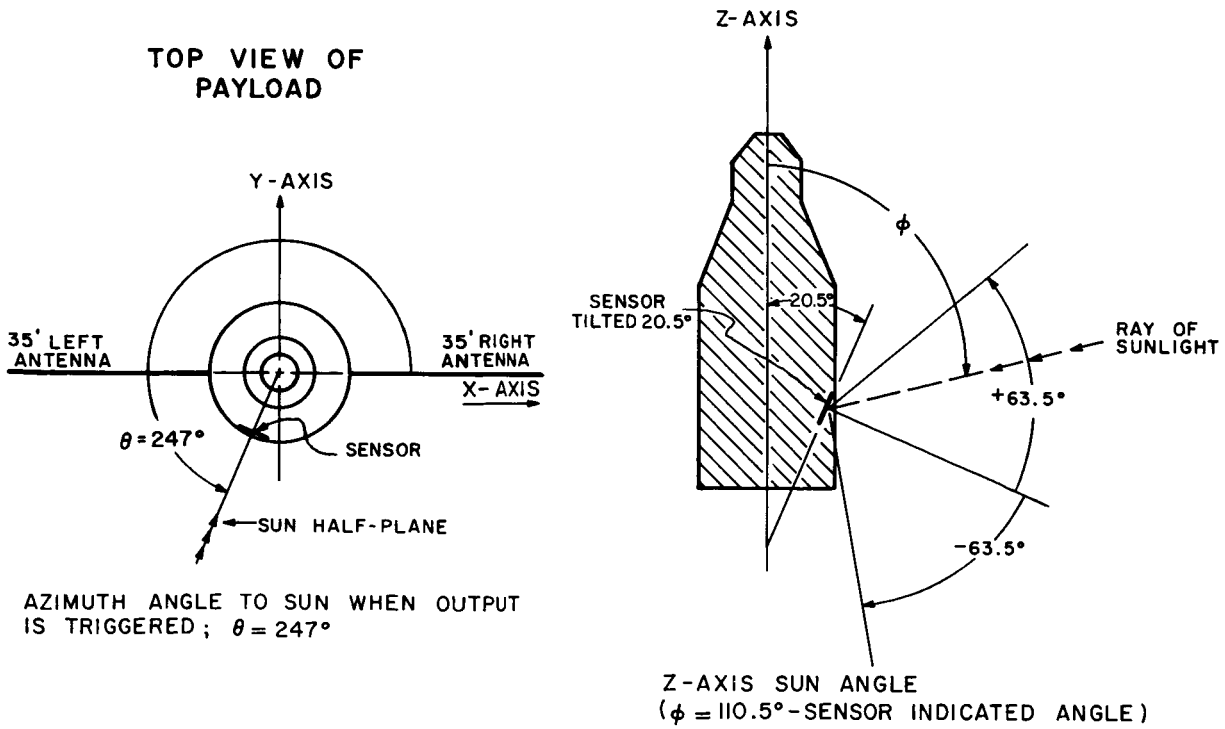

Figure 47. Solar aspect sensor angular relations.

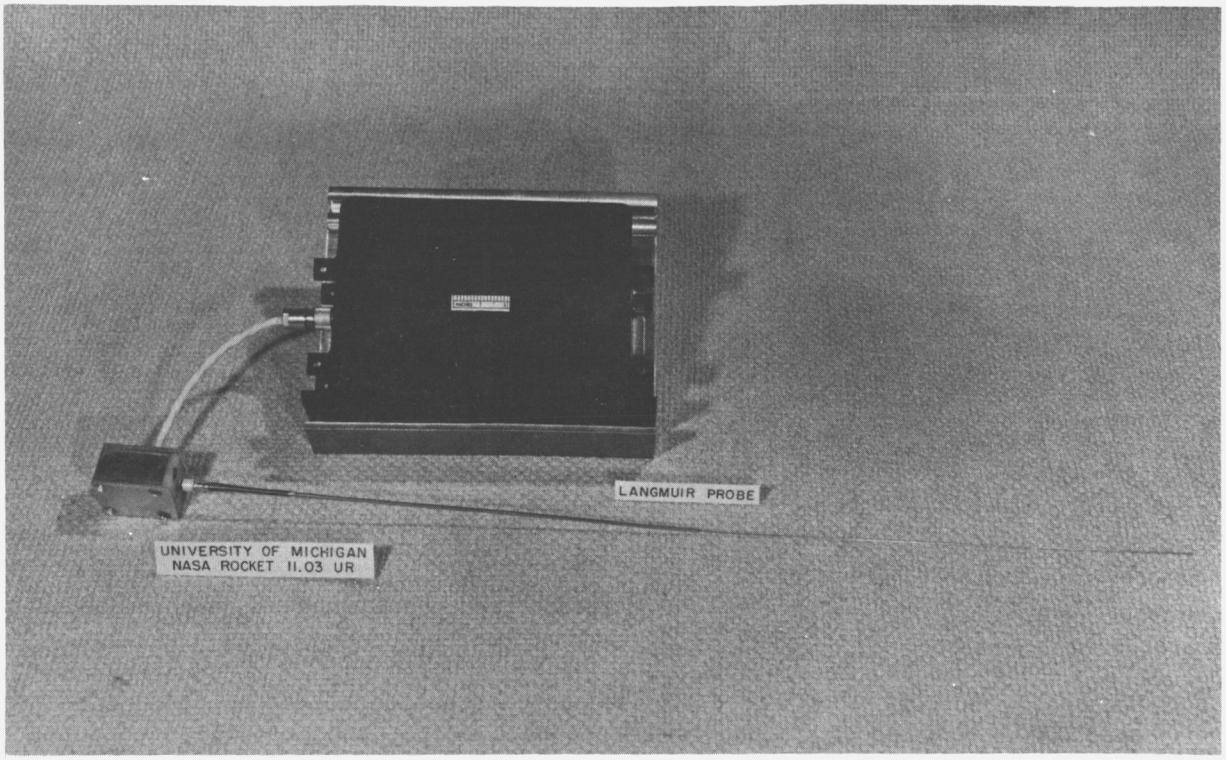

Figure 48. Langmuir probe.

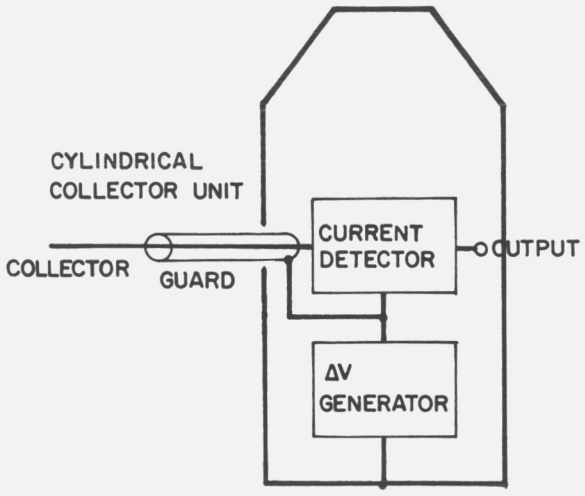

Figure 49. Langmuir probe experiment.

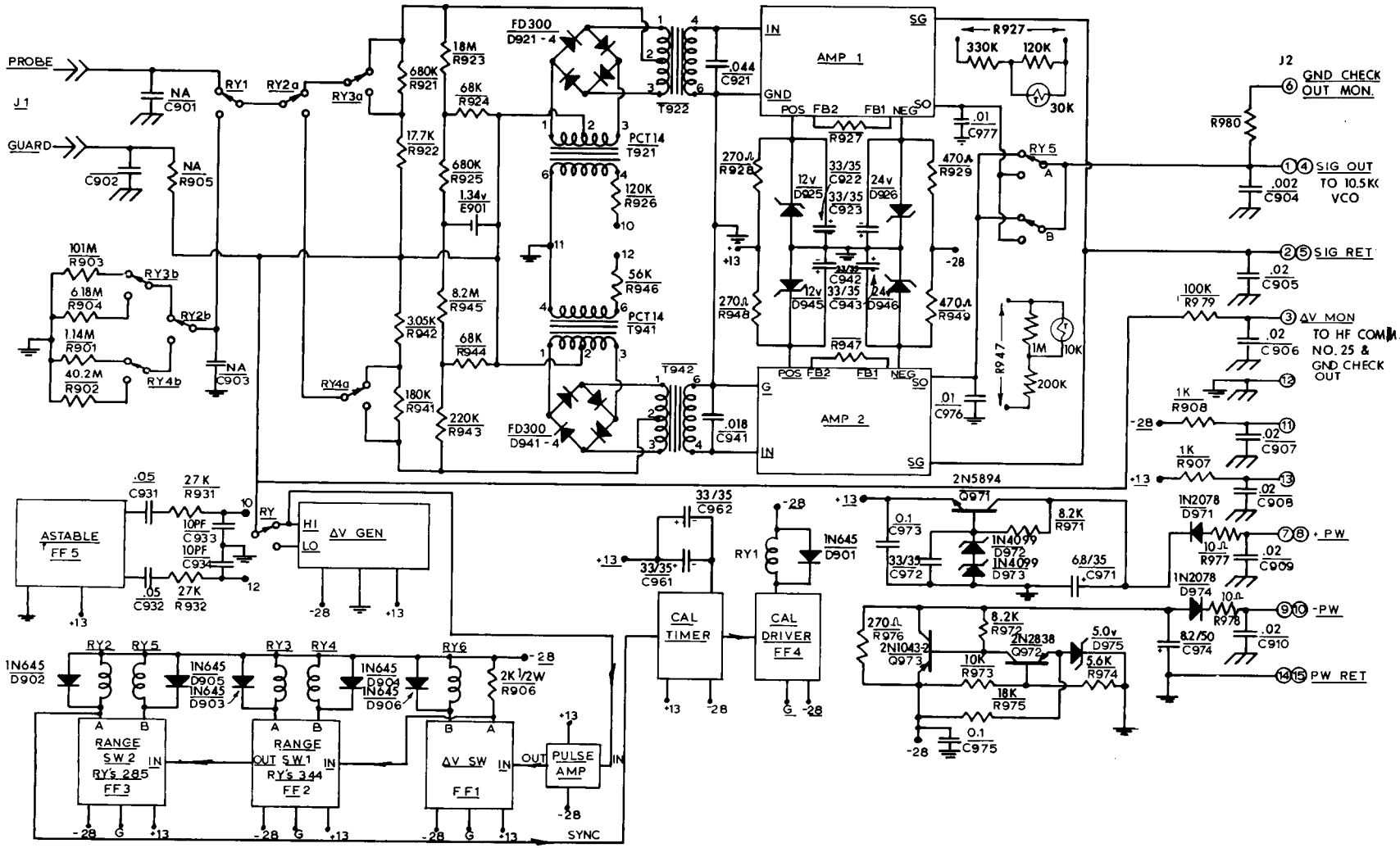

Figure 50. Schematic diagram, Langmuir probe.

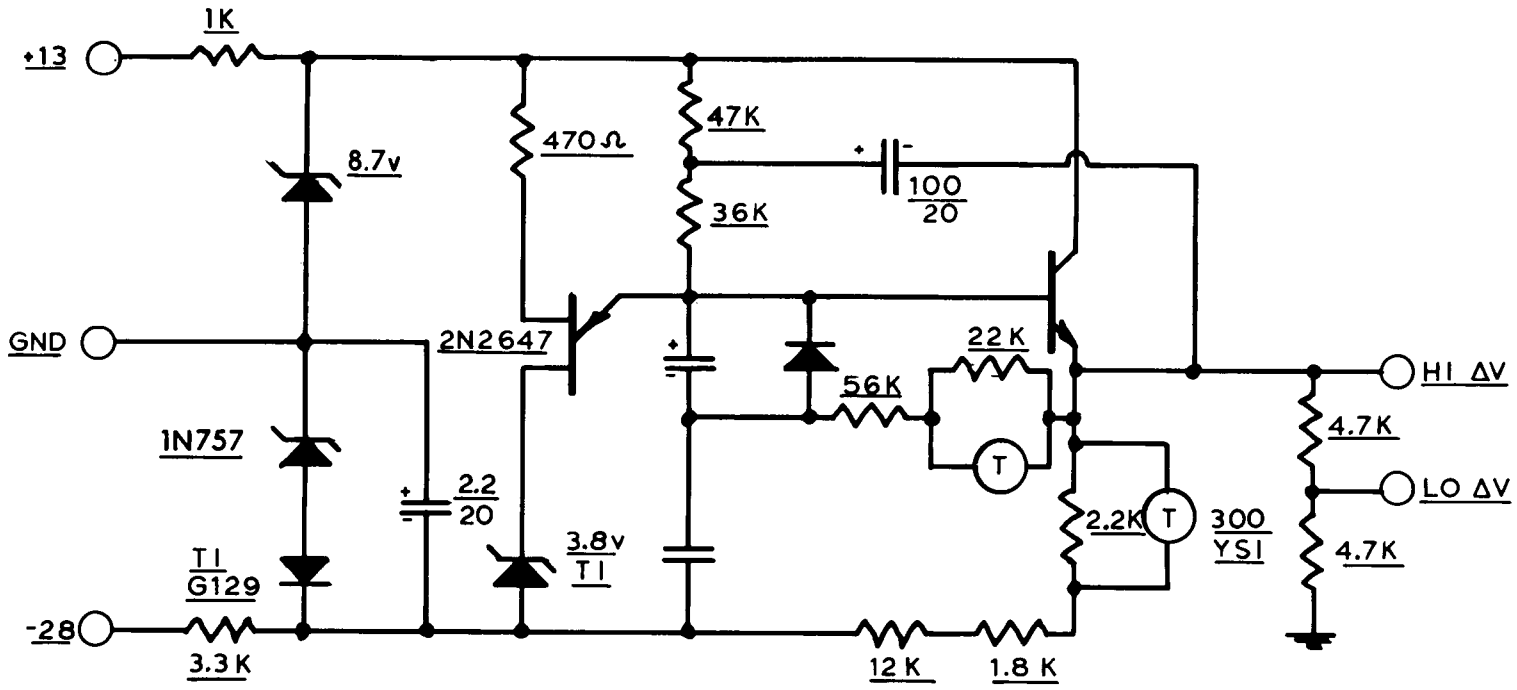

Figure 51. ΔV generator, Langmuir probe.

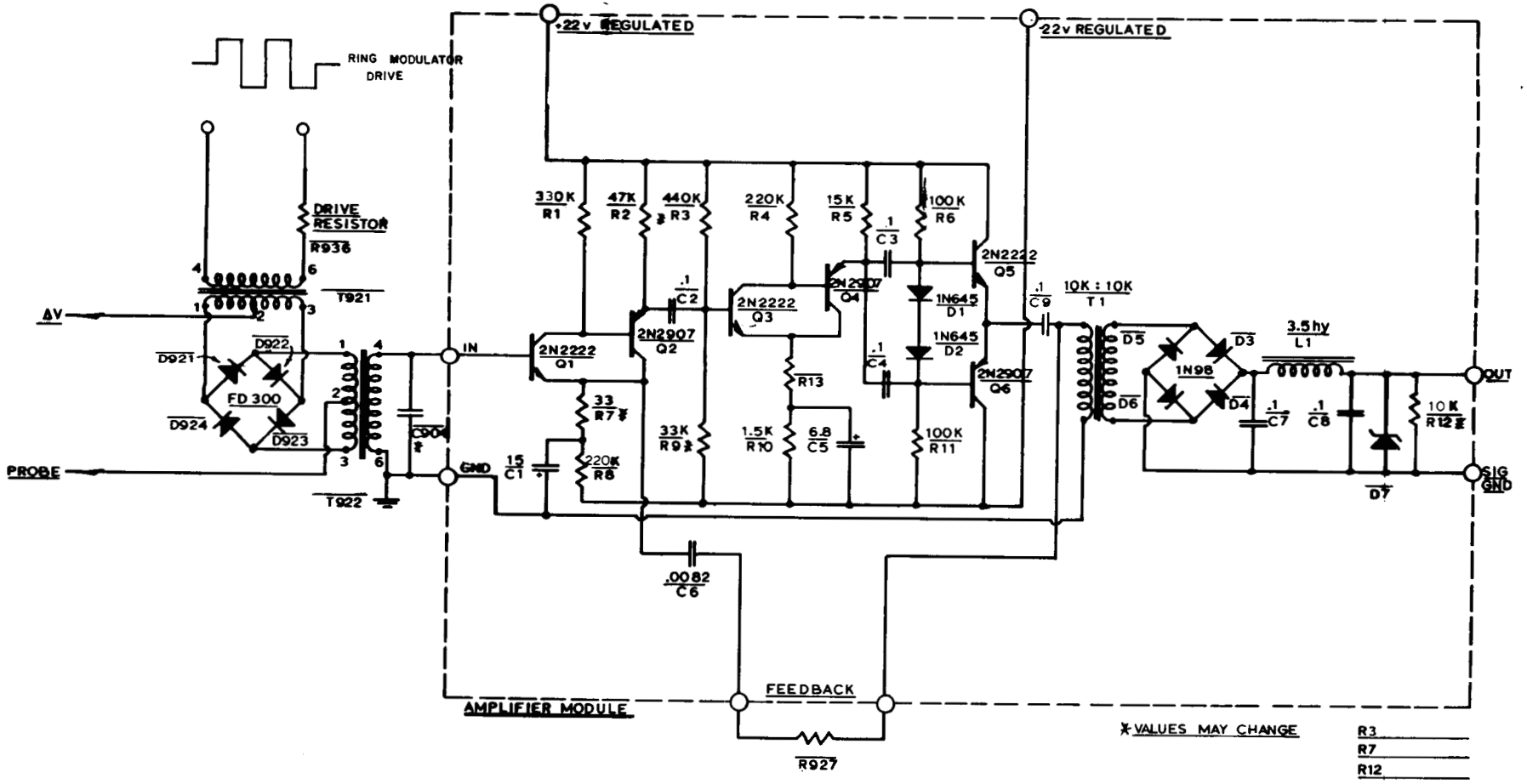

Figure 52. Solid state current amplifier, Langmuir probe.

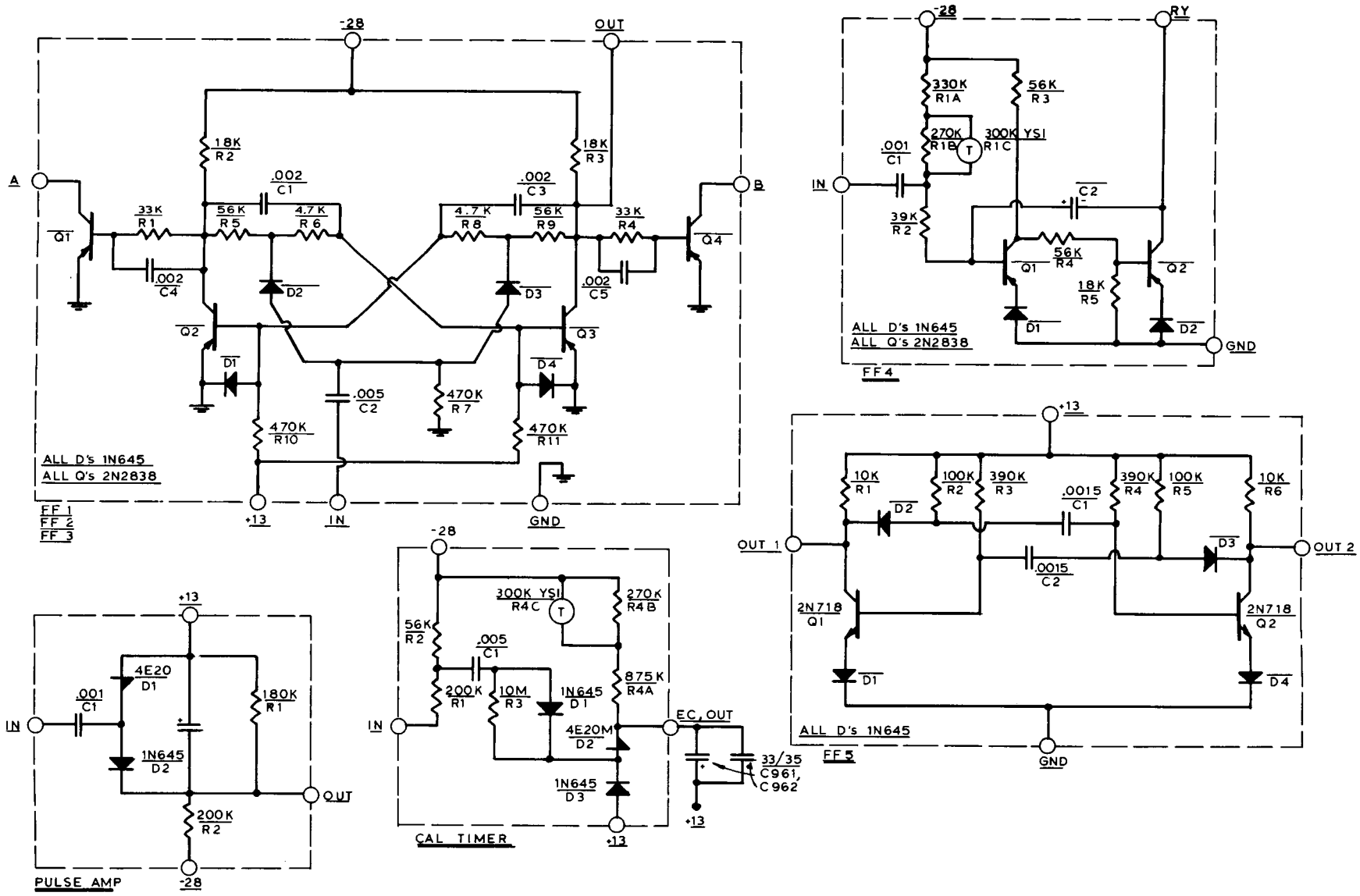

Figure 53. FF and timing modules, Langmuir probe.

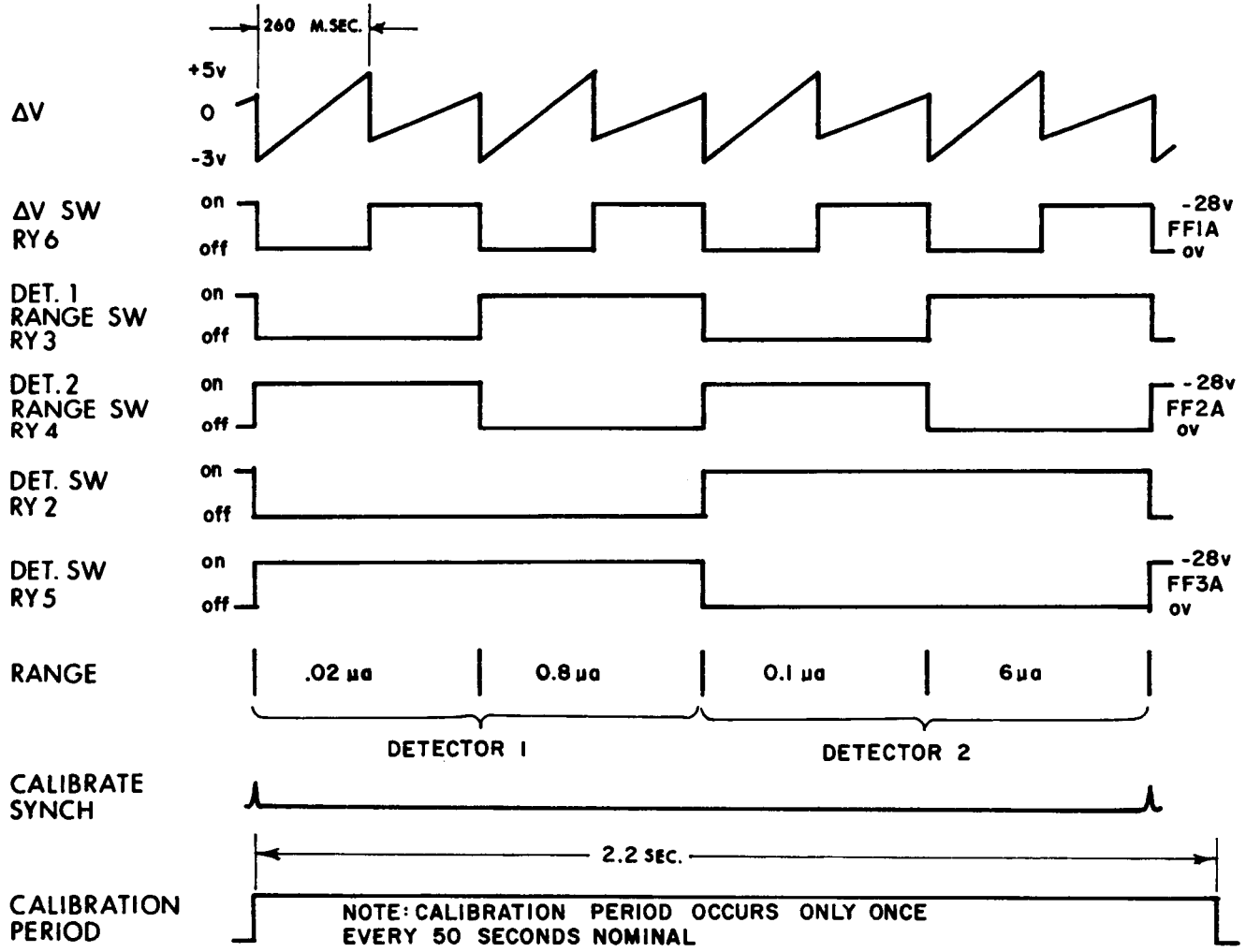

Figure 54. Timing sequence, Langmuir probe.

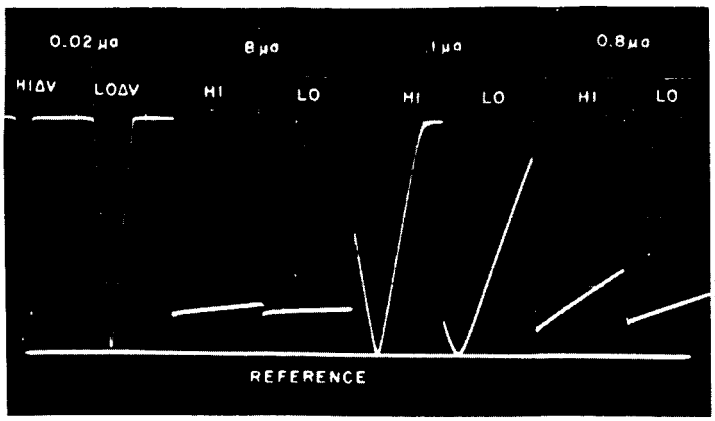

Figure 55. Output waveforms with dummy resistance, Langmuir probe.

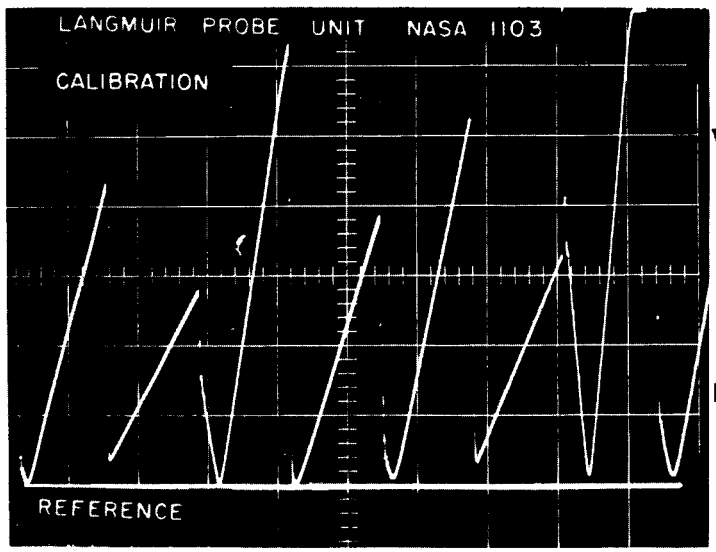

Figure 56. Calibration waveforms, Langmuir probe.
R_d = 22 Meg.

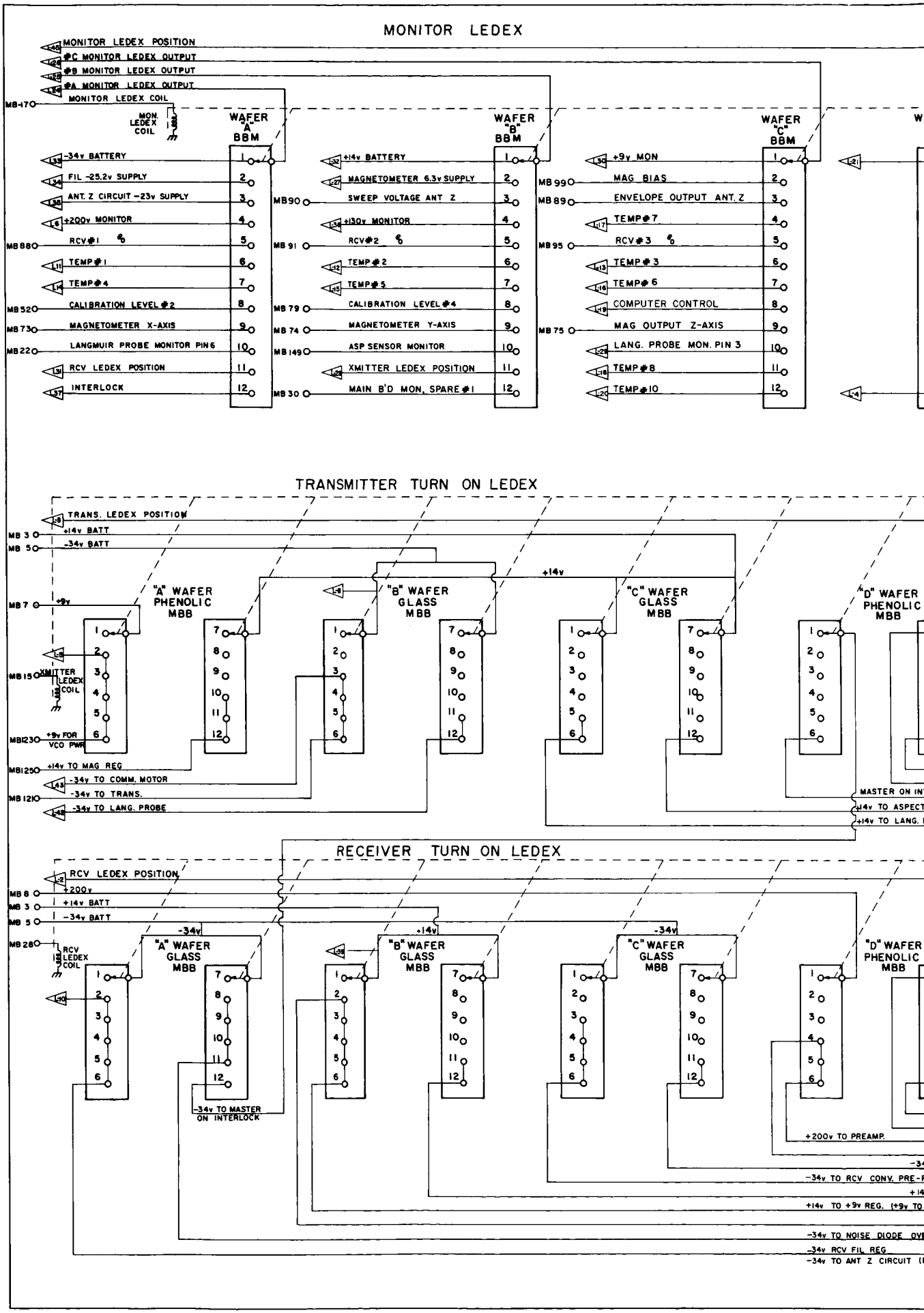
MONITOR LEDEX
MONITOR LEDEX POSITION
#C MONITOR LEDEX OUTPUT
#B MONITOR LEDEX OUTPUT
#A MONITOR LEDEX OUTPUT
MONITOR LEDEX COIL
MB-17
MON. LEDEX COIL
WAFER "A" BBM
WAFER "B" BBM
WAFER "C" BBM
-34v BATTERY
FIL -25.2v SUPPLY
ANT. Z CIRCUIT -23v SUPPLY
+200v MONITOR
RCV#1 %
TEMP#1
TEMP#4
CALIBRATION LEVEL#2
MAGNETOMETER X-AXIS
LANGMUIR PROBE MONITOR PIN 6
RCV LEDEX POSITION
INTERLOCK
+14v BATTERY
MAGNETOMETER 6.3v SUPPLY
SWEEP VOLTAGE ANT Z
+130v MONITOR
RCV#2 %
TEMP#2
TEMP#5
CALIBRATION LEVEL#4
MAGNETOMETER Y-AXIS
ASP SENSOR MONITOR
XMITTER LEDEX POSITION
MAIN B'D MON, SPARE#1
+9v MON
MAG BIAS
ENVELOPE OUTPUT ANT. Z
TEMP#7
RCV#3 %
TEMP#3
TEMP#6
COMPUTER CONTROL
MAG OUTPUT Z-AXIS
LANG. PROBE MON. PIN 3
TEMP#8
TEMP#10
TRANSMITTER TURN ON LEDEX
TRANS. LEDEX POSITION
+14v BATT
-34v BATT
+14v
+9v
"A" WAFER PHENOLIC MBB
"B" WAFER GLASS MBB
"C" WAFER GLASS MBB
"D" WAFER PHENOLIC MBB
XMITTER LEDEX COIL
+9v FOR VCO PWR
+14v TO MAG REG
-34v TO COMM. MOTOR
-34v TO TRANS.
-34v TO LANG. PROBE
MASTER ON IN
+14v TO ASPECT
+14v TO LANG.
RECEIVER TURN ON LEDEX
RCV LEDEX POSITION
+200v
+14v BATT
-34v BATT
-34v
+14v
RCV LEDEX COIL
"A" WAFER GLASS MBB
"B" WAFER GLASS MBB
"C" WAFER GLASS MBB
"D" WAFER PHENOLIC MBB
-34v TO MASTER ON INTERLOCK
+200v TO PREAMP.
-34v TO RCV CONV. PRE-
+14v TO +9v REG. (+9v TO
-34v TO NOISE DIODE OV
-34v RCV FIL REG
-34v TO ANT Z CIRCUIT

Figure 57.

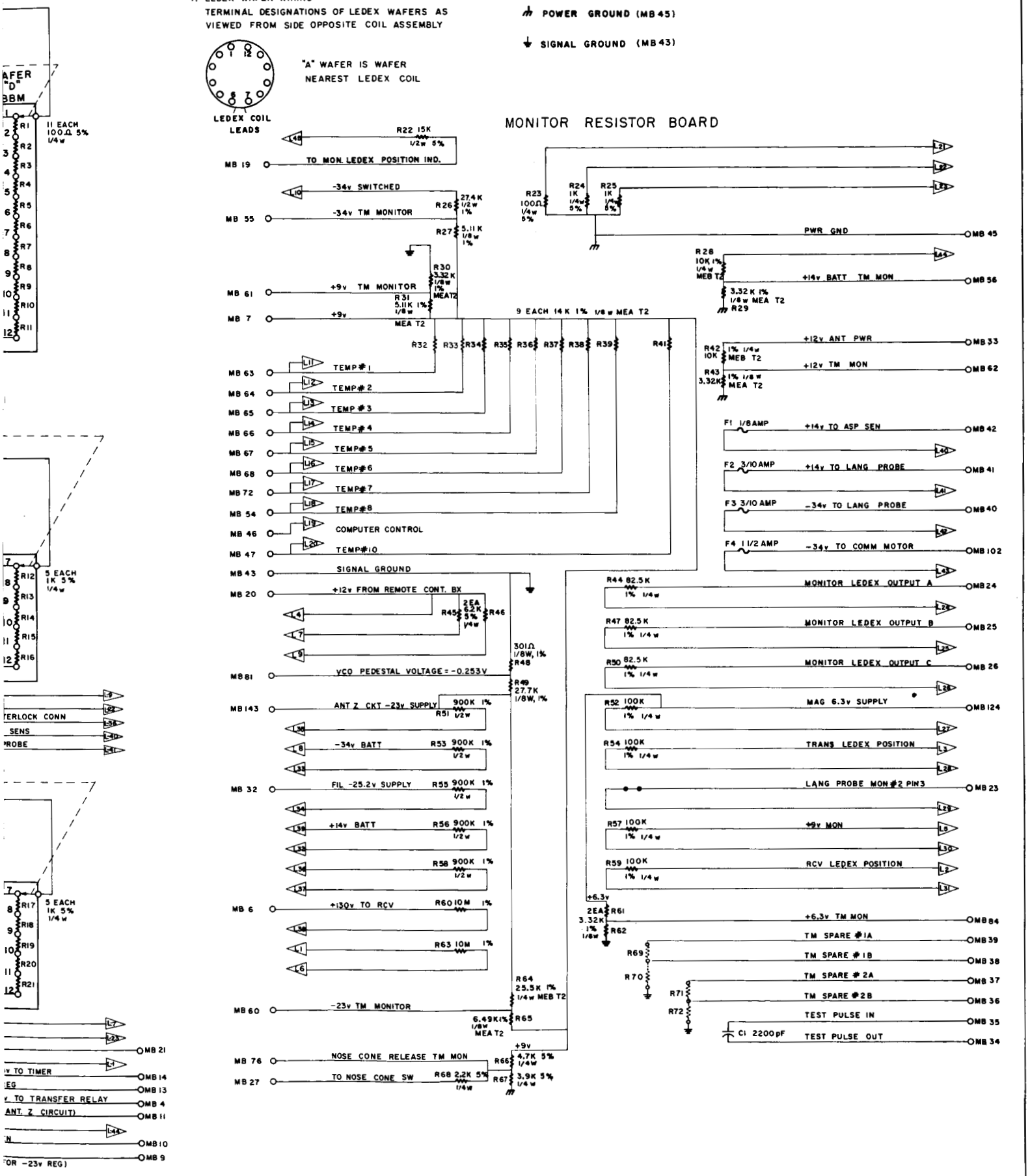

Ledex chassis wiring diagram.

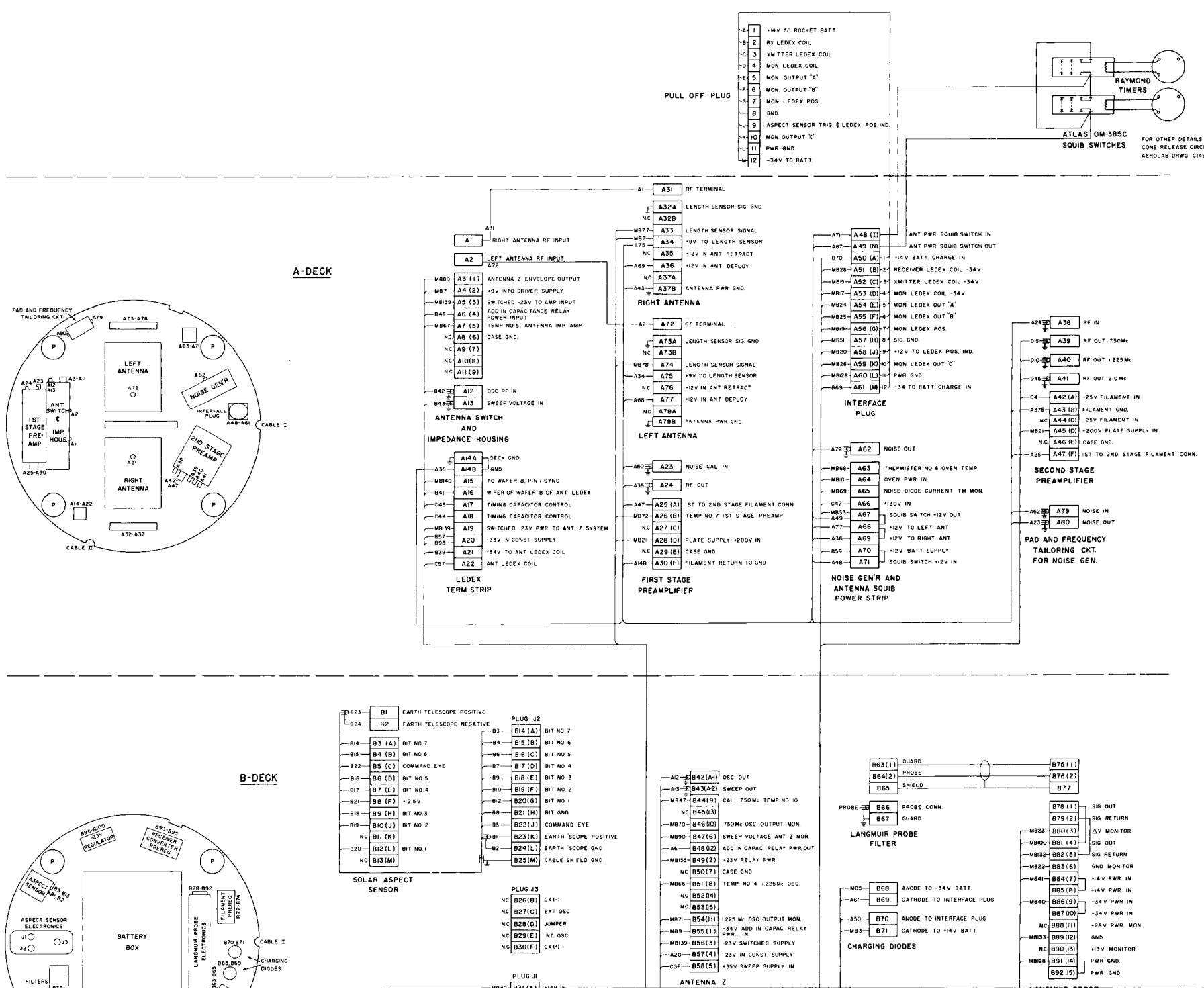
PULL OFF PLUG
A 1 +14V TO ROCKET BATT
B 2 RX LEDEX COIL
C 3 XMITTER LEDEX COIL
D 4 MON. LEDEX COIL
E 5 MON. OUTPUT "A"
F 6 MON. OUTPUT "B"
G 7 MON. LEDEX POS
H 8 GND.
J 9 ASPECT SENSOR TRIG. & LEDEX POS. IND.
K 10 MON. OUTPUT "C"
L 11 PWR. GND.
M 12 -34V TO BATT.
RAYMOND TIMERS
ATLAS OM-385C SQUIB SWITCHES
FOR OTHER DETAILS OF NOSE CONE RELEASE CIRCUITRY, SEE AEROLAB DRWG. C14972
A-DECK
A31 RF TERMINAL
A32A LENGTH SENSOR SIG. GND
A32B
A33 LENGTH SENSOR SIGNAL
A34 +9V TO LENGTH SENSOR
A35 -12V IN ANT RETRACT
A36 +12V IN ANT DEPLOY
A37A
A37B ANTENNA PWR GND.
RIGHT ANTENNA
A1 RIGHT ANTENNA RF INPUT
A2 LEFT ANTENNA RF INPUT
A72 RF TERMINAL
A73A LENGTH SENSOR SIG. GND.
A73B
A74 LENGTH SENSOR SIGNAL
A75 +9V TO LENGTH SENSOR
A76 -12V IN ANT RETRACT
A77 +12V IN ANT DEPLOY
A78A
A78B ANTENNA PWR GND.
LEFT ANTENNA
A3 (1) ANTENNA Z ENVELOPE OUTPUT
A4 (2) +9V INTO DRIVER SUPPLY
A5 (3) SWITCHED -23V TO AMP INPUT
A6 (4) ADD IN CAPACITANCE RELAY POWER INPUT
A7 (5) TEMP NO 5, ANTENNA IMP. AMP
A8 (6) CASE GND.
A9 (7)
A10(8)
A11(9)
A12 OSC RF IN
A13 SWEEP VOLTAGE IN
ANTENNA SWITCH AND IMPEDANCE HOUSING
A14A DECK GND
A14B GND
A15 TO WAFER B, PIN 1 SYNC
A16 WIPER OF WAFER B OF ANT LEDEX
A17 TIMING CAPACITOR CONTROL
A18 TIMING CAPACITOR CONTROL
A19 SWITCHED -23V PWR TO ANT. Z SYSTEM
A20 -23V IN CONST SUPPLY
A21 -34V TO ANT LEDEX COIL
A22 ANT LEDEX COIL
LEDEX TERM STRIP
A23 NOISE CAL IN
A24 RF OUT
A25 (A) 1ST TO 2ND STAGE FILAMENT CONN
A26 (B) TEMP NO 7 1ST STAGE PREAMP
A27 (C)
A28 (D) PLATE SUPPLY +200V IN
A29 (E) CASE GND.
A30 (F) FILAMENT RETURN TO GND
FIRST STAGE PREAMPLIFIER
A48 (I) ANT PWR SQUIB SWITCH IN
A49 (N) ANT PWR SQUIB SWITCH OUT
A50 (A) +14V BATT. CHARGE IN
A51 (B) RECEIVER LEDEX COIL -34V
A52 (C) XMITTER LEDEX COIL -34V
A53 (D) MON. LEDEX COIL -34V
A54 (E) MON. LEDEX OUT "A"
A55 (F) MON. LEDEX OUT "B"
A56 (G) MON. LEDEX POS.
A57 (H) SIG. GND.
A58 (J) +12V TO LEDEX POS. IND.
A59 (K) MON. LEDEX OUT "C"
A60 (L) PWR. GND.
A61 (M) -34 TO BATT. CHARGE IN
INTERFACE PLUG
A62 NOISE OUT
A63 THERMISTER NO. 6 OVEN TEMP
A64 OVEN PWR IN
A65 NOISE DIODE CURRENT TM MON.
A66 +130V IN
A67 SQUIB SWITCH +12V OUT
A68 +12V TO LEFT ANT
A69 +12V TO RIGHT ANT
A70 +12V BATT SUPPLY
A71 SQUIB SWITCH +12V IN
NOISE GEN'R AND ANTENNA SQUIB POWER STRIP
A38 RF IN
A39 RF OUT 750Mc
A40 RF OUT 1225Mc
A41 RF OUT 2.0Mc
A42 (A) -25V FILAMENT IN
A43 (B) FILAMENT GND.
A44 (C) -25V FILAMENT IN
A45 (D) +200V PLATE SUPPLY IN
A46 (E) CASE GND.
A47 (F) 1ST TO 2ND STAGE FILAMENT CONN.
SECOND STAGE PREAMPLIFIER
A79 NOISE IN
A80 NOISE OUT
PAD AND FREQUENCY TAILORING CKT. FOR NOISE GEN.
PAD AND FREQUENCY TAILORING CKT.
A79
A73-A78
A80
A63-A71
LEFT ANTENNA
A72
A62
NOISE GEN'R
INTERFACE PLUG
A48-A61
CABLE I
A24 A23 S1 A12 A13 A3-A11
ANT. SWITCH & IMP. HOUS.
A2
A1
1ST STAGE PRE-AMP
A25-A30
A31
RIGHT ANTENNA
A42 A47
A38 A39 A40 A41
2ND STAGE PREAMP
A14-A22
A32-A37
CABLE II
B-DECK
B1 EARTH TELESCOPE POSITIVE
B2 EARTH TELESCOPE NEGATIVE
B3 (A) BIT NO 7
B4 (B) BIT NO 6
B5 (C) COMMAND EYE
B6 (D) BIT NO 5
B7 (E) BIT NO 4
B8 (F) -12.5V
B9 (H) BIT NO 3
B10 (J) BIT NO 2
B11 (K)
B12 (L) BIT NO 1
B13 (M)
SOLAR ASPECT SENSOR
PLUG J2
B14 (A) BIT NO 7
B15 (B) BIT NO 6
B16 (C) BIT NO 5
B17 (D) BIT NO 4
B18 (E) BIT NO 3
B19 (F) BIT NO 2
B20 (G) BIT NO 1
B21 (H) BIT GND
B22 (J) COMMAND EYE
B23 (K) EARTH SCOPE POSITIVE
B24 (L) EARTH SCOPE GND
B25 (M) CABLE SHIELD GND
PLUG J3
B26 (B) CK(-)
B27 (C) EXT OSC
B28 (D) JUMPER
B29 (E) INT. OSC
B30 (F) CK(+)
PLUG J1
B31 (A) +14V IN
B32 (B) +14V IN
B33 (C) -34V IN
B34 (D) -34V IN
B35 (E) GND
B36 (F) GND
B37 (H) SIG. OUT
B38 (J) SIG. RETURN
B39 (K) ΔV MONITOR
B40 (L) SIG. OUT
B41 (M) SIG. RETURN
B42 (N) GND. MONITOR
B43 (P) +14V PWR. IN
B44 (R) +14V PWR. IN
B45 (S) -34V PWR IN
B46 (T) -34V PWR IN
B47 (U) -28V PWR. MON.
B48 (V) GND
B49 (W) +13V MONITOR
B50 (X) PWR GND
B51 (Y) PWR GND
ANTENNA Z
A12 B42 (A1) OSC OUT
A13 B43 (A2) SWEEP OUT
B47 (9) CAL. 750Mc TEMP NO 10
B45 (13)
B46 (10) 750Mc OSC OUTPUT MON.
B47 (6) SWEEP VOLTAGE ANT Z MON.
B48 (12) ADD IN CAPAC. RELAY PWR. OUT
B49 (2) -23V RELAY PWR
B50 (7) CASE GND
B51 (8) TEMP NO 4 1225Mc OSC.
B52 (14)
B53 (15)
B54 (11) 1225 Mc OSC OUTPUT MON.
B55 (1) -34V ADD IN CAPAC RELAY PWR. IN
B56 (3) -23V SWITCHED SUPPLY
B57 (4) -23V IN CONST. SUPPLY
B58 (5) +35V SWEEP SUPPLY IN
B63 (1) GUARD
B64 (2) PROBE
B65 SHIELD
B75 (1)
B76 (2)
B77
PROBE
B66 PROBE CONN.
B67 GUARD
LANGMUIR PROBE FILTER
B68 ANODE TO -34V BATT.
B69 CATHODE TO INTERFACE PLUG
B70 ANODE TO INTERFACE PLUG
B71 CATHODE TO +14V BATT.
CHARGING DIODES
B78 (1) SIG OUT
B79 (2) SIG. RETURN
B80 (3) ΔV MONITOR
B81 (4) SIG. OUT
B82 (5) SIG. RETURN
B83 (6) GND. MONITOR
B84 (7) +14V PWR. IN
B85 (8) +14V PWR. IN
B86 (9) -34V PWR IN
B87 (10) -34V PWR IN
B88 (11) -28V PWR. MON.
B89 (12) GND
B90 (13) +13V MONITOR
B91 (14) PWR GND
B92 (15) PWR GND
B96-B100 -25V REGULATOR
B93-B95 RECEIVER CONVERTER PREREG.
ASPECT SENSOR
B1, B2
B3-B13
ASPECT SENSOR ELECTRONICS
J1
J3
J2
BATTERY BOX
FILTERS
B78-B92
LANGMUIR PROBE ELECTRONICS
FILAMENT PREREG
B72-B74
B63-B65
B70,B71
CABLE I
B68,B69
CHARGING DIODES

1-85

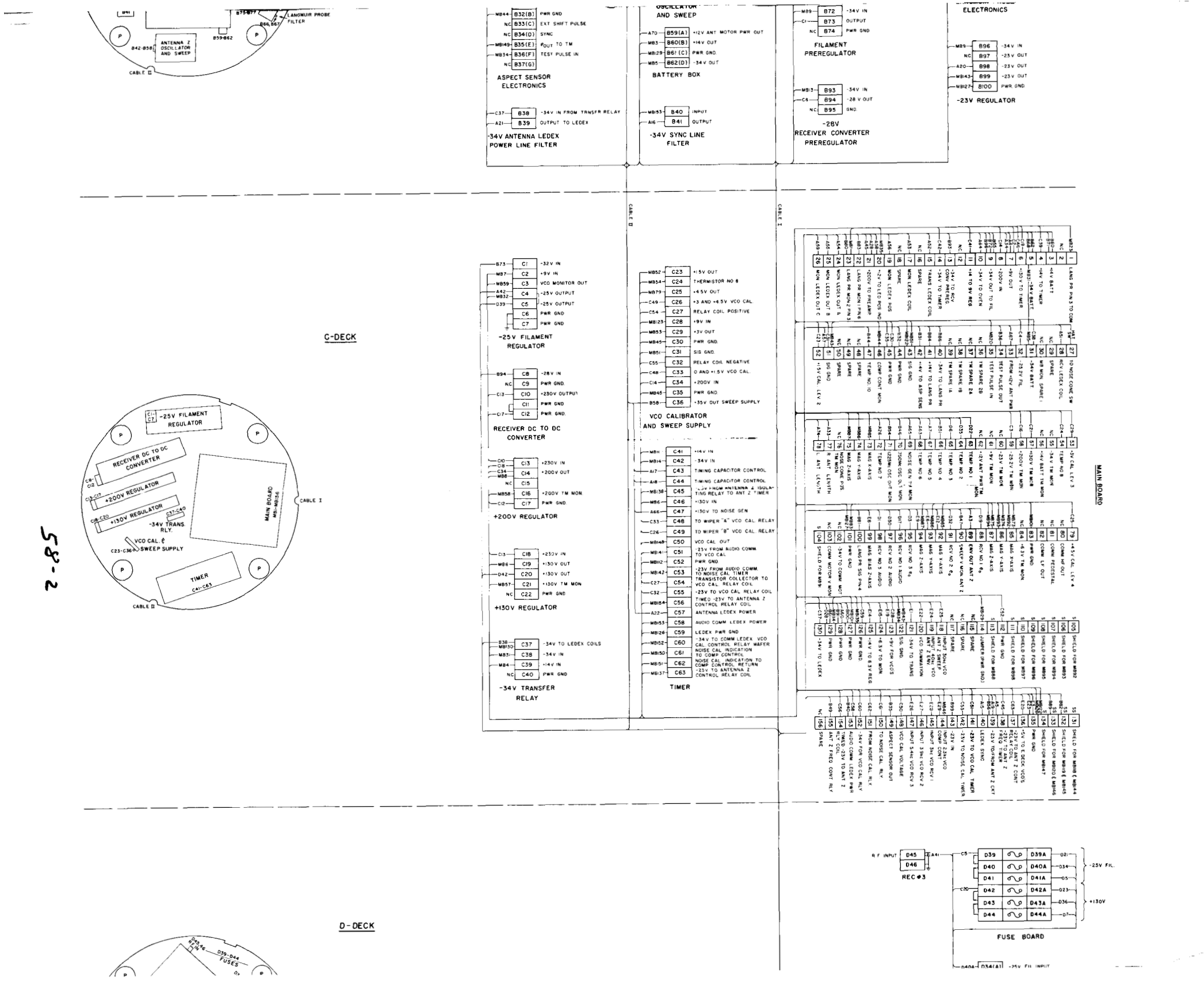
LANGMUIR PROBE FILTER
ANTENNA Z OSCILLATOR AND SWEEP
CABLE II
ASPECT SENSOR ELECTRONICS
-34V ANTENNA LEDEX POWER LINE FILTER
OSCILLATOR AND SWEEP
BATTERY BOX
-34V SYNC LINE FILTER
FILAMENT PREREGULATOR
-28V RECEIVER CONVERTER PREREGULATOR
ELECTRONICS
-23V REGULATOR
C-DECK
-25V FILAMENT REGULATOR
RECEIVER DC TO DC CONVERTER
+200V REGULATOR
+130V REGULATOR
-34V TRANS. RLY.
VCO CAL. & SWEEP SUPPLY
TIMER
MAIN BOARD
CABLE I
-25V FILAMENT REGULATOR
RECEIVER DC TO DC CONVERTER
+200V REGULATOR
+130V REGULATOR
-34V TRANSFER RELAY
VCO CALIBRATOR AND SWEEP SUPPLY
TIMER
MAIN BOARD
D-DECK
FUSES
REC #3
FUSE BOARD
-25V FIL.
+130V

58-2

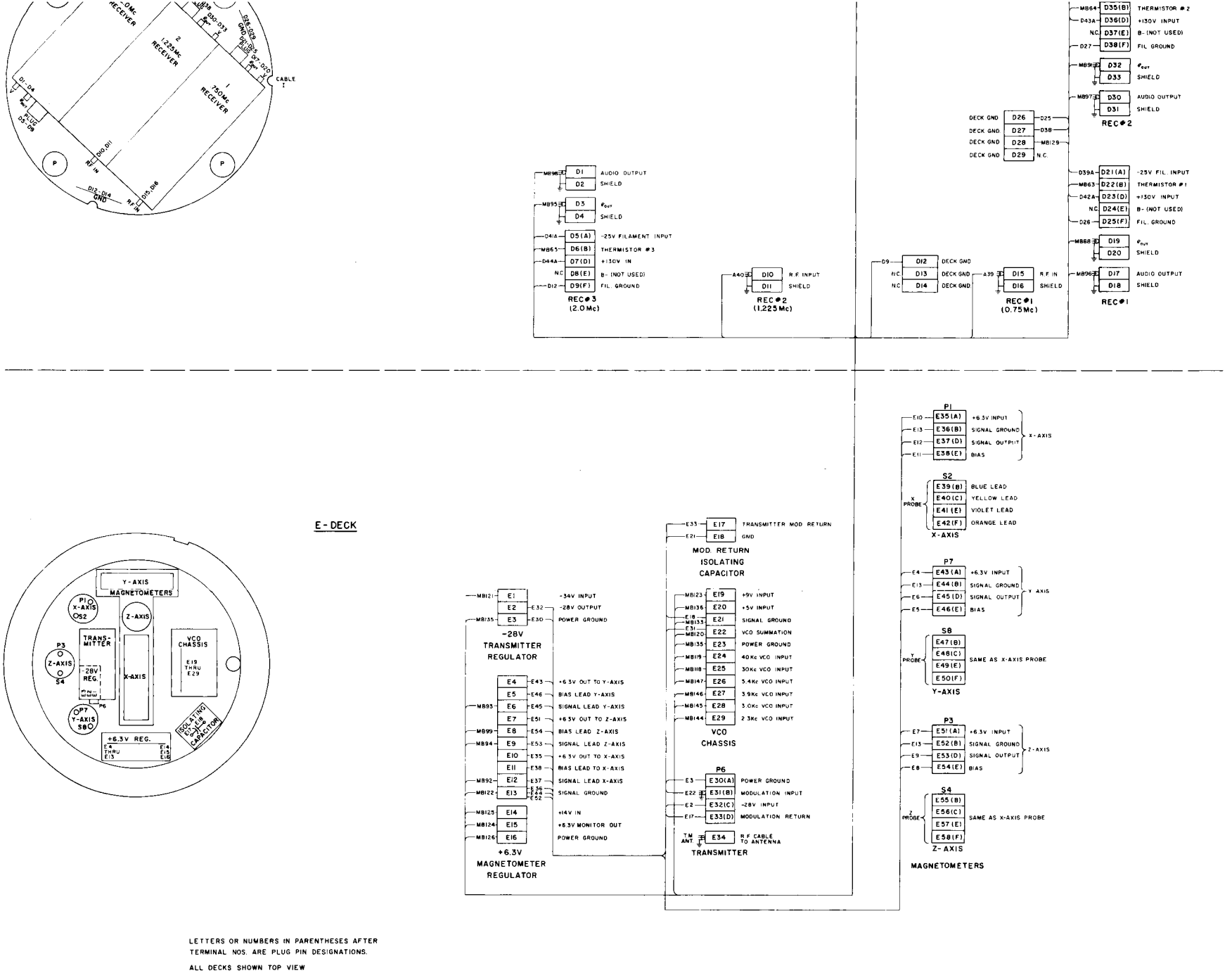

Figure 58. Payload interconnect diagram.

Figure 59. Remote control box and operator.

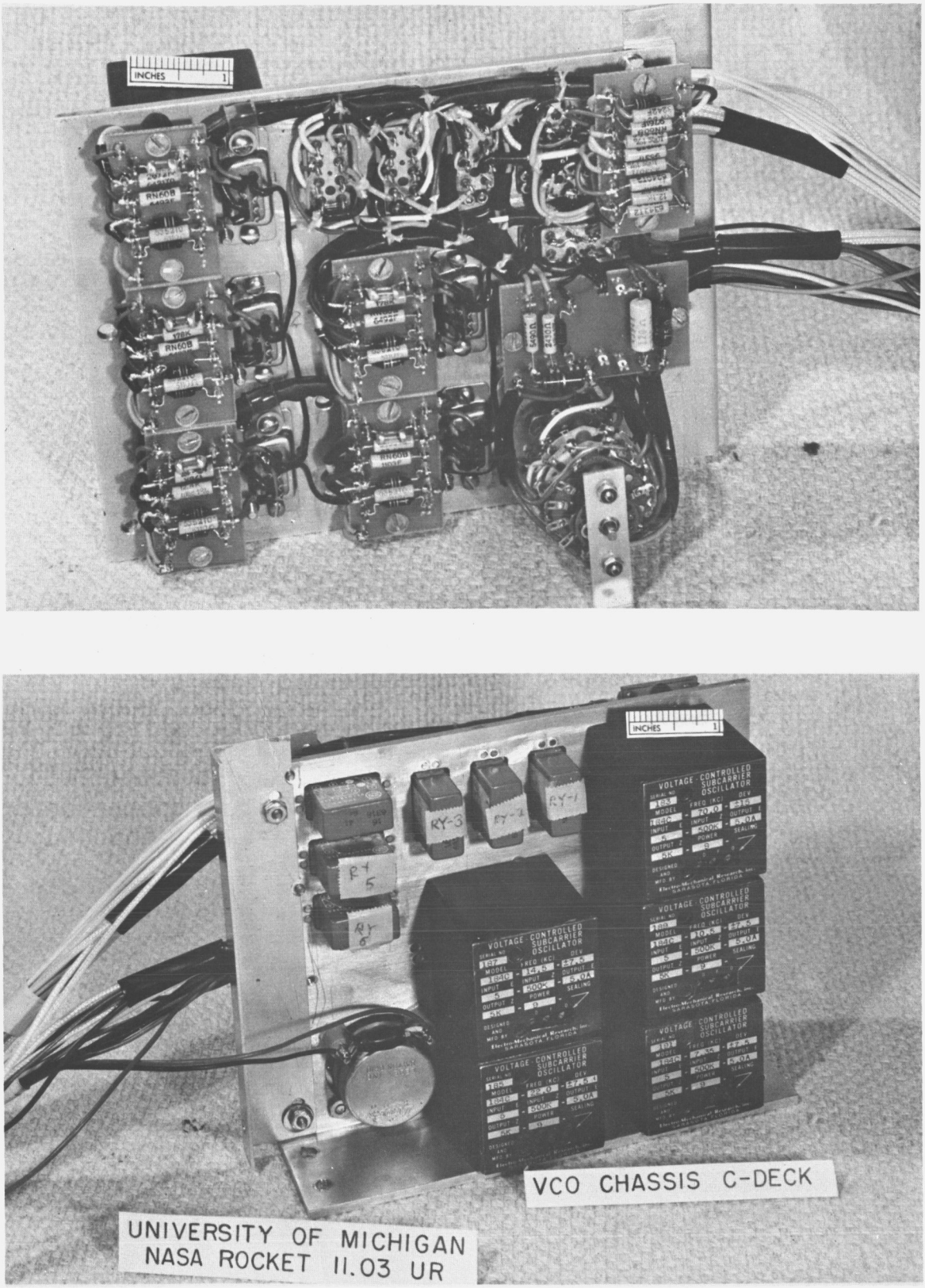

Figure 60. VCO chassis "C" Deck.

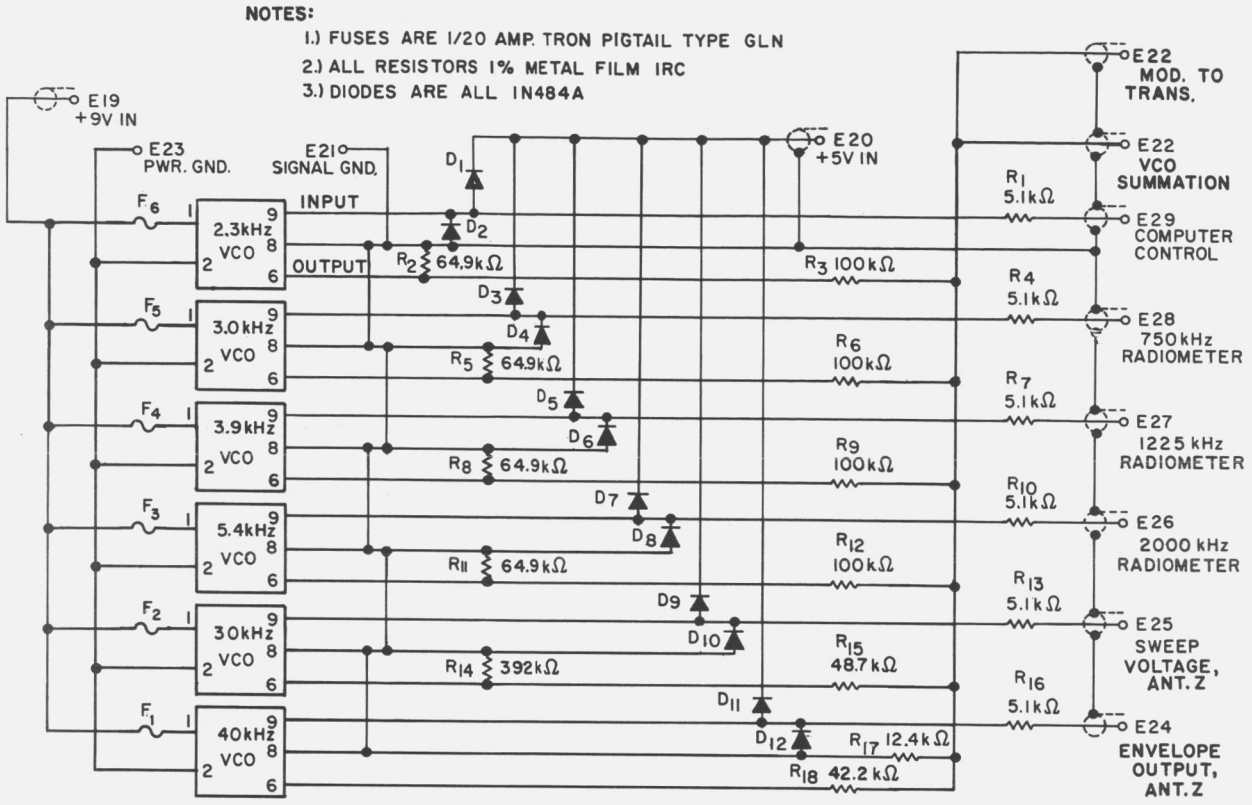

Figure 61. VCO board "E" Deck.

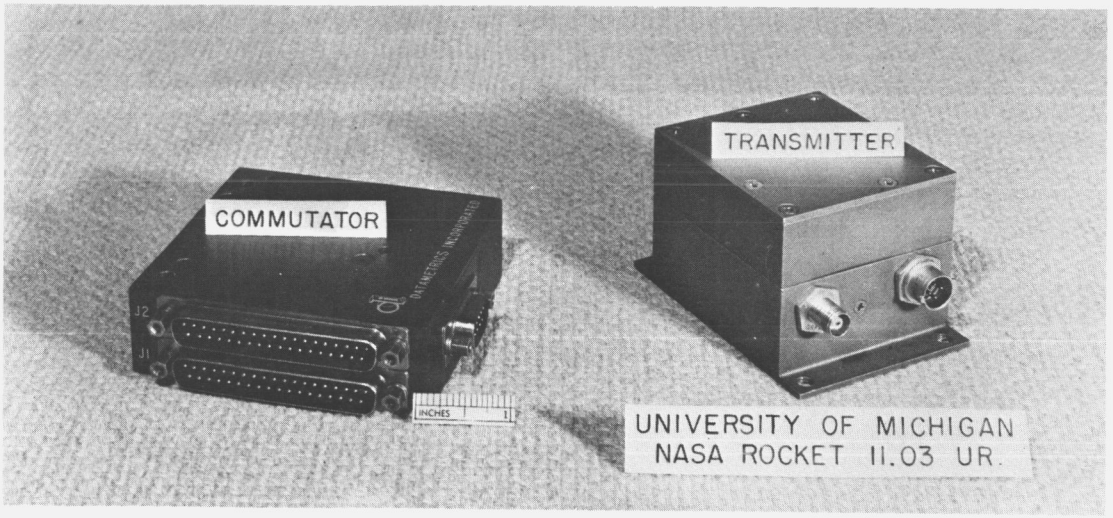

Figure 62. Commutator.

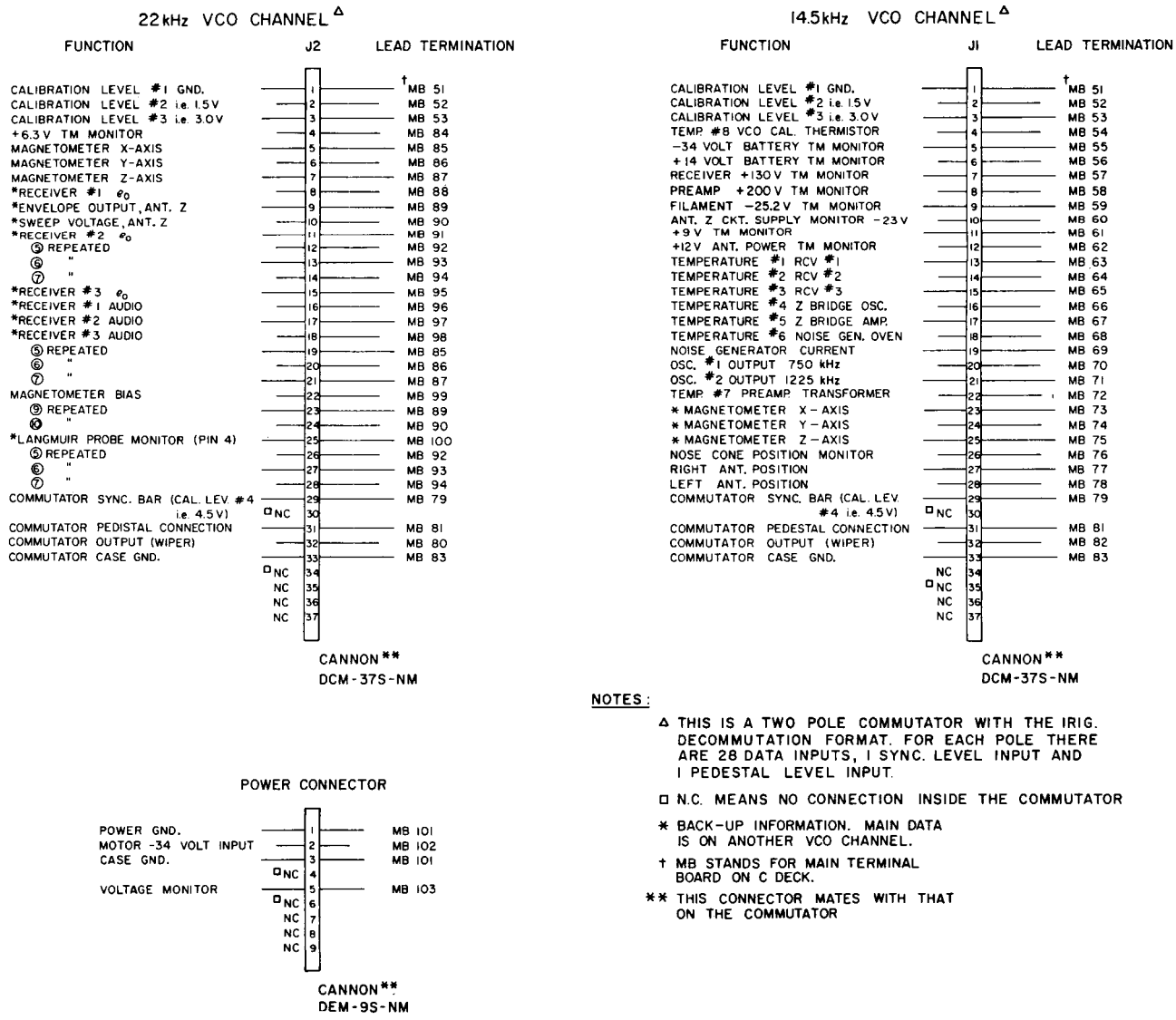

NOTES:

Δ THIS IS A TWO POLE COMMUTATOR WITH THE IRIG. DECOMMUTATION FORMAT. FOR EACH POLE THERE ARE 28 DATA INPUTS, 1 SYNC. LEVEL INPUT AND 1 PEDESTAL LEVEL INPUT.

□ N.C. MEANS NO CONNECTION INSIDE THE COMMUTATOR

* BACK-UP INFORMATION. MAIN DATA IS ON ANOTHER VCO CHANNEL.

† MB STANDS FOR MAIN TERMINAL BOARD ON C DECK.

** THIS CONNECTOR MATES WITH THAT ON THE COMMUTATOR

Figure 63. Commutator channel assignments.

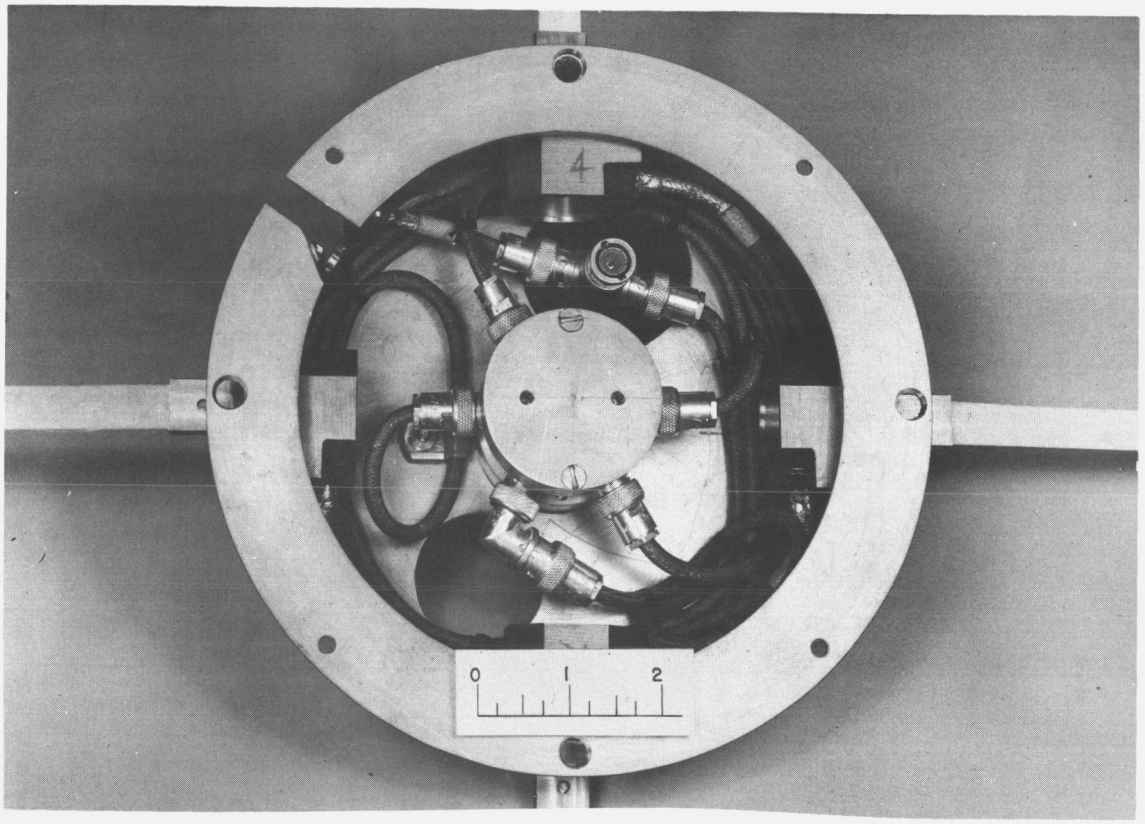

(a)

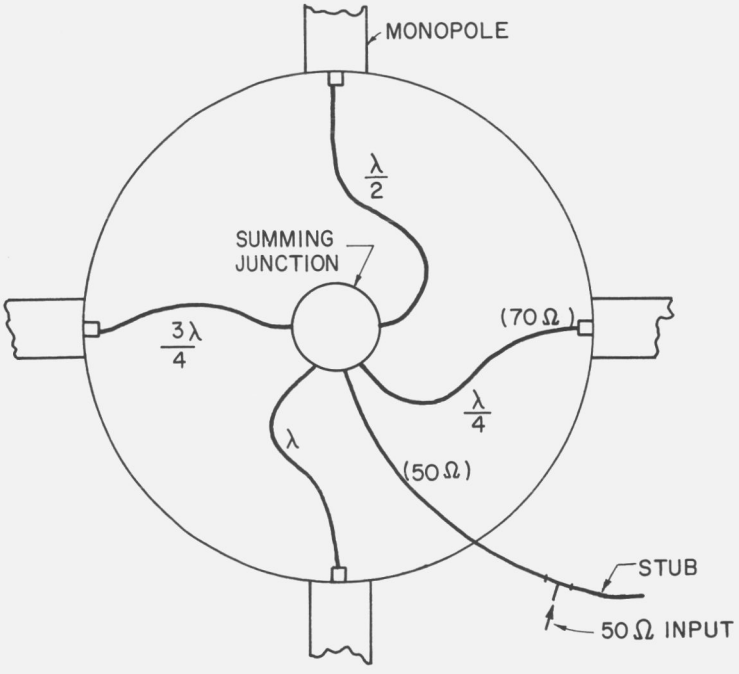

(b)

Figure 64. Antenna matching network.

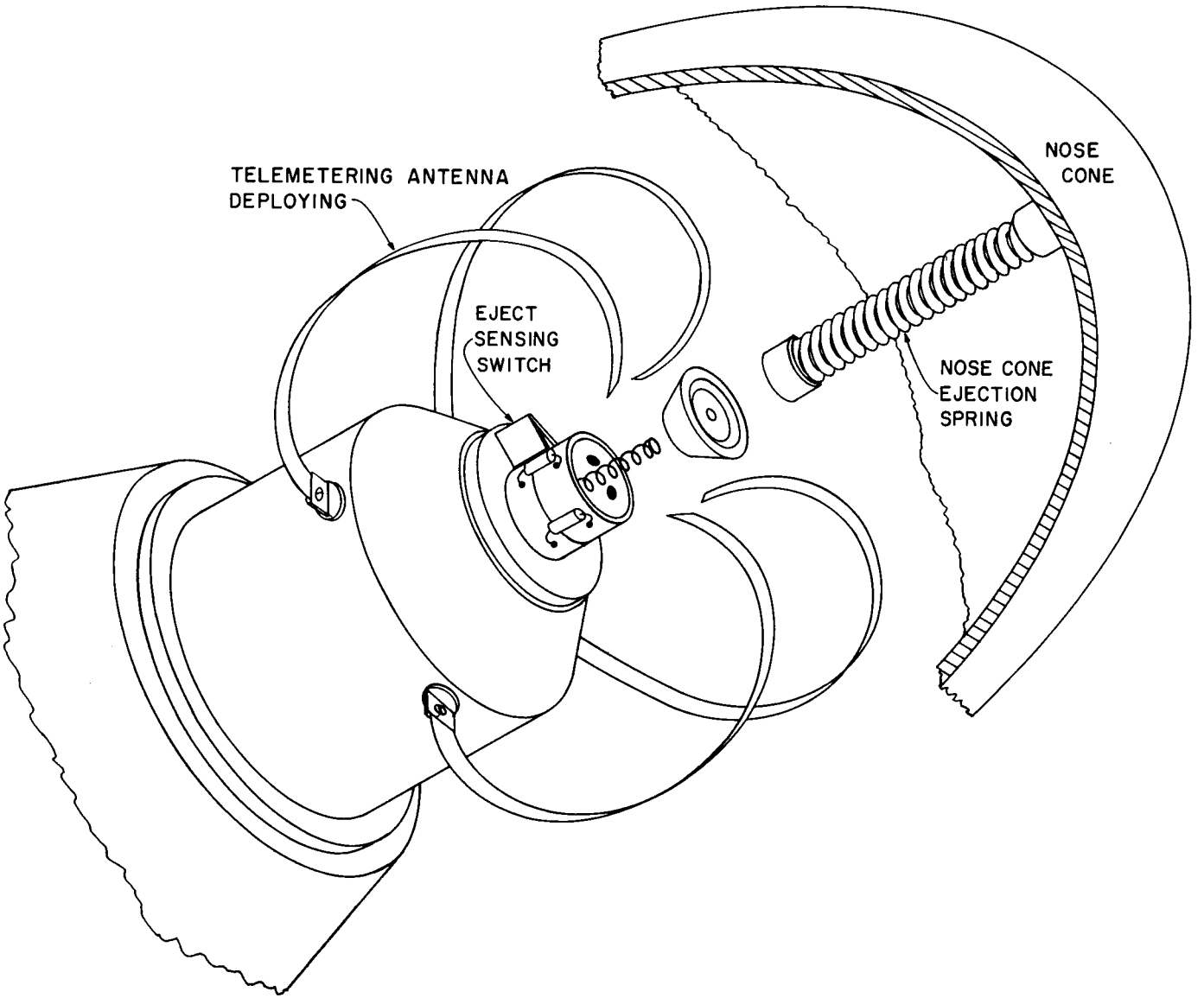

Figure 65. Turnstile deployment.

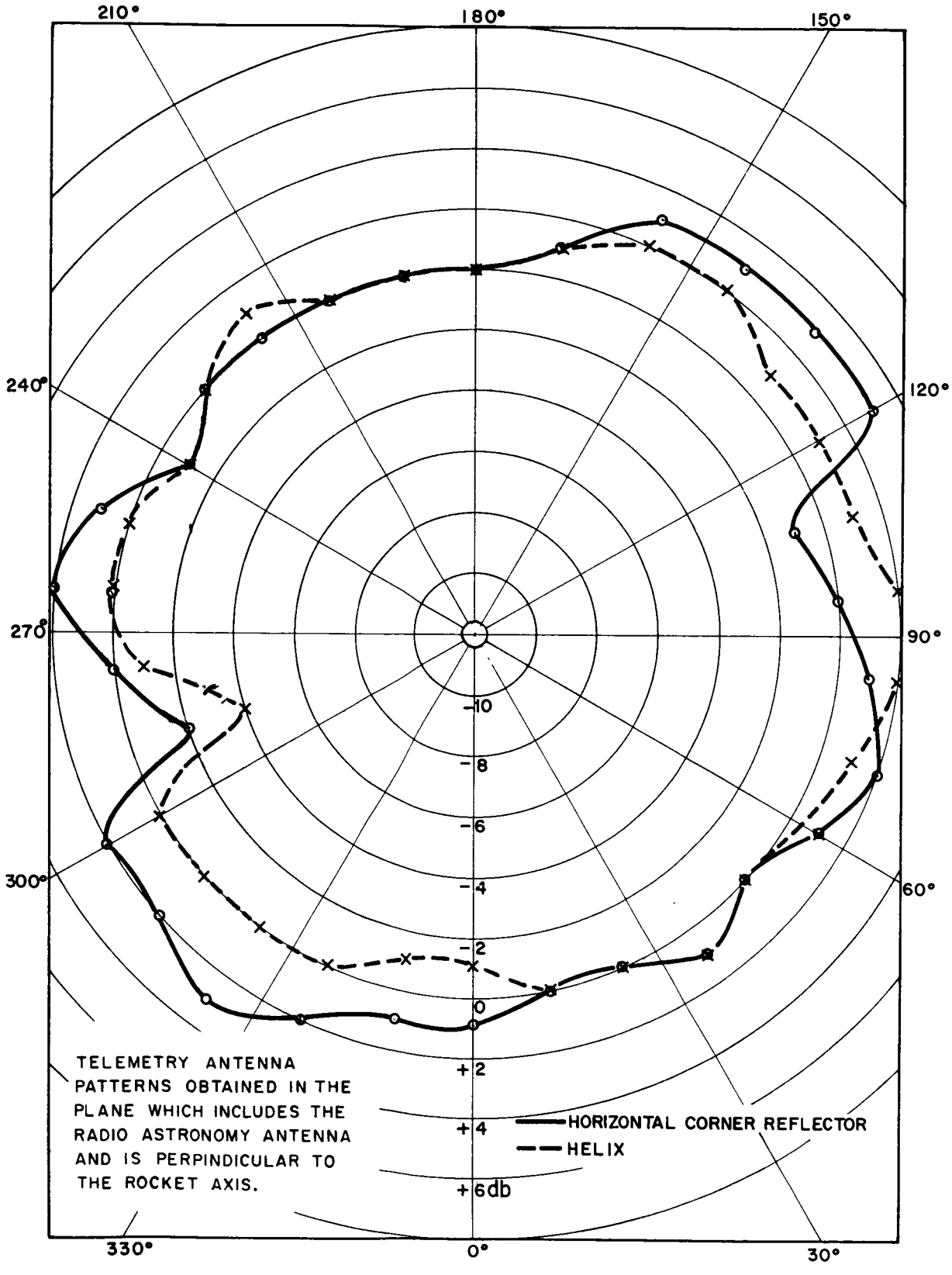

Figure 66. Turnstile antenna pattern.

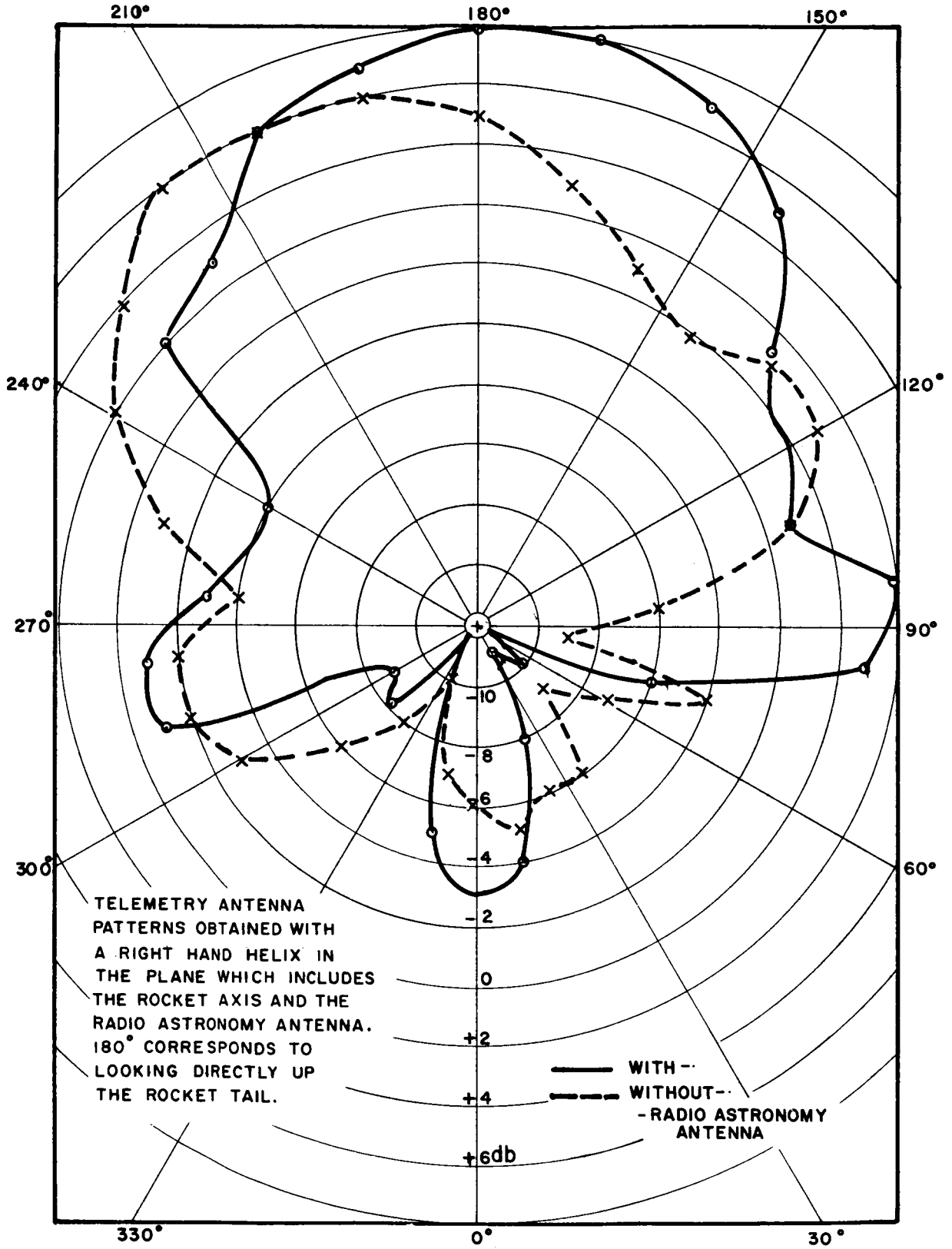

Figure 67. Turnstile antenna pattern.

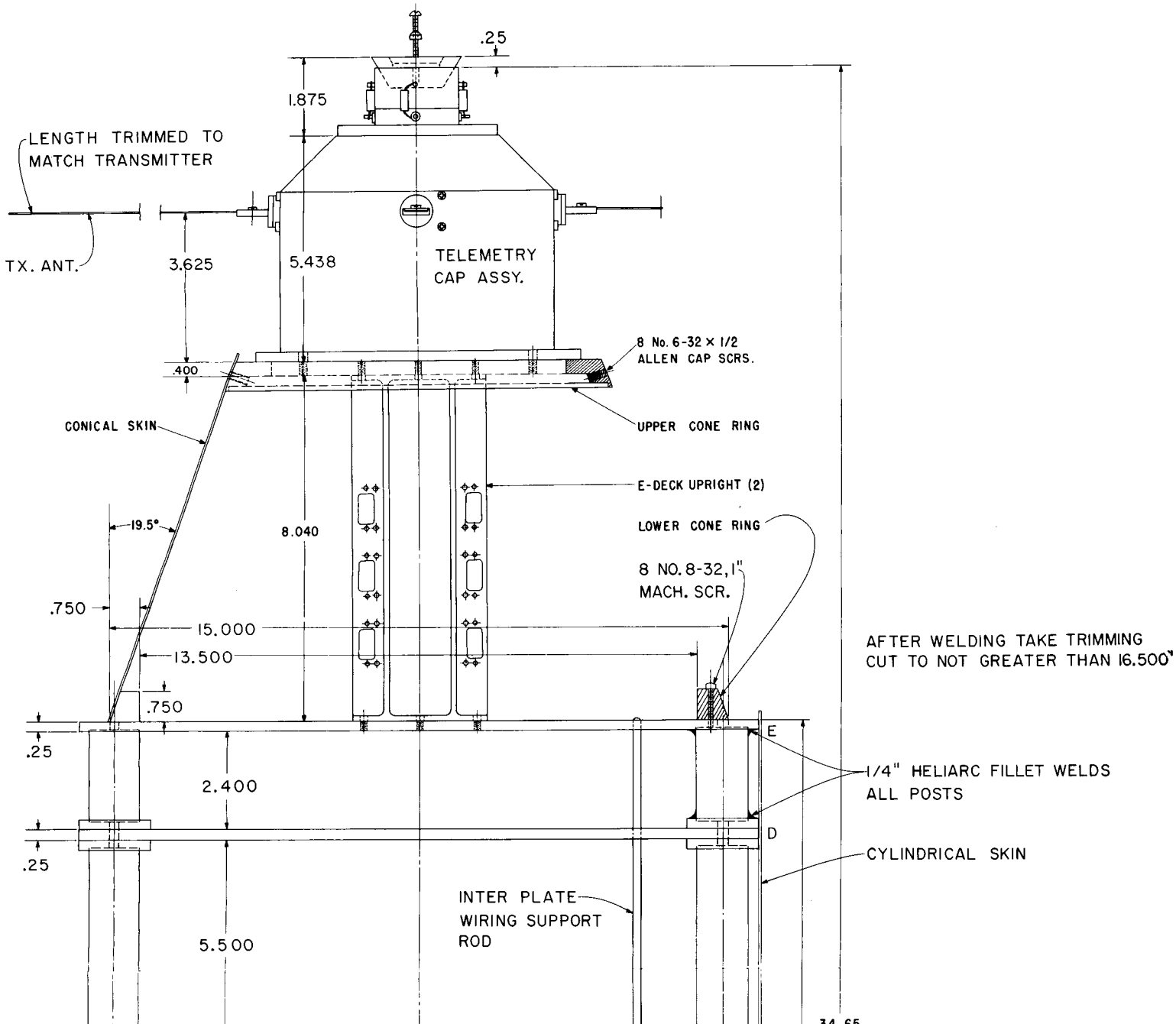
.25
1.875
LENGTH TRIMMED TO
MATCH TRANSMITTER
TX. ANT.
3.625
5.438
TELEMETRY
CAP ASSY.
8 No. 6-32 × 1/2
ALLEN CAP SCRS.
.400
CONICAL SKIN
UPPER CONE RING
E-DECK UPRIGHT (2)
19.5°
8.040
LOWER CONE RING
8 NO. 8-32, 1"
MACH. SCR.
.750
15.000
13.500
.750
AFTER WELDING TAKE TRIMMING
CUT TO NOT GREATER THAN 16.500"
.25
2.400
E
1/4" HELIARC FILLET WELDS
ALL POSTS
D
.25
CYLINDRICAL SKIN
INTER PLATE
WIRING SUPPORT
ROD
5.500
34.65

1-89

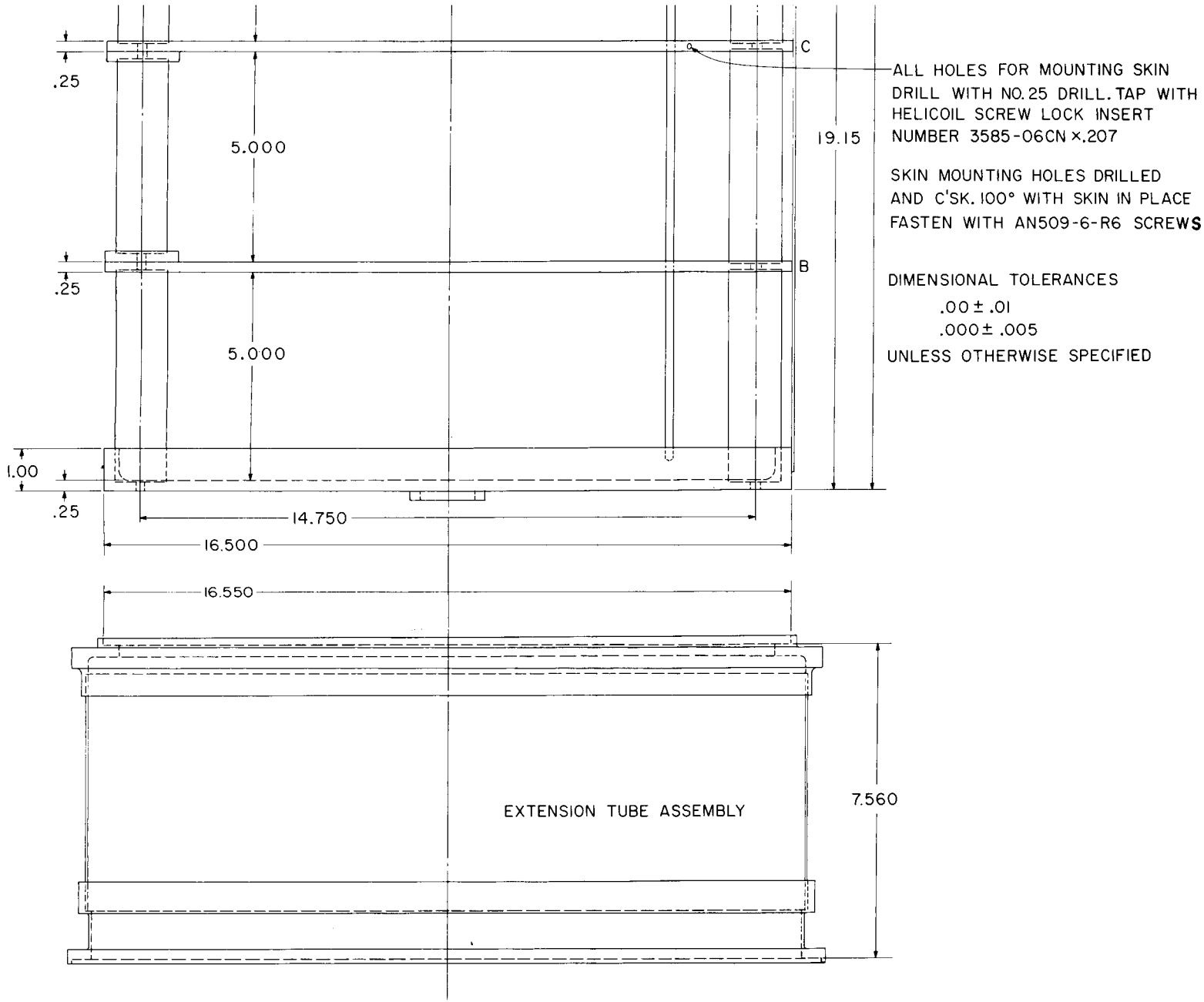

Figure 68. Instrument rack mechanical design.

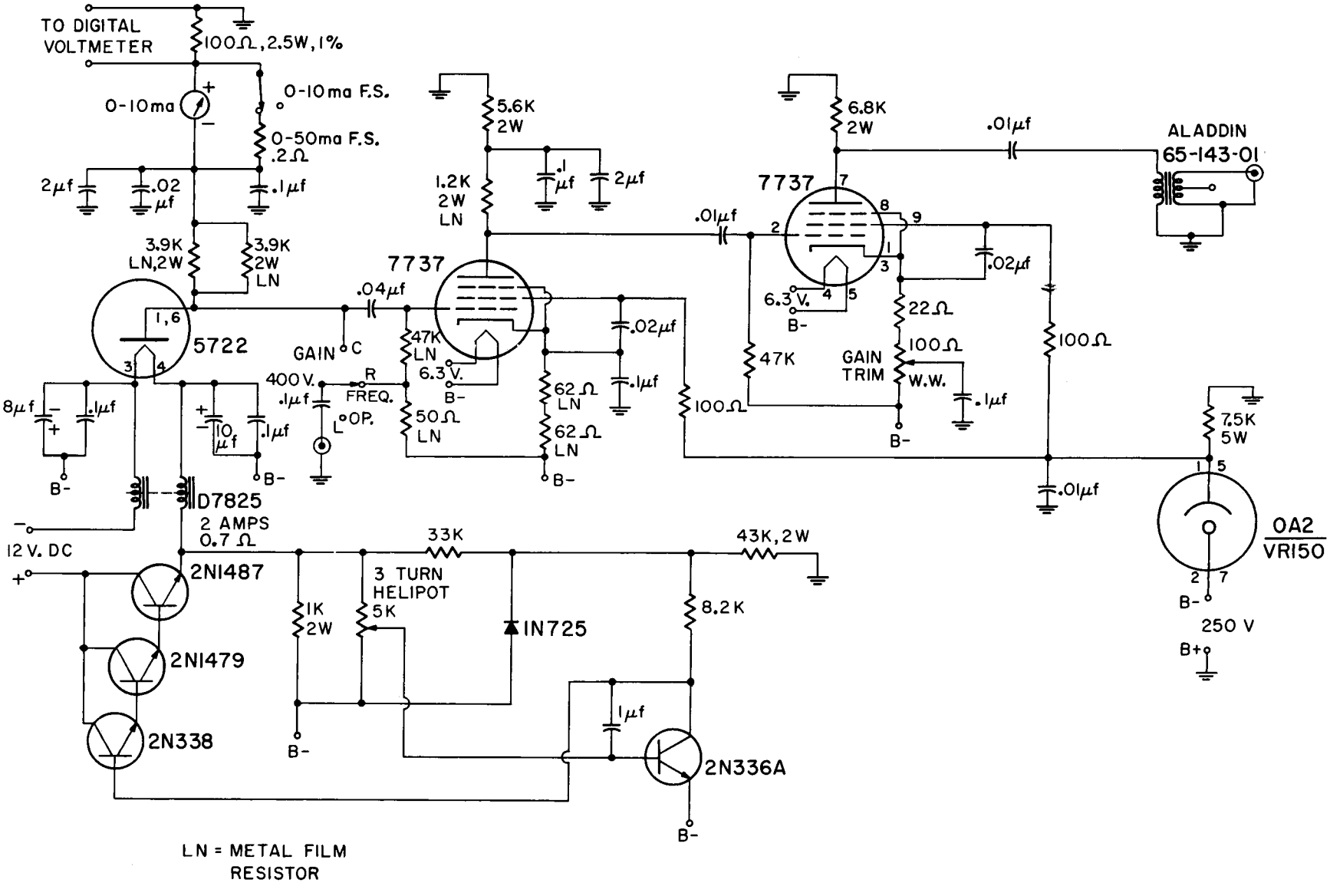

Figure 69. Laboratory noise generator.

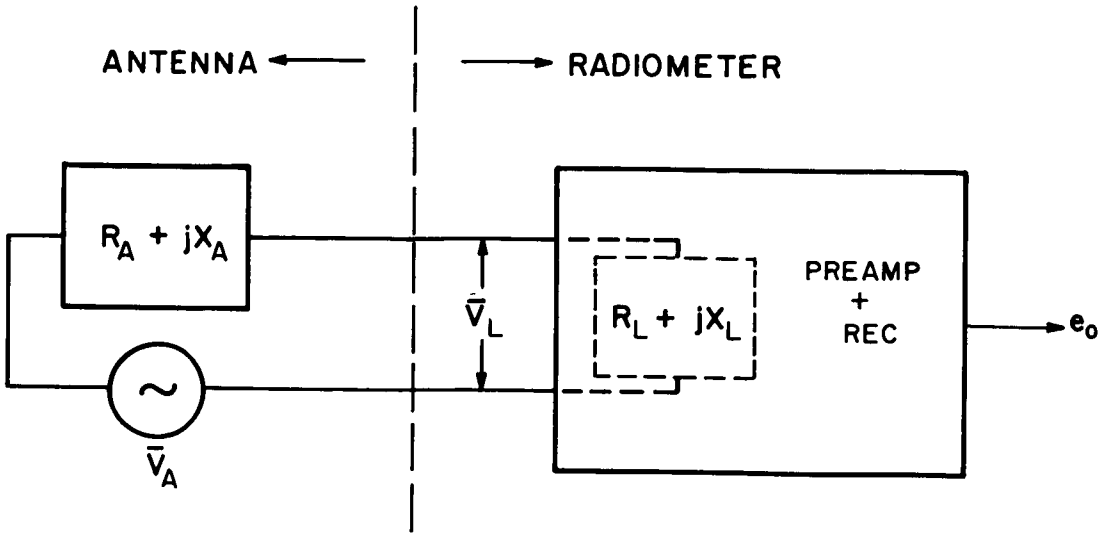

Figure 70. Equivalent circuit for preflight noise calibration.

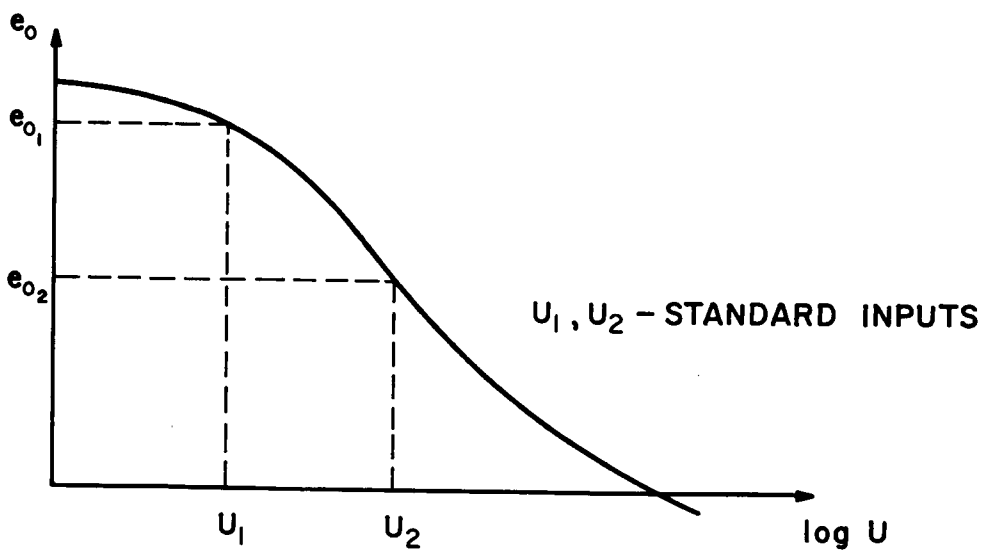

Figure 71. Reference response curve.

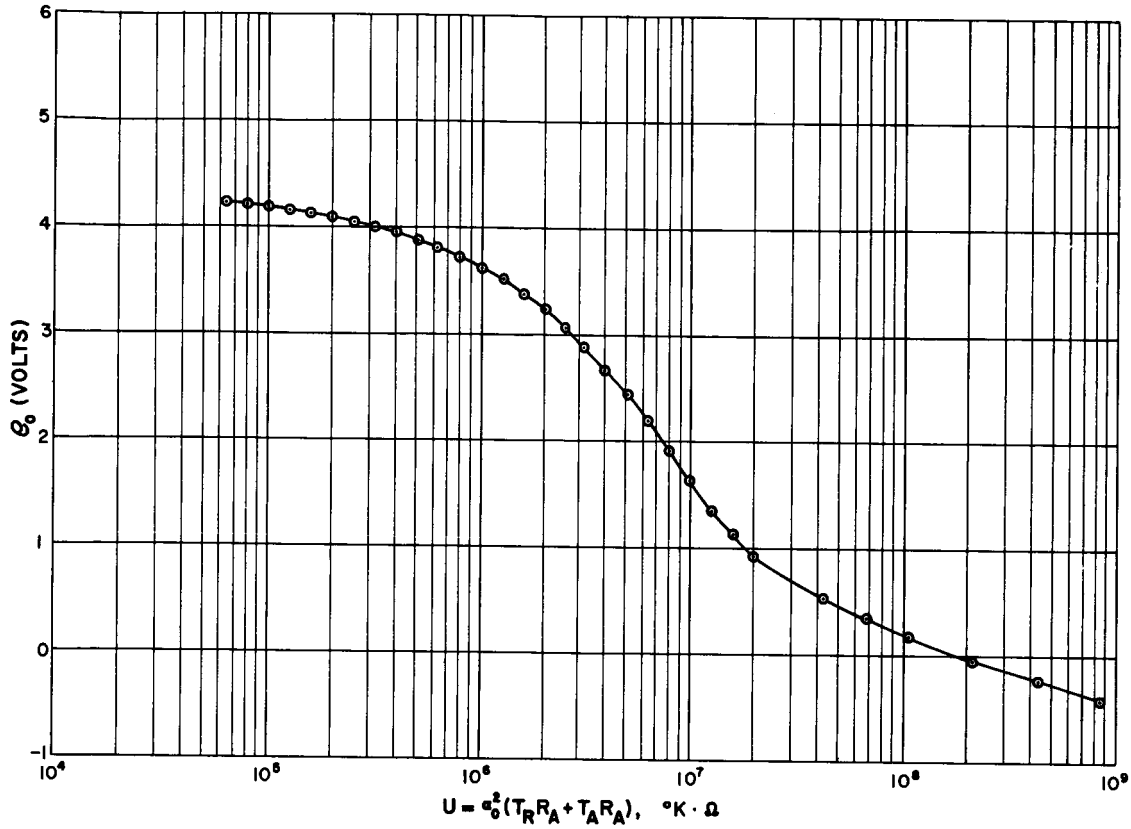

Figure 72. 750 kHz radiometer dynamic response.

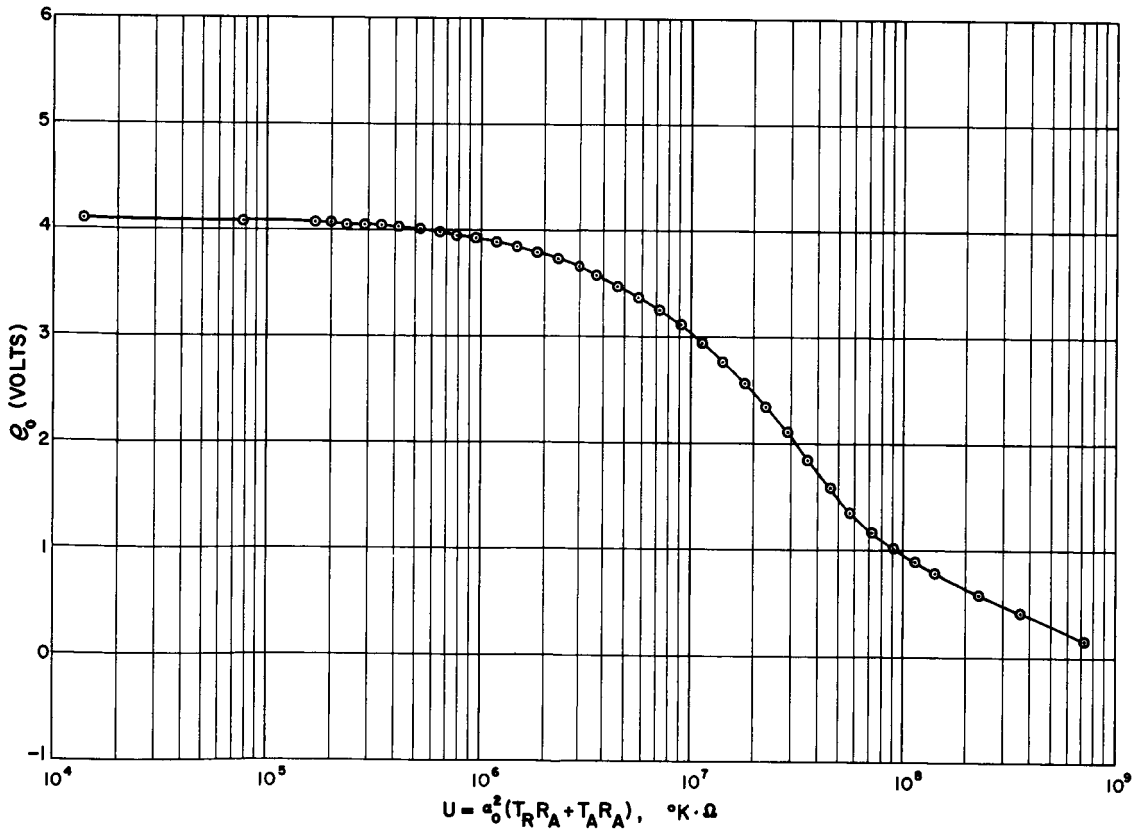

Figure 73. 1225 kHz radiometer dynamic response.

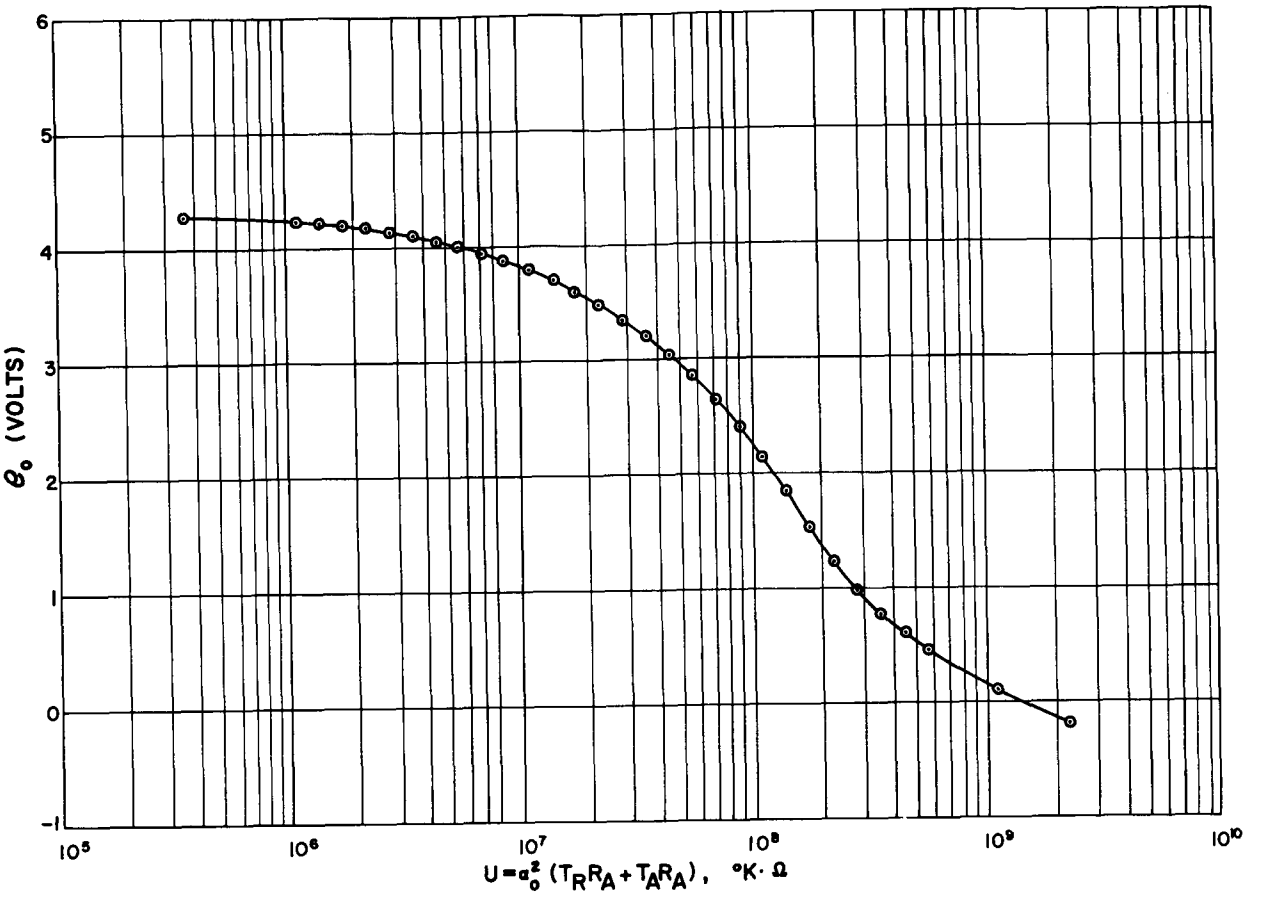

Figure 74. 2000 kHz radiometer dynamic response.

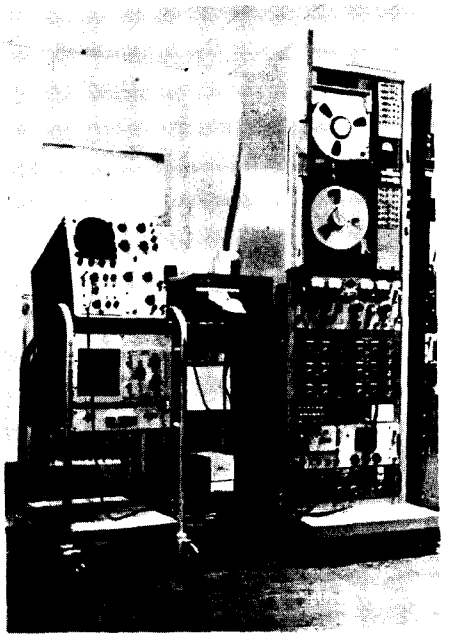

Figure 75. Ground station.

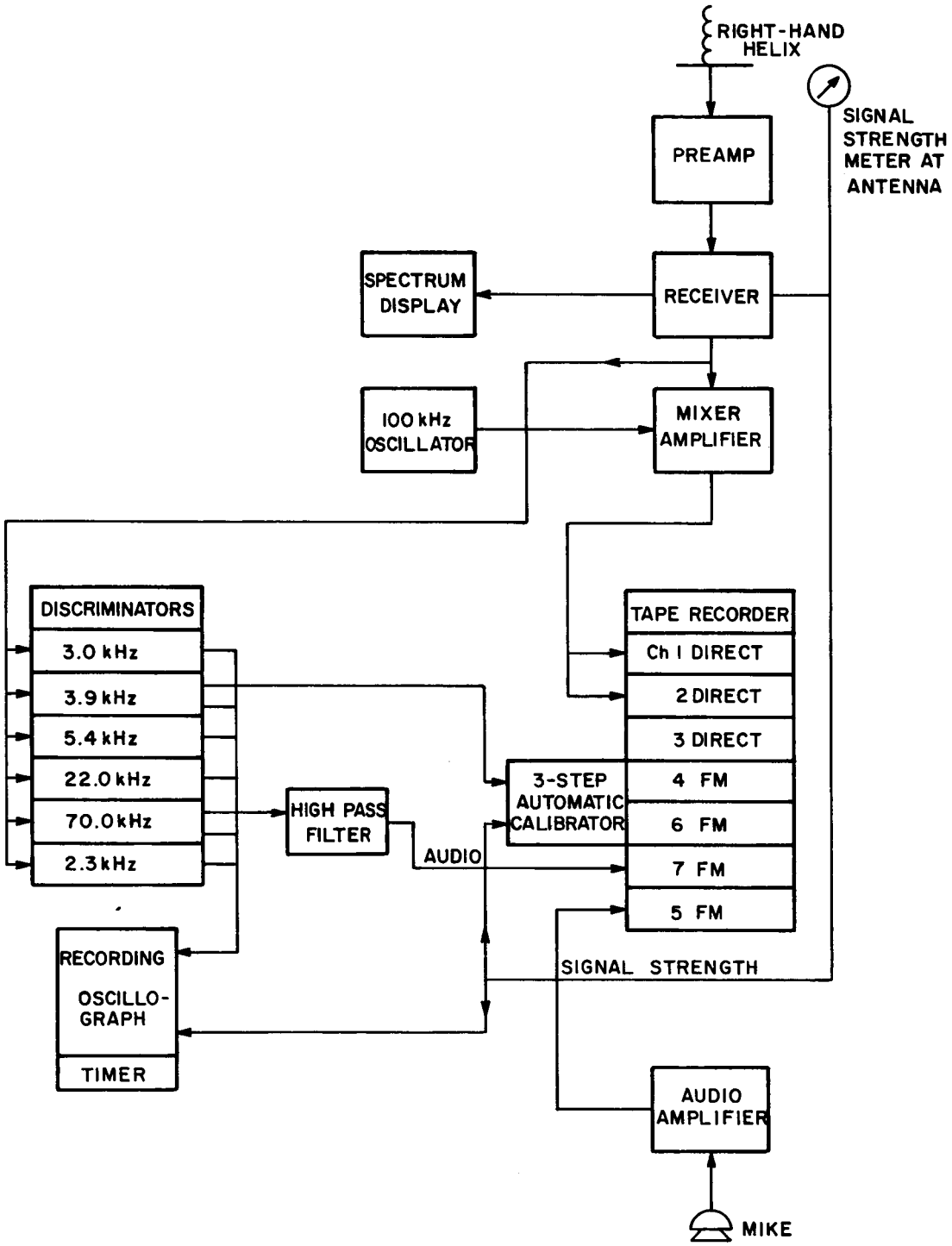

Figure 76. Ground station block diagram.

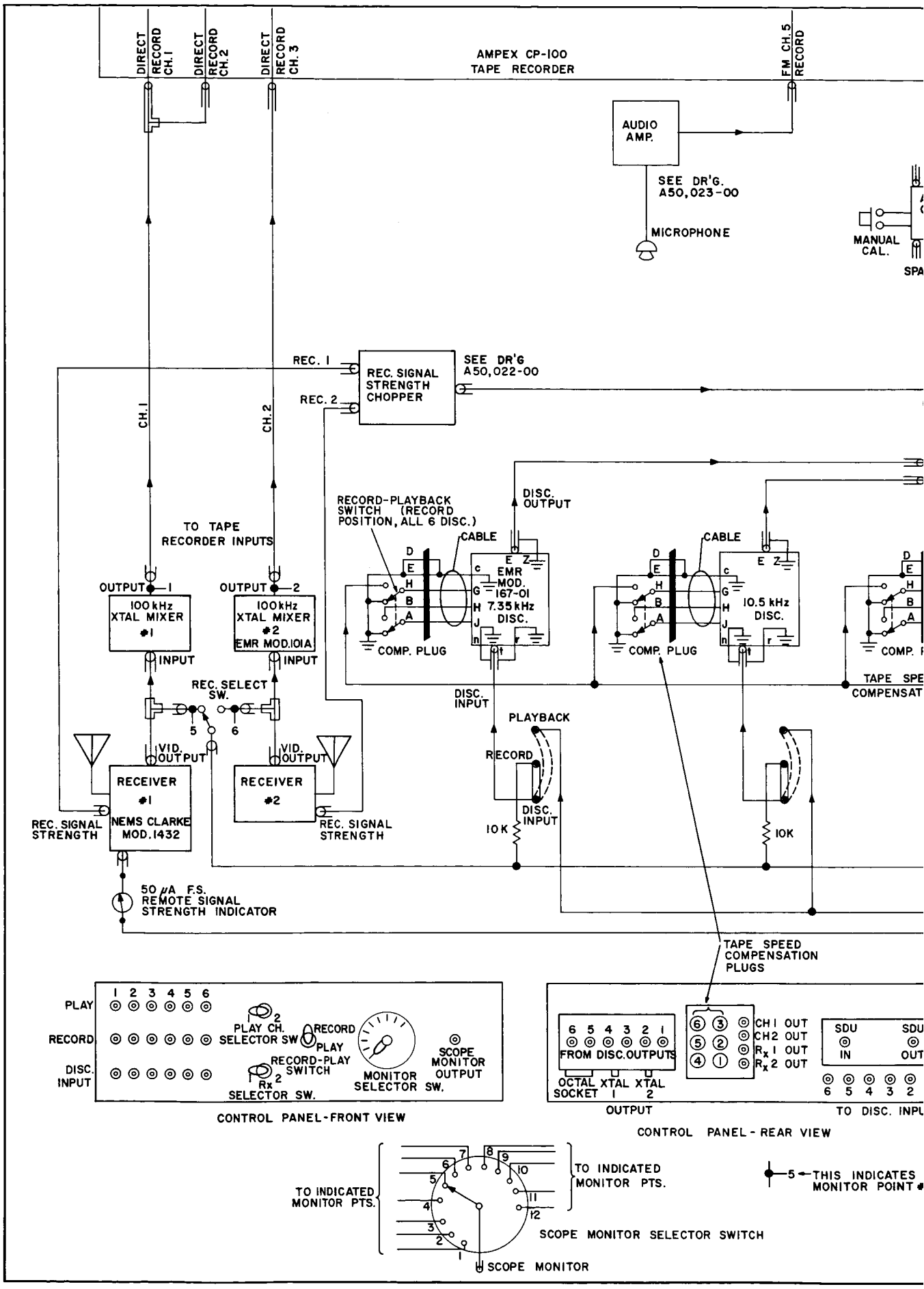

Figure 77. Telemetering

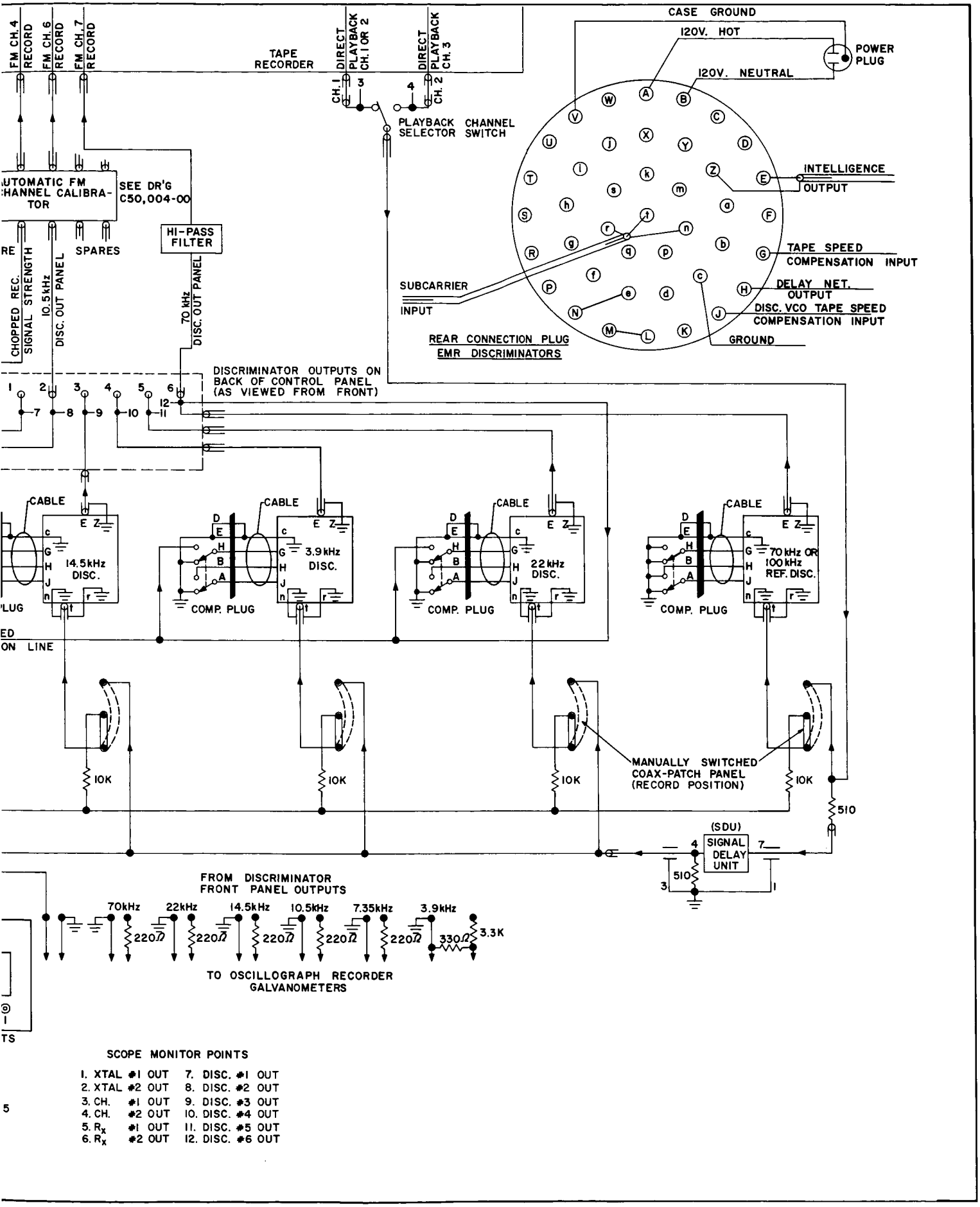

SCOPE MONITOR POINTS

1. XTAL #1 OUT	7. DISC. #1 OUT
2. XTAL #2 OUT	8. DISC. #2 OUT
3. CH. #1 OUT	9. DISC. #3 OUT
4. CH. #2 OUT	10. DISC. #4 OUT
5. R_x #1 OUT	11. DISC. #5 OUT
6. R_x #2 OUT	12. DISC. #6 OUT

ground station interconnect diagram.

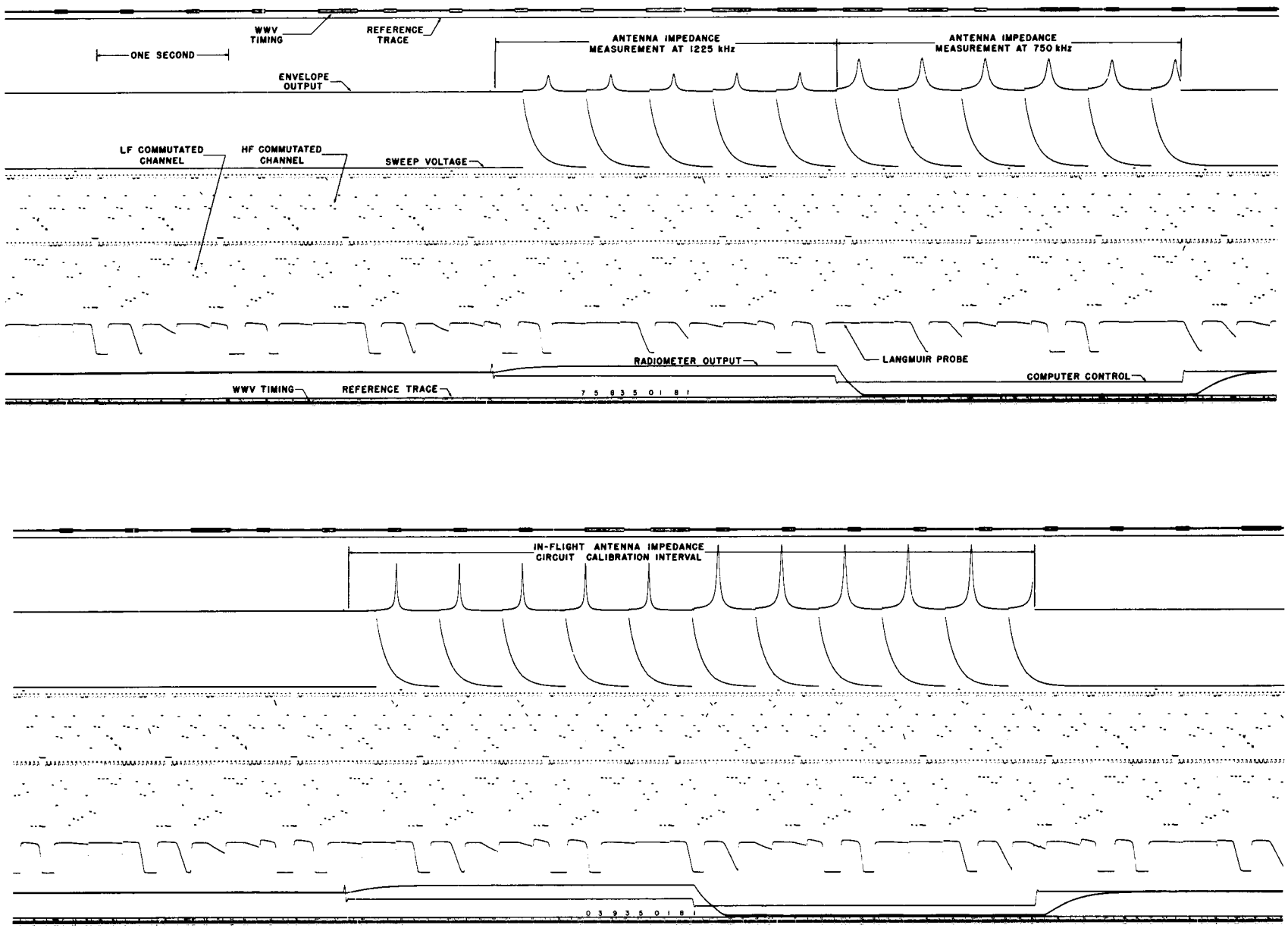

Figure 78. Sample of telemetry record.

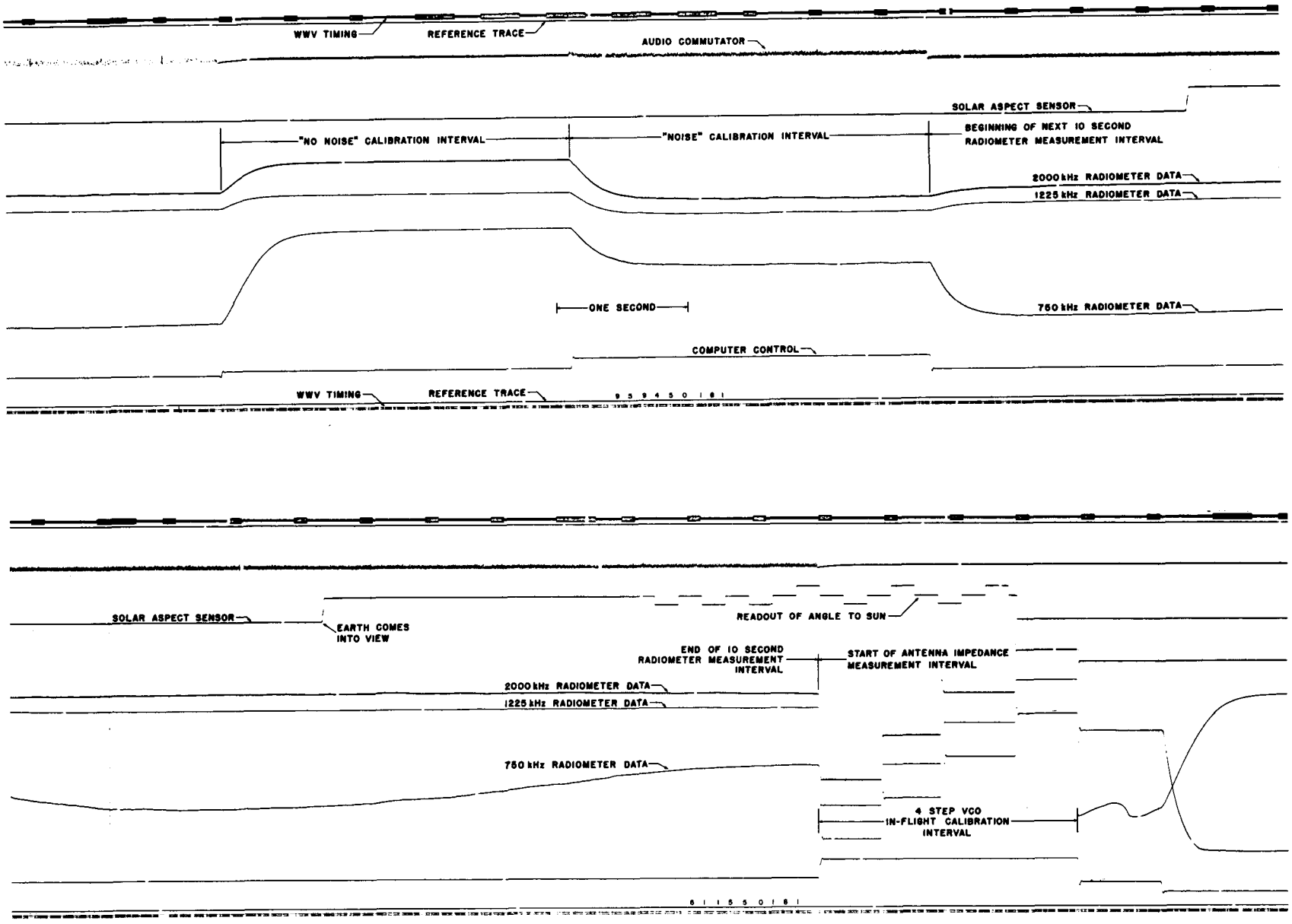

Figure 79. Sample of telemetry record.

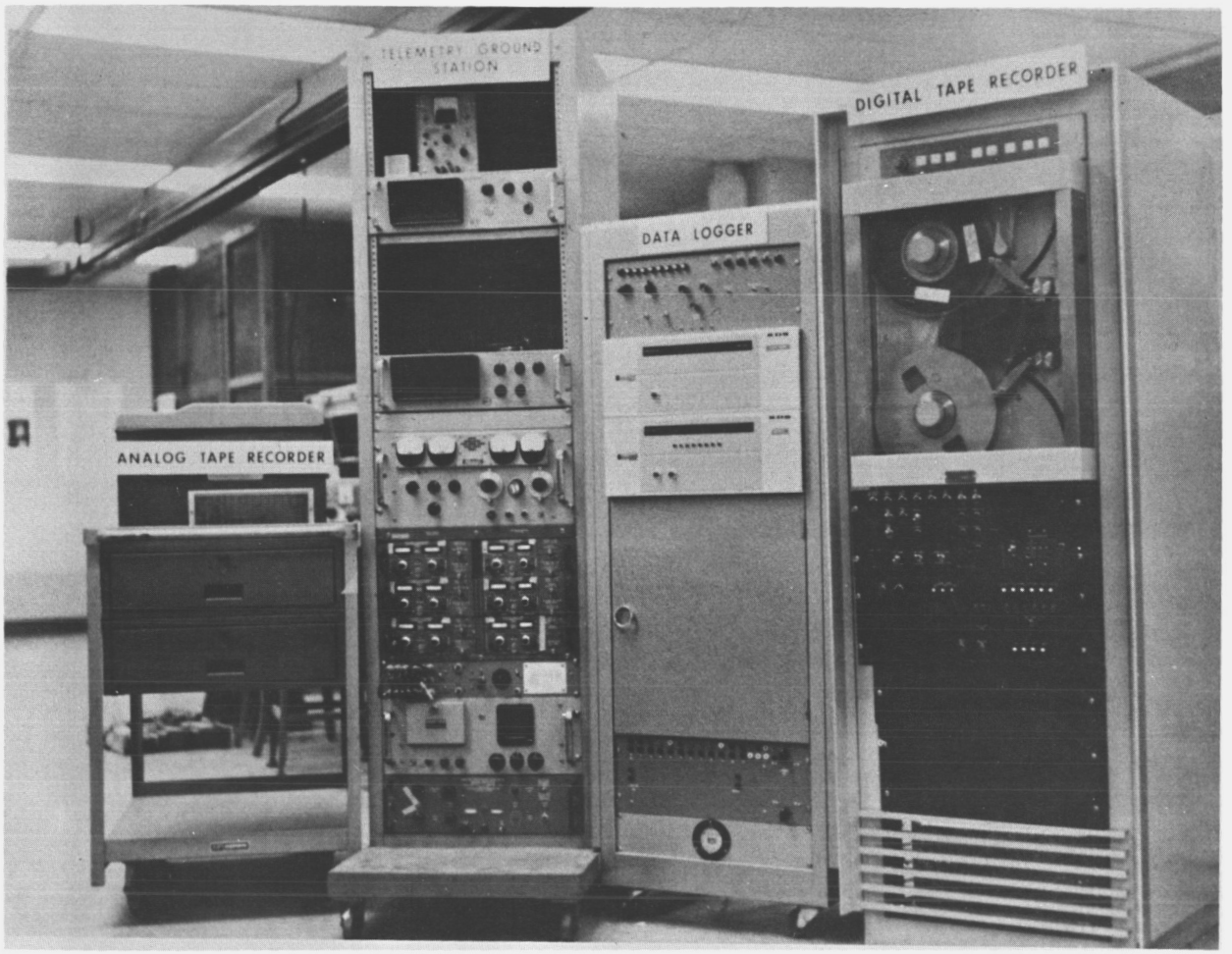

Figure 80. Data logger equipment.

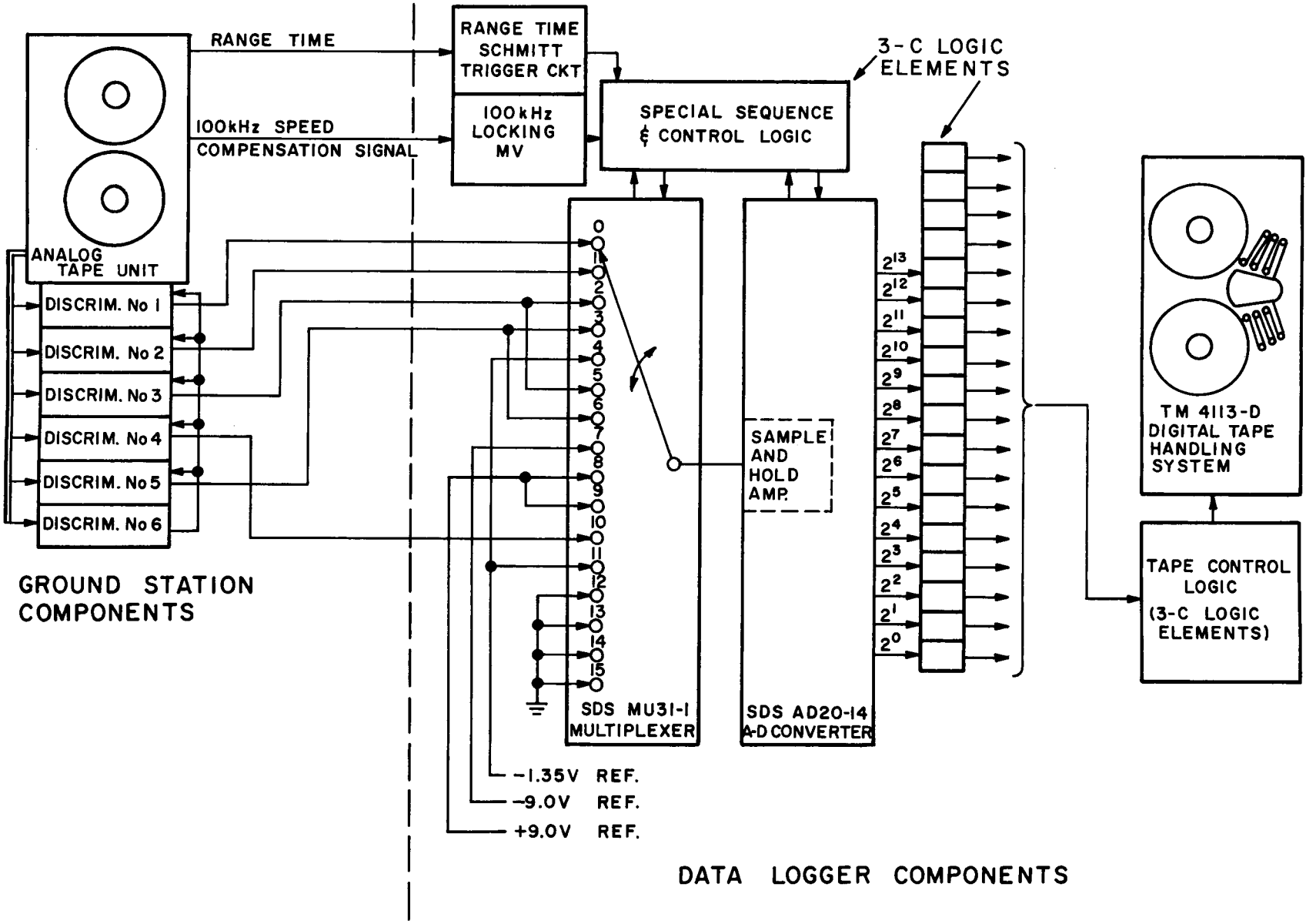

Figure 81. Block diagram of data logging operation.